

THESIS FOR THE DEGREE OF DOCTOR OF PHILOSOPHY

Chemical Interactions between Potassium, Nitrogen, Sulfur and Carbon Monoxide in Suspension-Fired Systems

THOMAS ALLGURÉN



Energy Technology
Department of Space, Earth and Environment
CHALMERS UNIVERSITY OF TECHNOLOGY
Göteborg, Sweden 2017

Chemical Interactions between Potassium, Nitrogen, Sulfur and Carbon Monoxide in
Suspension-Fired Systems

THOMAS ALLGURÉN

ISBN-978-91-7597-601-3

© THOMAS ALLGURÉN, 2017

Doktorsavhandlingar vid Chalmers tekniska högskola

Ny serie nr 4282

ISSN0346-718X

Energy Technology

Department of Space, Earth and Environment

CHALMERS UNIVERSITY OF TECHNOLOGY

SE-412 96 Göteborg

Sweden

Phone: +46 (0)31-772 10 00

Printed by Chalmers Reproservice

CHALMERS UNIVERSITY OF TECHNOLOGY

Göteborg, Sweden 2017

Chemical Interactions between Potassium, Nitrogen, Sulfur and Carbon Monoxide in
Suspension-Fired Systems

THOMAS ALLGURÉN

Energy Technology

Department of Space, Earth and Environment

Chalmers University of Technology

Abstract

Drastic cuts in global CO₂ emissions are needed to mitigate global warming and limit the average temperature increase to well below 2°C. The power generation sector is largely based on fossil fuels and generates a significant share of the global CO₂ emissions. Thus, new power generation processes with substantially reduced CO₂ emissions need to be employed to mitigate global warming. Two alternatives that may be part of the solution is the replacement of coal with biomass or to apply the concept of carbon capture and storage (CCS). In CCS processes the CO₂ is captured and processed on the plant site and thereafter transported to a storage location. Oxy-fuel combustion, which has been studied in this thesis, has been demonstrated in large-scale pilot plants (30-60 MW). This work investigates the possibilities to co-combust biomass and coal in oxy-fuel combustion with CO₂ capture. Biomass combined with CO₂ capture has the potential to contribute to negative CO₂ emissions. However, the high temperature corrosion (HTC) and the related K-Cl-S chemistry need to be studied in detail to determine the potential consequences for corrosion on heat transfer surfaces. This, since the use of biomass in power generation is problematic due to the relative high content of alkali (mainly potassium) and chlorine. Together these compounds form KCl, a salt that causes corrosive deposits and subsequent issues with so called high temperature corrosion (HTC). When sulfur is present, alkali sulfates may form instead of alkali chlorides. Sulfates have a higher melting point and causes less problems with corrosion and sulfates are therefore preferred instead of chlorides.

The work in this thesis is based on experiments performed in a 100 kW combustion unit and modelling of chemical kinetics. Both the experimental and modelling results show that a high SO_x concentration is preferable to achieve a high degree of sulfation of the alkali chlorides. In oxy-fuel combustion, the SO_x concentration is typically high due to flue gas recycling that enables almost complete potassium sulfation in some of the studied oxy-combustion atmospheres. This makes oxy-fuel combustion an attractive process for co-combustion of coal and biomass, since alkali chloride formation can be suppressed. In addition, the effect of KCl and SO₂ on the CO oxidation and NO formation has been studied in both experimental and modelling work. The results show that KCl can promote CO-oxidation in a CO₂ rich environment. However, no change was observed for the total burnout time even though the CO concentration was decreased locally. Regarding the nitrogen chemistry, KCl was found to inhibit the formation of NO whereas SO₂ promotes the oxidation of already formed NO to NO₂.

Keywords: alkali, CO-oxidation, NO-formation, combustion, experiments, modelling, oxy-fuel, sulfation

List of Publications

This thesis include the work presented in the following papers;

- I. Modeling the Alkali Sulfation Chemistry of Biomass and Coal Co-firing in Oxy-fuel Atmospheres
Ekvall, T.; Normann, F.; Andersson, K.; Johnsson, F., Energy and Fuels 2014, 28 (5), 3486-3494
- II. K-Cl-S chemistry in air and oxy-combustion atmospheres
Ekvall, T.; Andersson, K.; Leffler, T.; Berg, M., Proceedings of the Combustion Institute 36 (2017) 4011-4018.
- III. The influences of carbon monoxide oxidation on alkali sulfation in nitrogen and carbon dioxide atmospheres
Allgurén, T.; Andersson, K., submitted to Energy & Fuels
- IV. Experimentally Observed Influences of KCl and SO₂ on CO Oxidation in an 80 kW Oxy-Propane Flame
Ekvall, T.; Andersson, K., The Proceedings of Pittsburgh Coal Conference, 2017, Pittsburgh, USA
- V. The influence of KCl and SO₂ on NO formation in C₃H₈ flames
Allgurén, T.; Andersson, K., accepted for publication in Energy & Fuels

Thomas Allgurén (previously Thomas Ekvall) is the main author and responsible for the modelling and experimental work presented in all five papers. Associate Professor Fredrik Normann has contributed with guidance in the modelling work together with discussions and editing of the first paper. Professor Filip Johnsson took also part in discussions and the editing work of Paper I. Tomas Leffler and Magnus Berg contributed with their expertise regarding the IACM™ and contributed also to the editing work of Paper II. Professor Klas Andersson has contributed with guidance and discussion regarding both modelling and experiments as well as editing of all five papers.

Acknowledgement

I would like to start to show my appreciation to the Swedish Research Council (621-2011-4699) for supporting this project financially. I am also thankful for all the help I have received from my examiner Prof. Filip Johnson. My supervisors Prof. Klas Andersson and Assoc. Prof Fredrik Normann are greatly acknowledged for all their support. You always have time for discussions and together we have found a solution no matter the problem.

I have spent many hours in Kraftcentralen where Johannes Öhlin, Rustan Marberg and Jessica Bohwalli have supported me when I needed it. Tomas Leffler is acknowledged for his contribution with both equipment and expertise regarding alkali measurements. The experiments carried out in this work would not have been possible without the help of Adrian Gunnarsson, Daniel Bäckström and Rickard Edland. You have not only made it possible but also much more enjoyable to spend all these hours in Kraftcentralen. A special thanks to Daniel Bäckström with whom I spend most of my time in Kraftcentralen. Daniel has not only helped with experiments but also the development of new experimental systems.

It is easy to forget, but there are a lot of things behind the scenes that must be done. A big thanks to the “A-team” for all the help with a little bit of everything. I appreciate the working environment at the division and would like to thank everyone at Energy Technology for their contribution. Some extra appreciation is directed to Verena Heinisch for all the board game events she has arranged. When you share office with a person it means that you spend a lot of time together. If that person happens to be Stefania “Stebba” Ósk Garðarsdóttir it is nothing but a pleasure. I do not think I have spent a single day with you without at least one laugh. Thankful for having you as a friend, I am.

I would like to thank my friends and family, with a special thanks to my parents, for all the support. It is a natural part of life to question yourself and what you are doing, but some times are tougher than others. There was a time when also the teachers had doubts regarding my choices. If it would not have been for the unquestionable support from my parents I would most likely not have been where I am today.

My, you said “It is dangerous to go alone. Take this!” and gave me your hand. A hand which I took and that has supported me every day since. Your encouragement has meant the world to me. There are, however, things where a child is superior to an adult. I do not think there is a better way of gaining perspective and motivation than spending time with my son. Finally, work is not everything and I am truly grateful to have my family to share my life with.

To everyone – May the force be with you!

Thomas Allgurén

August 2017, Lövsveden – Dalarna - Sweden

Table of content

1	Introduction	1
1.1	Objective.....	3
1.2	Outline of the thesis	3
2	Background	5
2.1	Fuel characteristics	5
2.2	Oxy-fuel combustion	6
2.3	Co-combustion.....	7
2.4	High temperature corrosion	8
2.5	Co-combustion and flue gas recirculation	8
3	N, S and alkali chemistry related to combustion.....	11
3.1	The release of inorganic species during combustion.....	11
3.2	Formation of alkali-containing aerosols	12
3.3	Alkali sulfation	13
3.4	Effects of interactions between S, K and Cl species on CO oxidation.....	16
3.5	NO formation.....	18
4	Experimental setup.....	21
4.1	Combustion experiments	21
4.2	Measurement techniques	23
4.3	Evaluation of sulfation measurement methods.....	32
5	Modelling	39
5.1	Reaction mechanisms	39
5.2	Sulfation simulations	42
5.3	NO simulations	44
6	Results	47
7	Discussion	57
8	Summary & outlook.....	61
	Nomenclature	63
	References	65

1 Introduction

Today, it is generally accepted that the global temperature increase is largely a result of anthropogenic use of fossil fuels [1]. As a consequence, interest in alternative energy sources such as biomass and waste-based fuels, has increased drastically in recent years. The global total primary energy supply has increased by an average annual rate of 1.9% since 1990, while at the same time, the primary energy supply from renewable sources has grown at a rate of 2.2%. In 2014, 13.8% of the global total primary energy supply was generated from renewable energy sources [2]. Despite this increase in renewable energy supply there has been an increase in fossil CO₂ emissions of almost 40% between 1990 and 2014. The largest share of global CO₂ emissions, 42%, is attributed to heat and power generation [3]. According to the IEA, in Year 2014 more than 65% of the global electricity generation was based on the combustion of fossil fuels and more than 40 % was from coal alone. Hydro represents the largest source of renewable electricity production (16%), whereas only 2% of the worldwide electricity generation is from the combustion of biofuels and waste. In addition, solar and wind, which are believed to play an important role in the future electricity production mix, are together with geothermal generation responsible for 4% of the total electricity production [4]. Thus, there is a long way to go towards replacing the present use of fossil fuels.

An alternative pathway towards the replacement of fossil fuels is to lower the emissions of CO₂ from the use of fossil fuels in stationary combustion facilities by adopting the concept of carbon capture and storage (CCS). CCS allows for the continued use of fossil fuels without emissions to the atmosphere of carbon dioxide; CCS is often referred to as a bridging technology that will allow for fast and drastic cuts in emissions while more sustainable energy sources are being developed that can be adopted in a cost-effective and secure manner in the future. Four of the capture concepts discussed are: 1) pre-combustion, in which the carbon is removed through gasification before combustion; 2) post-combustion, in which the CO₂ is separated from the flue gases using, for example, absorption [5]; 3) oxy-fuel combustion [6], where the fuel is combusted in an oxygen-flue gas mixture instead of air; and 4) chemical-looping combustion, in which the fuel is oxidized by a metal oxide rather than air [7]. A schematic of the concepts is shown in Figure 1. The CCS concept entails that the captured or separated CO₂ is stored underground at a suitable location, such as an aquifer or a depleted oil well, preventing the CO₂

from reaching the atmosphere [8]. Before transportation from the source to the storage point, the CO₂ stream is cleaned from impurities, such as water, particulates, NO_x and SO_x. Employment of CCS typically reduces the emissions by 90%–95% from combustion of any fossil fuel. However, all of these approaches are associated with a considerable additional cost that is specific for each concept. It is therefore important to seek understanding of these processes so that they – in the future – may become as cost-effective as today’s conventional combustion processes.

An interesting possibility to reduce global warming is to combine the combustion of biofuels and CCS; this is commonly referred to as “bioenergy with carbon capture and storage” (BECCS). BECCS not only can help to reach a zero-emission target for power or industrial plants, but also to achieve negative emissions locally. BECCS could be used to compensate for fossil CO₂ emissions from sources for which a reduction might be more difficult to achieve. BECCS has also been proposed for the actual removal of CO₂ from the atmosphere. Azar et al. [9] have shown that it possible to reach the 2°C target even if we, for a while, reaches an atmospheric concentration of greenhouse gases otherwise considered too high, provided that BECCS is deployed.

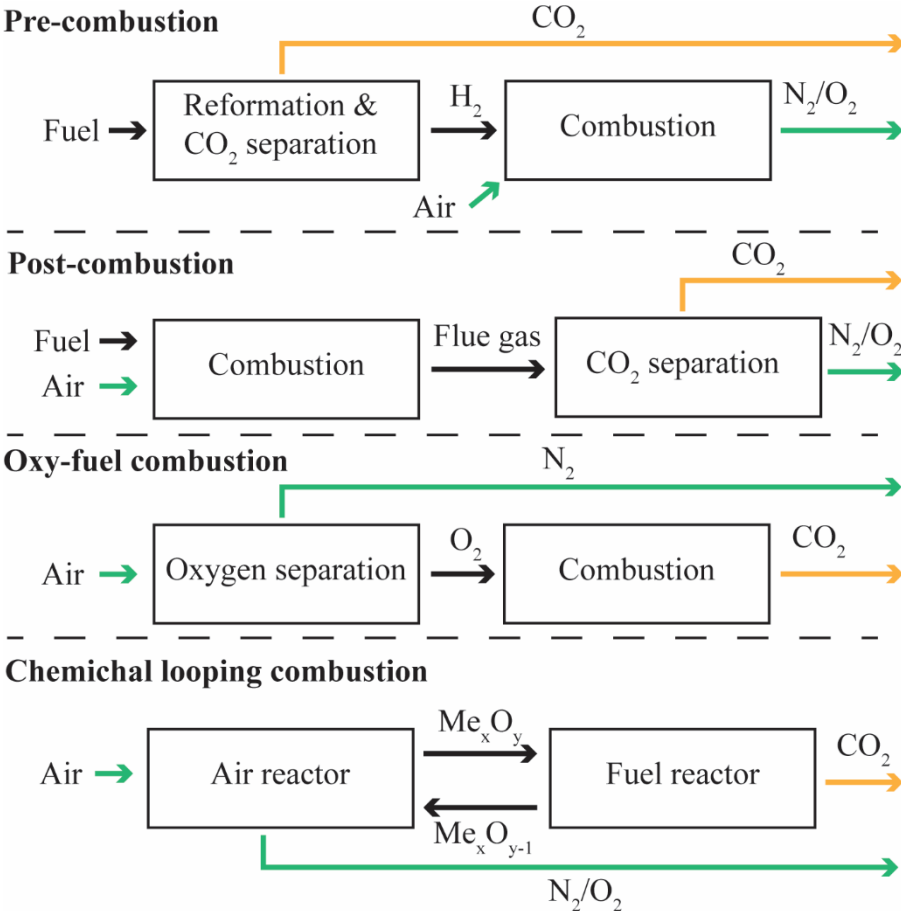


Figure 1. Schematic of the four main concepts for CO₂ separation for heat and power generation. Only the main components (on a dry basis) of each stream are indicated; the CO₂ streams might also contain, for example, NO_x and SO_x, which need to be removed before transportation and storage.

1.1 Objective

This thesis investigates the combustion chemistry relevant to fuel or fuel mixes with high concentrations of alkali, chlorine and sulfur that are used in suspension-fired systems in both air-fuel and oxy-fuel combustion systems. Compared to coal, biomass contains high levels of alkali metals and chlorine and low levels of sulfur. Given the fuel composition, significant amounts of alkali chlorides may be formed during the combustion of biomass, which increases the risk of HTC. However, during co-combustion of coal and biomass, the fuel-bound sulfur in the coal may promote the sulfation rather than the chlorination of the alkali metals. The formation of HTC-related alkali species is investigated in the present work under both in-flame and post-flame conditions. These compounds may, however, also influence other aspects of the combustion chemistry, such as fuel oxidation and NO formation. The focus of this investigation is on the homogenous gas-phase chemistry and includes both experimental work and detailed kinetic modeling. The work includes the development and evaluation of a new experimental setup that is designed to investigate the chemistry of the alkalis in technical-scale combustion test units. The results obtained are discussed in the contexts of the following questions:

- Which key parameters control the sulfation of alkali chlorides?
- Are there any differences in the alkali-sulfur interactions between air-fuel and oxy-fuel combustion?
- How is the combustion process influenced by the presence of alkali and sulfur?

1.2 Outline of the thesis

This thesis is based on the following five papers, as shortly described below.

Paper I includes modeling work that focuses on the homogenous sulfation of potassium chloride. The modeling includes a comparison of co-combustion with air-fuel and oxy-fuel systems, together with an evaluation of the related chemistry and the most important parameters.

Paper II presents both experimental results and the results from the kinetic modeling to investigate the homogenous gas-phase sulfation of potassium chloride. The work includes a sensitivity analyses with respect to the concentration of sulfur and the flue gas recirculation mode applied, the latter when comparing air-fuel and oxy-fuel atmospheres.

Paper III is a continuation of the work presented in Paper II. In this work, chemical kinetic modelling is used to study the changes that may occur when replacing nitrogen with carbon dioxide in the combustion atmosphere, *i.e.* in further detail compared to Paper II.

Paper IV focuses on the influences of potassium, chlorine, and sulfur on CO oxidation in the flame zone. The work includes both experiments and kinetic modeling for conditions relevant to both air-fuel and oxy-fuel combustion.

Paper V examines how potassium chloride and sulfur dioxide affect the formation of NO during the combustion of propane in air. This involves measurements of the NO concentration in the flue gas when an 80 kW flame is doped with KCl and SO₂. Reaction simulations are also performed in addition to the experiments.

2 Background

In this chapter the concept of oxy-fuel combustion is presented and describes how it differs from conventional air-fuel combustion. In addition, the characteristics of biomass (or types of biomasses) will be presented together with the effects of introducing biomass into an air-fuel or oxy-fuel combustion system.

2.1 Fuel characteristics

Coal is the main fuel used for heat and power generation, whereas only a few percent of the global electricity production originates from biomass combustion [4]. Two subcategories of biomass, forest-derived and agriculture-derived biomass, are commonly used as fuel for heat and power generation purposes. The properties of these biomass types differ considerably from those of coal. For example, the moisture content of biomass is typically higher, which is also the case for alkali metals (sodium and potassium) and chlorine [10-13]. The composition of the fuel not only differs between the various types of biomass, but it is also related to the pretreatment of the biomass before it is fed into the combustion process, e.g., wood chips, saw dust or torrefied wood, whereby the latter process tends to alter the sulfur and chlorine contents [14]. Some examples of the different types of biomasses are shown in Figure 2. In the present work, the most common types of biomass are considered, i.e., forest or agricultural biomass that has not been pretreated with thermal or similar processes. The simulated contents of alkali and chlorine, in both the experiments and the modeling of this work, are therefore significant. This is also typically the case when biomass is used in the current heat and power generation plants.



Figure 2. Heat and power can be generated from various types of biomass, which can be pretreated in several different ways. Some examples are: a) demolition wood; b) rice husk; c) torrefied wood; and d) pelletized wood.

2.2 Oxy-fuel combustion

In oxy-fuel combustion, the fuel is combusted in an almost-nitrogen-free atmosphere that is created by mixing pure oxygen with recycled flue gases. Thus, the nitrogen is mainly replaced by CO_2 or a mixture of CO_2 and H_2O for dry or wet flue gas recirculation, respectively. The concept of oxy-fuel combustion and the differences between dry and wet flue gas recirculation are described in Figure 3. The figure also shows examples of components that differentiate between streams. The difference in gas composition in relation to air-fuel combustion affects the physical properties, such as the specific heat capacity and the emissivity of the gases, resulting in a different temperature profile compared to air-firing [15-17]. To compensate for these differences, the concentration of oxygen in the oxidizer is often set higher than 21% [6].

The amount of recirculated flue gas is directly related to the feed gas oxygen concentration; a higher concentration of oxygen requires less recirculated flue gas. Furthermore, the minor species, in addition to CO_2 and H_2O , in the flue gases will also be recirculated (if they are not separated before recirculation). Therefore, recirculation will influence the concentrations of these species; the concentration of SO_2 is typically more than 3 or 4-fold higher in oxy-fuel combustion than in air-fuel combustion [18, 19]. The level of NO is, however, reduced due to reburning effects that result from the flue gas recirculation [20, 21]. Although the concentrations of substances such as SO_x and NO_x are low, the differences between the levels of SO_x and NO_x can be of importance for the chemical reactions.

The recirculation itself is not the only factor that affects the gas composition in the furnace. The composition of the gases will also be changed if flue gas cleaning equipment is placed in the recirculation loop of the system, thereby separating solids before recirculation and removing, for example, condensed alkali species (the species indicated in red in Figure 3). Another item of equipment that can be used is a flue gas condenser, which will remove water (referred to as ‘dry recirculation’) and soluble compounds, such as HCl and $\text{SO}_3/\text{H}_2\text{SO}_4$ (the species indicated in blue in Figure 3). In this way, flue gas cleaning equipment can be used as a means to achieve a favorable combustion atmosphere. However, if the cleaning apparatus is placed before the recirculation, the cost for that specific component will increase due to the larger gas flow, as compared to the cost associated with positioning the cleaning apparatus outside the loop [6].

In this work, the oxy-fuel system considered is similar to the one presented in Figure 3. Thus, the system will always include ash removal before recirculation of the flue gas, and there is the possibility to choose, whether or not, the flue gas condenser should be used. If a flue gas condenser is used before the recirculation it will be referred to as ‘dry flue gas recirculation’ and, if not, it will be referred to as ‘wet flue gas recirculation’ (Fig. 3).

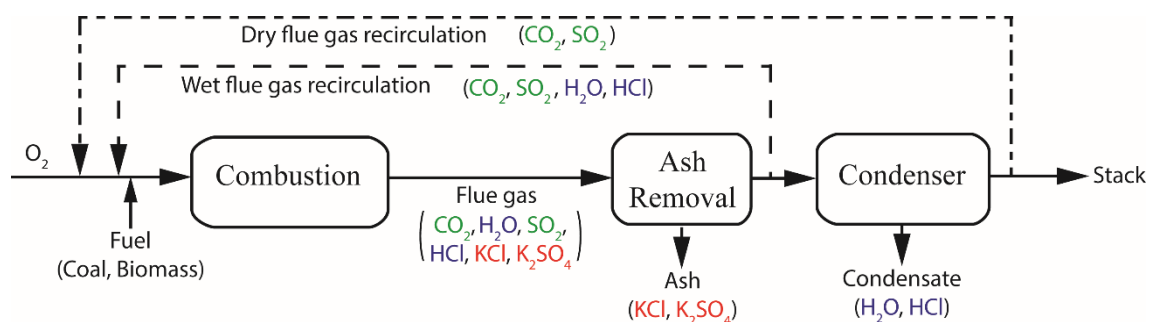


Figure 3. Overview of the oxy-fuel combustion process, indicating potential compositional differences arising from using solids separation and a flue gas condenser. The species indicated in parentheses are examples to clarify differences between the streams. Red, solids; blue, condensable species; green, gaseous species.

2.3 Co-combustion

Co-combustion is a way to introduce biofuels to fossil-fuel fired units to achieve a reduction in CO_2 emissions with a fuel of fossil origin. Biofuels may be co-combusted with coal, either directly or indirectly. During indirect co-combustion, the two fuels are combusted separately and the systems are connected on either the steam side or the flue gas side. In the direct co-combustion system, the fuels are combusted in the same furnace, with the fuels being mixed and fed together, either to a bed (fixed or fluidized) or to a burner with suspension-based combustion [22].

For the existing suspension-fired units in which biomass could be introduced for co-firing purposes, the fuel mills typically set the technical limitation for the share of biomass that may be blended into the fuel mix, as discussed by Savolainen [23]. Savolainen attempted to mix coal and saw dust (in a 315-MW_{fuel} boiler) and found that for large fractions of saw dust (>30% vol), the drying capacity of the mills was insufficient. When the share on a volume basis was >50% the boiler capacity was reduced by 25%. However, not only the drying capacity was affected. The fraction of coarse coal particles increased with the share of biomass in the mills [23]. The energy required (both thermal and mechanical) to prepare the biomass varied with both size and the concept chosen, as well as with moisture content, in that a higher moisture content required more energy [24]. A second option for introducing biomass into a pulverized coal boiler is to treat the biomass separately. This option requires an extra biomass mill/crusher and a specialized biomass burner. The new burner can be constructed either so it can be fired with pure biomass or a blend of coal and biomass [23]. Co-firing biomass with coal may affect emissions, such as NO_x and SO_x, as well as other properties, such as ignition delay [23, 24]. The size and share of biomass particles may also have a positive or negative effect on the outlet CO concentration, i.e., the burnout conditions [24].

2.4 High temperature corrosion

High temperature corrosion (HTC) is a problem that affects the heat transfer surfaces in a boiler. HTC is caused mainly by alkali-based salts that possess a high melting point and that easily are deposited on heat transfer surfaces. Compounds that contain alkali metals and chlorine are among the most aggressive agents, which is why HTC is primarily a problem for power plants that are fired with biomass rather than coal [25-27]. To counteract HTC in biomass-fired power plants, the steam temperature in the boiler is often lowered, which leads to a decreased electrical efficiency [10]. The risk for alkali-related HTC can be reduced by the co-combustion of coal and biomass (relative to the combustion of biomass alone) owing to the relatively high levels of fuel-bound sulfur in coal, which favors the formation of the less-corrosive sulfates over chlorides [11, 28, 29]. Oxy-fuel derived flue gases have for example been shown by Syed et al. [30] to be more corrosive than those derived from air-fuel combustion. However, they assumed that the level of deposition and the composition of the deposits were the same for both the air-fuel and oxy-fuel flue gases, which is not necessarily the case, and this is a topic that will be discussed further in this work.

2.5 Co-combustion and flue gas recirculation

As mentioned above, the flue gas recirculation applied in oxy-fuel combustion increases the concentrations of SO_x and NO_x compared to air-fuel combustion [21, 31]. In this work, the SO_x components are studied in detail, components whose concentrations are typically 3–4-fold higher in oxy-fuel flue gases than in air-fuel flue gases [19, 31]. An increased concentration of SO_x will also increase the S/K-ratio of the flue gases if the ash (which contains the potassium) is removed before flue gas recirculation. The theoretical relationship between the S/K-ratios of the fuel and the flue gases is shown in Figure 4. The calculations are theoretical and are based on the assumptions that all fuel-bound sulfur and alkali species are being released to the gas phase, and that the formed alkali gas-phase species are captured in the condenser water and/or extracted as solids before the flue gas is recirculated to the burner (see Figure 3). The ratio of the S/K in the flue gas to that in the fuel is one for air-fuel combustion and approximately five

for the OF25 dry case (oxy-fuel operation with dry flue gas recycling and with 25 vol.% oxygen in the feed gas). The amount of sulfur in the flue gases is then decreased for higher concentrations of oxygen and for wet recirculation in relation to dry recirculation. To summarize, the S/K-ratio of the flue gases will always be higher during oxy-fuel combustion if the recirculated flue gas contains sulfuric species. If no sulfur is recirculated it will be a one-to-one relationship similar to combustion in air. SO₂ is shown to inhibit the oxidation of CO during both air-fuel and oxy-fuel combustion, which means that it influenced the overall combustion process [32, 33]. In addition, a high concentration of SO₂ seems to favor the sulfation of alkali metals [11, 34, 35]. The SO₂ concentration is therefore important for both in-flame and post-flame conditions. It also implies that there is a difference in performance between air-fuel and oxy-fuel combustion systems, which is attributed to the increase in SO₂ concentration for the latter case.

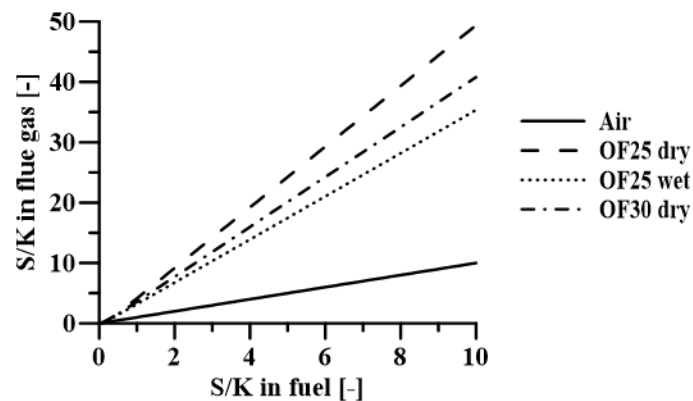


Figure 4. Molar sulfur to potassium (S/K)-ratio in the flue gases and how this varies with respect to the S/K-ratio of the fuel. The theoretical variations are shown for air-fuel combustion and oxy-fuel (OF) combustion. There are three cases representing different oxygen concentrations (25 vol.% and 30 vol.%) and different recirculation strategies (wet or dry). In air, the S/K-ratio of the flue gas is the same as that of the fuel. The trends are based on the assumption that all the sulfur- and potassium-containing species are released to the gas phase. Source: Paper I.

3

N, S and alkali chemistry related to combustion

The combustion of solid fuels includes the following steps: heating of the fuel; release of volatile matter; oxidation of gaseous species; and char combustion. Fuel oxidation, which is the main part of the combustion, is not the only reaction taking place. Depending on the composition of the fuel, a large variety of different compounds, both gaseous and solid, can be formed at concentrations that are low (<1 vol.%) but still important from the boiler performance or environmental perspective. Nitrogen, sulfur, chlorine, and alkali-metals are examples of such compounds. In this chapter, we describe how these compounds are released and interact with each other in the combustion process. Note that in the present work, K represents the overall alkali-metal content of the flue gases. In a practical combustion system, sodium (Na) is also typically present, even though potassium is usually the main alkali specie. In addition, sodium has been reported to follow a reaction mechanism similar to that of potassium [11, 13, 36, 37].

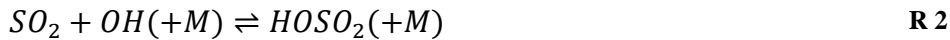
3.1 The release of inorganic species during combustion

Some of the main inorganic elements released during combustion and devolatilization are N, S, Cl, and K. Their relative rates of release and in which form they are released are, however, highly dependent upon the overall fuel composition and temperature. The inorganic species are released to the gas phase as a result of increased temperature. Chlorine is released early in the heating process, with up to 50 wt.% of the chlorine being released already at 500°C [38]. Chlorine is released mainly in the forms of HCl and KCl. A minor share of the chlorine might, however, be released as chlorinated hydrocarbons which often react soon after their release, with subsequent formation of HCl during combustion [38-40]. Potassium is mainly released as KCl, if Cl is present, otherwise it is released as atomic potassium (K) or as potassium hydroxide (KOH) [38-41]. The release of K has been shown to be strongly coupled to the release of chlorine [38]. Cl-species have a stronger tendency to react with char than K-species, which indirectly affects the release of K, since less Cl is available for KCl formation to occur [40]. The release rates of Cl and K are also affected by the ash composition. Silicates, especially aluminum silicate (during co-combustion of coal and biomass mainly derived from coal), are the main component responsible for inhibiting the release of alkali chlorides [29, 41-45]. In addition, the state in which the species is released depends on the combustion temperature, in relation to the melting and evaporation temperatures for each specific compound, and also the compositions of the fuel and the flue gas [38, 40, 41, 43-48].

Sulfur is released to the gas phase in the form of simple reduced species, such as CS₂, COS, and H₂S [39, 49, 50]. In the presence of oxygen, these compounds form oxides (mainly SO₂), which are more stable in a reducing environment [39, 49]. The formation of SO₃ is thermodynamically favored at temperatures <600°C, although the kinetics inhibit the SO₂/SO₃ equilibrium from being reached. The homogenous formation of SO₃ from SO₂ is the result of either:



at higher temperatures or the combination of the following reactions:



during the flue gas cooling process. The homogenous formation of SO₃ is well known compared to the possible heterogeneous reactions, which may involve fuel and ash particulates contributing to SO₃ formation [39, 49].

During devolatilization of a solid fuel, the nitrogen component may either be released as volatile species or be retained in the char. How much of the total fuel-bound nitrogen becomes volatile and in which form it is released depends not only on the fuel composition, but also on the temperature and residence time [51]. Glarborg et al. [52] collected data from several different studies found in the literature regarding mainly coals, although some peat and biomass data were also included. Despite the large variation between the different fuels, there was a clear trend towards less nitrogen being detected in the char as the temperature increased [52]. Biomass and lignite show, in general, higher retention of nitrogen at lower temperatures, as compared to coals of higher rank [53, 54]. The nitrogen is released from coal during the first stage of the pyrolysis process, mainly as aromatic compounds [55]. These compounds are however decomposed during the second stage of the pyrolysis process, releasing nitrogen in the form of HCN or NH₃. HCN is the main volatile nitrogen species released during the pyrolysis of high-rank coals. However, the share of NH₃ increases for coals of lower rank and for biomasses [52]. Finally, there is also the possibility for the nitrogen to be bound to the soot that is formed during the latter part of devolatilization. The amount of nitrogen detected in the soot varies with the fuel composition, and is most often insignificant, although it has been reported that up to 25% of the nitrogen released during pyrolysis is bound to soot [56, 57].

3.2 Formation of alkali-containing aerosols

The aerosols formed during biomass combustion vary in size distribution and concentration, as well as composition depending on the fuel composition and combustion conditions used. An example of experimental results from particle measurements at different facilities is given in Table 1. The results represent the combustion of different biomasses and variations of the combustion conditions in terms of different combustion technologies and thermal load conditions. The sampling temperature also varies, from for the lowest temperature of 100°C (in the work of Wierzbicka et al. [58]) up to 850°C (in the work of Valmari et al. [59]). However, K, S, Cl and C (excluding eventual oxygen) are the most commonly found elements found in particles from combustion, especially among the smaller particles of diameter up to 1 μm [58-63].

Table 1. Experimental results from the literature, showing the variations in composition, size, and concentration of aerosols formed during the combustion of biofuels.

Reference	Boiler type	Thermal effect [kW]	Fuel	Sampling temperature [°C]	Particle load [mg/Nm ³]	Main size (by mass) [µm]	Main components (by mass)
Wierzbicka et al. [58]	Grate	1000-1500	Sawdust pellets, forest residues	100–175	51-120	5	K, S, Cl
Valmari et al. [59]	CFB*	35000	Forest residues, willow	810–850	600-1200	~10	Ca, Si, P, K, S, Cl
Pagles et al. [63]	Grate	1000–6000	Forest residues	150–215	79-145	1–10	K, S, C
Johansson et al. [62]	Pellets burner	11–22	Wood pellets, wood briquettes	-	34-240	<1	K, S, Cl
Boman et al. [60]	Pellets burner	10–15	Pellets	-	-	~0.3	K, Cl, S, C
Christansen and Livbjerg [61]	-	15000	Straw	120	3-500	~0.3	K, Cl, S

*CFB = circulating fluidized bed.

When gaseous potassium chloride condenses in an inert atmosphere (*via* homogeneous nucleation) the condensed phase consists of both monomers and dimers. Such a system will always be in equilibrium [64]. Nucleation is a continuous process in which more and more aerosols form until the particle concentration is sufficient to on-set coagulation. According to Jensen et al. [65], the coagulation half-time for particle number concentrations is >10 s at a particle concentration of $3 \times 10^7 \text{cm}^{-3}$. The system examined by Jensen and co-workers had a residence time of <2 s, and for this reason the impact of coagulation was omitted in their model. These assumptions, together with mathematical expressions describing, for example, size distribution density functions, were used by Jensen *et al.* [65] to describe the homogenous nucleation of potassium chlorides in a plug flow reactor. They showed that when SO₂ was introduced to their experimental set-up the number of particles dramatically increased, which also followed from the model results. Potassium, which is homogeneously sulfated, has a vapor pressure that is several orders of magnitude lower than that of KCl, which means that the sulfates are supersaturated and form aerosols through homogenous nucleation [65].

Alkali-metals may form carbonates rather than sulfates in the flue gas. The carbonization has been suggested to follow a heterogeneous reaction pathway, due to the thermodynamic instability of K₂CO₃(g). Potassium carbonate is suggested to be formed *via* a reaction between KOH(s, l) and gaseous CO₂ [66]. Carbonates may only form at temperatures lower than the temperature at which homogenous sulfation can take place [36, 67, 68].

3.3 Alkali sulfation

The chlorinated form of potassium, KCl, is the main potassium compound released to the gas phase during biomass combustion. KCl may, however, be sulfated during combustion. This sulfation is considered complete when all that potassium has formed potassium sulfate (K₂SO₄). At temperatures <450°C, sulfated potassium may be found as pyrosulfate (K₂S₂O₇) [69]. Such low temperatures are, however, not relevant to the present work. The sulfation of potassium chloride follows one of two possible paths: 1) homogenous sulfation, where the sulfates are formed in the gas phase (and condense after their formation); or 2) heterogeneous sulfation, which includes surface reactions of non-gaseous chloride particles. Below follows a short summary of previous investigations of these two reaction pathways.

3.3.1 Heterogeneous alkali sulfation

The heterogeneous sulfation of KCl has been proposed by Steinberg and Schofield [70] as a surface reaction phenomenon that is manifested under post-flame conditions. In their work with hydrogen and propane flames, Steinberg and Schofield have concluded that sodium sulfate is too unstable under flame conditions to be responsible for the observed sulfation [70-72]. Experimental results presented by others have, in contrast, suggested that the heterogeneous pathway is too slow to describe the sulfation that typically occurs in industrial-scale boilers [67, 73].

Sengeløv et al. [68] have shown that the sulfation of condensed KCl increases with increases in temperature and oxygen concentration. The amount of water in the surrounding gas does not seem to influence the rate of sulfation. Sengeløv *et al.* [68] have suggested that only small KCl particles ($<1 \mu\text{m}$) can achieve a significant level of sulfation at residence times of $<1 \text{ s}$, even at high temperatures. However, KCl aerosols of this size are unlikely to be found at temperatures $>800^\circ\text{C}$, and at lower temperatures, the rate of sulfation of condensed KCl is $<20\%$ [68, 74]. These modeling results are in agreement with the experimental results in the literature [67, 73, 74]. This work focuses on the homogenous alkali-sulfating route, which is more relevant to the conditions studied here, as represented by flame temperatures up to about 1600°C . However, it should be noted that the findings presented are valid for residence times in the order of a number of seconds. Once deposited, the exposure time for sulfuric species will be order of magnitudes longer; for such conditions, the sulfation of condensed potassium chloride is no longer negligible [68].

3.3.2 Homogenous alkali sulfation

The alternative route to heterogeneous sulfation involves sulfation being governed by homogenous gas-phase reactions and K_2SO_4 being condensed soon after its formation. This is a theory that is in agreement with a series of experimental studies [61, 65, 67, 73, 75]. The sulfation of KCl can follow any one of the routes shown in **Error! Reference source not found.**, including reactions with both SO_2 and SO_3 . Regardless of the route, the final step is the condensation of gaseous K_2SO_4 , which is formed from either KHSO_4 or KSO_4 (R4-R7).

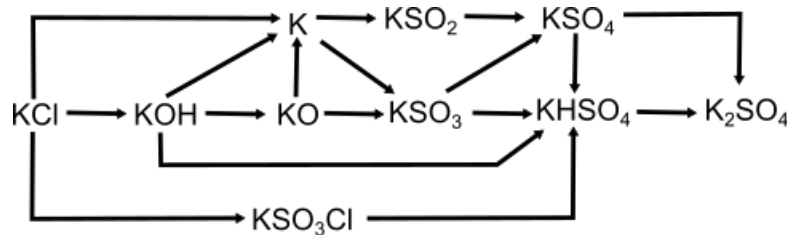
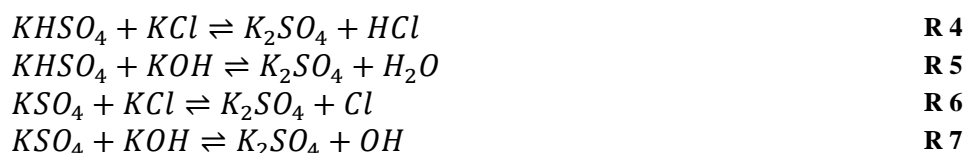


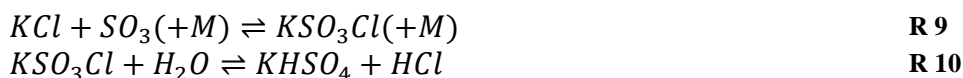
Figure 5. Illustration of the main reactions for the sulfation of KCl.



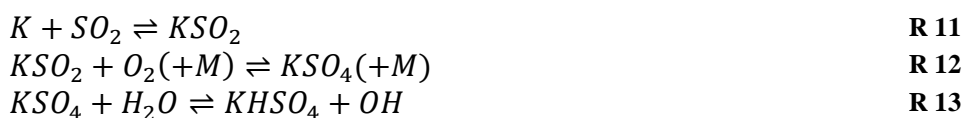
There are four main routes to the formation of $KHSO_4$, including either SO_2 or SO_3 . SO_3 may react directly with KOH :



or through a two-step reaction that starts with KCl :



$KHSO_4$ may then be formed *via* SO_2 in a three-step reaction that starts with K :



or starting with KSO_3 , which can be formed from either KO (involving SO_2) or K (involving SO_3):



KCl , KOH , KO , and K form the basis for the sulfating process. These compounds are linked together *via* several reactions, the most important of which are listed below. KOH may form from KCl *via* the following reaction with water:



KOH may react further to KO :



K is formed directly from KCl *via* one of the following reactions:



or indirectly *via* KOH or KO:



The present work focuses entirely on this suggested route involving homogenous alkali sulfation, as described by the reaction pathway schematic in **Error! Reference source not found.** Thus, this forms the basis for the modeling of the alkali sulfation chemistry covered in Papers III.

3.4 Effects of interactions between S, K and Cl species on CO oxidation

The oxidation of CO, R 26, may be influenced by alkali- and chlorine-containing species, as well by SO₂. The inhibitory effect has been experimentally observed for both hydrogen [76-79] and hydrocarbon-air flames [37, 80-87] (both in laboratory scale), and for HCl and SO₂ it has also been reported for pulverized coal combustion [88]. This phenomenon has also been examined under various conditions in flow reactors [89-92]. The interactions may either be direct or *via* the O/H radical pool, which is important for the chain branching that drives the combustion. There follows a theoretical discussion as to how these compounds may affect the oxidation of CO. The reactions discussed form the basis for the kinetic modeling carried out in Paper IV.



3.4.1 Sulfur-CO interactions

It is well known that SO₂ can influence the combustion chemistry, and depending on the local air-to-fuel ratio, the presence of SO₂ either inhibits or enhances the oxidation of CO [33]. Under fuel-lean conditions, a small fraction of the SO₂ can be oxidized to SO₃, the latter of which can be reduced back to SO₂ *via* a second reaction path that starts with $SO_2 + O(+M) \rightleftharpoons SO_3(+M)$ (R 1) followed by:



SO₂ has the most potent effect in a reducing environment, relative to an oxidizing environment [39]. Rasmussen et al. [33] have presented a more complex SO_x-cycle, which shows better agreement for both rich and lean conditions, including HOSO:



They also introduced a third loop that includes SO for better accuracy during flame combustion (higher temperatures):



Despite this more complex SO_x-cycle presented by Rasmussen et al. [33], there remain some sulfur-fuel interactions that are not captured by the mechanism [39].

3.4.2 Alkali-CO interactions

KCl has been reported in literature to influence CO oxidation but only for conditions relevant for fluidized bed (FB) combustion. Therefore, it remains unknown whether the reported effects presented here are applicable to suspension fired systems or not. This topic will be examined in this work. Alkali species in a combustion facility can be found both as solids and in the gas phase. However, the inhibitory effect of these species on CO oxidation has been shown for both physical states. The influences of alkali species are attributed to chemical interactions, whereas more chemically inert solids, such as silica powders, instead exert thermal influences [82, 87]. Although the details of the chemical mechanism underlying this phenomenon are still being discussed in the literature, it is often suggested to be based on reactions in the gas phase [39, 84, 86, 89, 93]. Based on gas-phase experiments conducted in previous studies [37, 78, 79, 84, 89, 94], a mechanism that includes R17 and R20-R22 has been suggested in which interactions *via* the O/H radical pool connect CO oxidation, R 24, with the potassium available in the gas phase. In order for these reactions to describe the observed inhibitory effect of alkali species on CO oxidation, the reaction rate for R 22 has to be higher than that confirmed previously. Hynes et al. [76] have proposed that an additional reaction involving KO₂ enables the reaction rate to be lower. although this reaction seems unlikely given the thermodynamic properties noted for alkali dioxides [89]. Potassium-containing compounds have been reported to inhibit CO oxidation in an oxygen-rich environment and to promote CO oxidation under certain conditions, e.g. in the presence of high NO_x concentrations [95, 96].

3.4.3 Chlorine-CO interactions

Chlorine-containing species are released already during pyrolysis, and are mainly found in the gas phase as chlorinated hydrocarbons or HCl and KCl [38, 39]. In the same way as for the alkali-metals, chlorine interacts with CO oxidation *via* the O/H radical pool in a cycle of reactions [39, 90]:



There is also a second cycle that includes CO directly [97]:



The relationship between these two cycles depends on whether the reaction between $Cl + HO_2$ follows R 37 or R 38. This is especially important, as the first route will inhibit CO oxidation, while the second will promote CO oxidation. The inhibitory effect of the first cycle may be reduced or changed to change the conditions in areas with higher Cl concentrations (e.g., the post-flame zone), thereby forcing R 34 and R 35 to reach equilibrium or even to reverse the reaction direction [39].

3.5 NO formation

There are two possible sources of nitrogen in a combustion process: N_2 from the air, and fuel-bound nitrogen, and NO may be formed from both of these sources. A general reaction scheme for NO formation from the two possible sources is shown in Figure 6. As discussed in Section 3.1, the fuel-bound nitrogen can be divided into volatile nitrogen (volatile-N) and char-bound nitrogen (char-N), reflecting the different ways in which nitrogen is bound to and released from the fuel. As indicated in Figure 6, both types of fuel-bound nitrogen can form N_2 or NO. These routes are, however, not considered in this work. Instead, the focus is on the chemistry related to the formation of NO from molecular nitrogen derived from the air (i.e., the routes within the gray-shaded area in Figure 6).

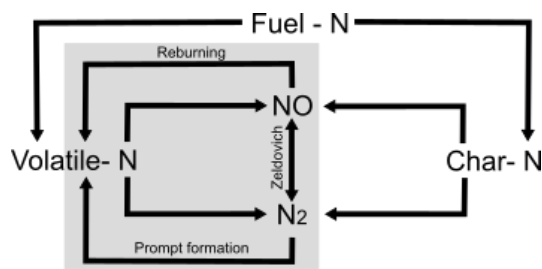


Figure 6. Reaction scheme for the general routes for NO formation. The area shaded gray indicates the aspects of nitrogen chemistry covered in this work.

Homogenous NO formation from molecular nitrogen is presented in greater detail in Figure 7. The corresponding reactions are presented here and in Paper V as the most important reactions describing homogenous NO formation from N_2 . All the presented reactions are potentially reversible, working in both directions depending on the conditions. The arrows in Figure 7 indicate the direction of the forward reaction.

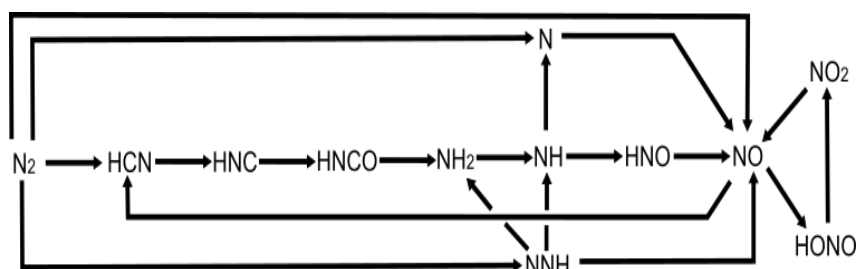


Figure 7. Schematic of the main reaction pathways towards NO formation, as described in Paper V.

According to the extended Zeldóvich mechanism [98-100], NO can be formed from N₂. As this occurs at high temperatures, it is referred to as ‘thermal’ NO formation. Molecular nitrogen is split into atomic nitrogen through the following reaction with atomic oxygen:



The atomic nitrogen can thereafter react with either OH or O₂ to form NO:



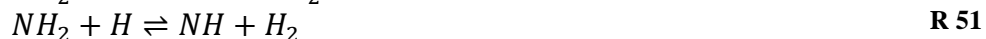
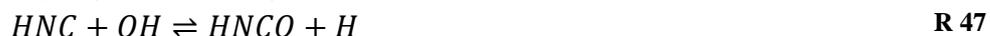
Once formed, NO can react with hydrocarbon radicals to form HCN:



Moreover, HCN can be formed from N₂, e.g., through reaction with CH, leading to the rapid formation of NO:



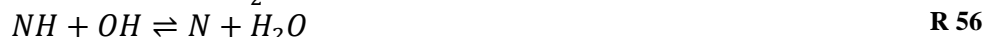
Kinetically-controlled NO formation is, in high-temperature systems, less important than thermal NO formation [101]. Following a long series of reactions, NO can be reformed from HCN. HCN may also cause NO to generate NH, with HNC and HNCO, as well as NH₂ as intermediates that react with H or OH:



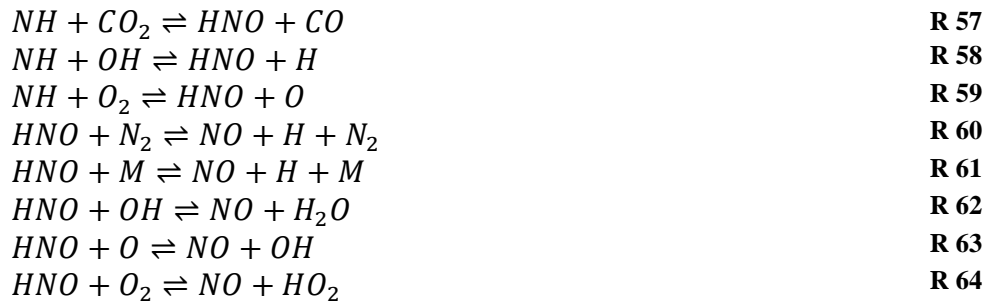
There are, however, also possibilities for HCN to form N₂ in a process that is termed ‘reburning’ [102]. A second route from molecular nitrogen towards NH is that *via* NNH, together with either O or OH. In both cases, NO is also formed:



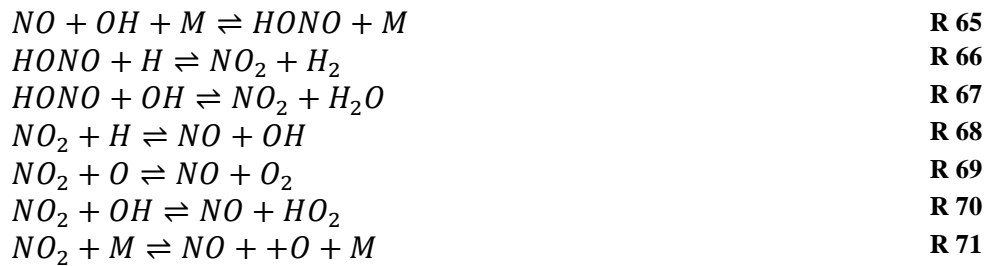
There are two possible ways to form NO from NH. First, atomic nitrogen can be formed *via* reaction with H or OH:



Once N is formed, NO can be formed via R 41 and R 42. The second possibility is to form NO with HNO as an intermediate:



Finally, there exists a pathway in which NO reacts with OH to form HONO, which may react back to NO *via* NO₂:



3.5.1 The influences of S and K on NO formation

Glarborg [39] simulated the influence of sulfur on NO formation during the combustion of methane in air and compared the results with the experimental results for hydrocarbon combustion in air found in the literature [103-105]. Both the experiments and the model indicated a decrease in the exit concentration of NO when sulfuric species were added. This was found for both fuel-lean and fuel-rich flames and was attributed by the model to radical recombination being catalyzed by the sulfur. This is achieved under reducing conditions following reactions R 28, R 29 and R 31, whereby the reduction in level of radicals inhibits the formation of N₂ from HCN and NH₃ [39]. Wendt et al. [103] also showed in their experiments that the addition of SO₂ increased the decay of NO in the post-flame zone. This was suggested by Glarborg [39] to be due to direct interactions between N and S, where the direction of the reactions varies depending on whether the conditions are reducing or oxidizing.



Regarding alkali-nitrogen interactions, sodium has been reported to increase the transformation of char-N to volatile-N, thereby altering the overall formation of NO [106]. Alkali-metals also influence the formation of NO, albeit only indirectly through an effect on CO oxidation [107, 108]. All these previous studies have focused on solid fuels and the relatively low combustion temperatures relevant to FB combustion. In contrast, the present work focuses on the formation of NO from molecular nitrogen during combustion in suspension, which entails much higher temperatures than fluidized bed combustion.

4 Experimental setup

The experimental series investigates the chemistry in a technical-scale combustor (100 kW_{th}) and includes the development of an experimental setup that includes systems for analyzing the gas and particle compositions. The experiments are performed and evaluated in ways that reflect the specific research question being posed. The experimental results are also used as inputs to the simulations. The 100-kW combustion unit used, as well as the different measurement techniques, are described in detail in the following sections. The results obtained from the experiments described here are parts of Papers II, IV, and V. In addition, some of the experimental results are used as a reference in Paper III. As these latter results are taken from the literature [109, 110], they are not presented here.

4.1 Combustion experiments

In this work, experiments were performed in the Chalmers 100-kW test unit, as presented in Figure 8. This unit can be operated in either air-fuel or oxy-fuel mode. The furnace is 800 mm in diameter and has a height of 2400 mm, with a propane burner mounted at the top of the furnace. There are four water-cooled rods for temperature control inside the furnace. The furnace has measurement ports at seven distances from the burner (M1–M7) and there are eight measuring ports (M8–M15) located further downstream in the flue gas path. The burner is fed with 1.73 g/s of propane and the oxidizer, corresponding to a stoichiometric ratio of 1.15. The experimental unit facilitates SO₂ injection directly into the oxidizer before entering the primary and secondary registers. As part of this work, an injection system for KCl has been developed to investigate the alkali chemistry during combustion experiments. The KCl is fed as an aqueous solution *via* a probe enters through the furnace ceiling (see Figure 8). At the tip of the probe, a nozzle sprays the solution directly into the flame, 40 mm downstream of the burner at a spray angle of 15°. The KCl-water solution is kept at a salt concentration of about 3.4 %_{wt}. The solution is stored in a separate tank with an internal circulation pump, to avoid salt precipitation. A metering pump is used to inject 0.9 l/h of the KCl(aq) solution into the flame. The KCl(aq) injection system is shown in Figure 9. The concentration is controlled over time by a hand held digital refractometer (ATAGO, PAL-49S) to ensure constant conditions.

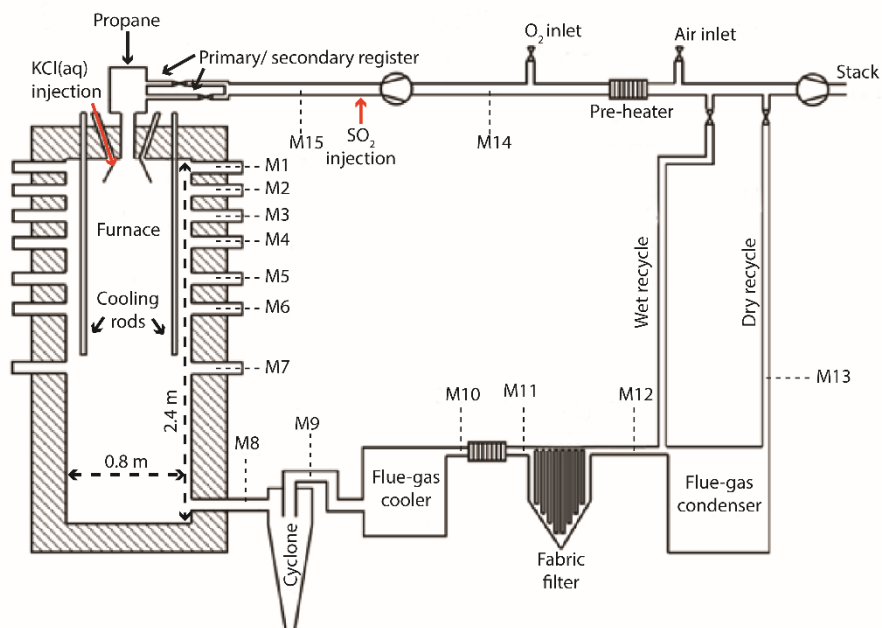


Figure 8. Schematic of the 100-kW test unit at Chalmers University of Technology. The red arrows indicate the positions for the injection of KCl and SO₂. The locations of the 15 measuring ports are indicated as M1–M15.

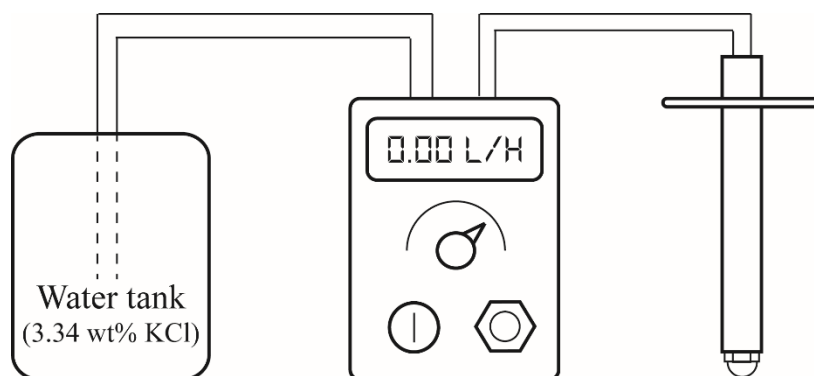


Figure 9. Schematic of the salt injection setup, including the storage tank, metering pump, and injection probe.

The injection flow rate of KCl(aq) was kept constant in all the experiments. In contrast, the concentration of KCl was varied for the CO experiments presented in Papers IV and V, respectively. In these studies, the injection of pure water (0.0 %wt KCl) was also done, to establish a reference effect caused by the water itself. In the CO experiments (Paper IV), the KCl content was also doubled in one case (6.68 %wt KCl). In those cases in which the S/K-ratio was altered (Paper II), this was achieved by adjusting the amount of SO₂ injected. The amount of SO₂ injected was set by a mass flow controller, as well as by adjusting the concentration in the oxidizer. The reason for this is that during operation with flue gas recycling, SO₂ is recycled to the burner inlet. Inevitably, some sulfur is lost in the flue gas system due to absorption by the condensing water and reactions with deposits in the filters. The SO₂ concentration was found to decrease by 11% between measuring ports M8 and M13. The concentration of sulfur in each oxy-fuel case was based on a decrease in SO₂ concentration of around 14% in the recirculation loop. This loss of sulfur in the loop varied with time, although the SO₂ concentration in the oxy-fuel oxidizer was kept constant for each case by adjusting the set-point in the mass flow controller.

Table 2 presents a summary of the conditions for which the degree of sulfation, as well as the NO and CO interactions were investigated. The standard sulfur injections used in Papers IV and V are based on an S/K-ratio of 4 (106 g of SO₂ per hour). Further details regarding each specific measurement can be found in the corresponding paper.

Table 2. *Running conditions for the experimental cases of Air and OF25.*

	Fuel feed [g/s]	O ₂ /fuel ratio [-]	O ₂ oxidizer [% wet]	O ₂ stack [% wet]
Air	1.73	1.15	21	2.55
OF25	1.73	1.15	25	3.00
S/K-ratio (injected)	KCl(aq) [l/h]	SO ₂ injection* [g/h]	SO ₂ oxidant [% wet]	
			Air	OF25
1	0.9	26.5	107	485
2	0.9	53.0	215	1126
4	0.9	106.0	429	2345
6	0.9	159.0	644	3559
8	0.9	212.0	1504	-
-	0.9 (0.00% wt KCl)	-	-	-
-	0.9 (6.68 %wt KCl)	-	-	-

*Varied to keep the inlet concentration constant for the OF25 case.

Measuring ports M2–M5, M7, and M8 were used for both compositional and temperature measurements inside the furnace. The oxidizer composition was measured at M15. The aerosol measurements were performed only in the center position of M3. More details regarding the specific measurement setups can be found in the following section.

4.2 Measurement techniques

Several measurement techniques were used in this work to characterize the alkali sulfation behavior, as well as to investigate the interactions between K, Cl, and S and examine how these interactions influence the overall combustion chemistry. Most of the measurements were gas composition measurements, although some aerosol measurements were also performed. All the measurement technologies, for both the gas composition and aerosol measurements, were extractive, except for the IACMTM system, which involves online analyses. The gas temperature was measured as a complement to the other measurements.

4.2.1 Gas composition

All the gas composition measurements performed were extractive, except for the IACMTM system (an online measurement). The same sampling system was used, even though different analyzers were used for the different components. The sampling was performed using a water-cooled probe with an outer diameter of 45 mm. The probe consisted of three coaxial tubes, whereby the inner tube had an inner diameter of 8 mm through which the gas was sampled (see Figure 10). The inner tube was electrically heated to maintain a constant temperature of 140°C, avoiding condensation. There was also the possibility to mount a ceramic filter at the front of the probe, to prevent particles from entering the probe together with the sampling gas. The back end of the probe was connected to a heated pump using a heated hose (both set at 180°C). After the pump, the sampled gas was led through a heated (180°C) hose either directly to the gas analyzer (if the analyzer was measuring on a wet gas basis) or *via* a condenser operating at 4°C (if the gases are to be analyzed on a dry gas basis).

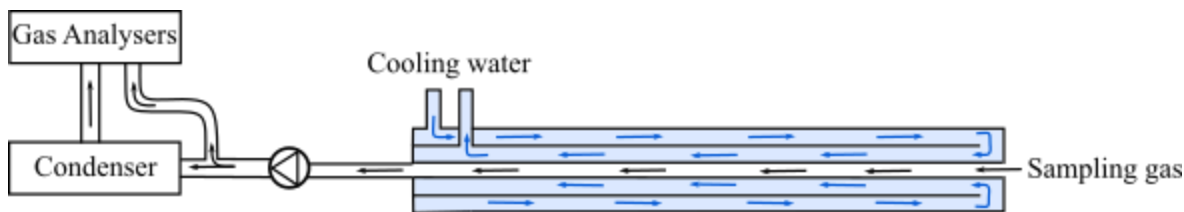


Figure 10. Schematic of the system used for measuring gas concentrations.

Four different analytical systems were used, which together covered a wide range of concentrations and different measuring principles. The NGA 2000 analyzer was used for measuring the levels of CO, CO₂, O₂ and SO₂. This instrument uses the paramagnetic principle (O₂), non-dispersive ultraviolet sensors (SO₂), and non-dispersive infrared sensors (CO and CO₂). The BINOS 100 analyzer was used to measure the levels of CO₂ and O₂ using IR and electrochemical sensors. Both the NGA 2000 and BINOS 100 instruments are from Emerson (St. Louis, Missouri, USA). Two different Fourier transform infrared spectroscopy (FTIR) systems were used: MB9100 (Bomem Inc., Quebec City, Quebec, Canada) and MultiGas 2030 (MKS Instrument Inc., Andover, Massachusetts, USA). These systems generally measure warm (190°C) and wet gases and can be used to detect a wide range of different compounds. In this work, they were, however, used to measure the levels of HCl (MB9100) and nitric oxides (MultiGas 2030).

4.2.1.1 Controlled condensation

Controlled condensation, which is a technique for measuring SO₃ (as H₂SO₄) in flue gases, has similar or superior accuracy compared to the “salt method” and isopropanol absorption under both air-fuel and oxy-fuel conditions [111, 112]. Therefore, this method was chosen for the present work. For this method, the flue gas sample is cooled in a water-bath to a temperature of between 80°C and 90°C (see Figure 11). For the concentrations found in flue gases, this temperature interval is located between the dew-point of sulfuric acid (H₂SO₄) and that of water vapor. In the presence of water vapor, SO₃ will form sulfuric acid, which will condense in the cooling tube, while the water vapor follows the main gas stream. The condensed acid is collected over a defined time period (a lower concentration requires a longer measurement time) and with a defined volume flow. The collected acid is quantified by titration, to determine the amount of sulfuric acid, from which the concentration of SO₃ in the flue gases is calculated. To avoid sampling losses, it is important to keep the flue gas temperature above the dew-point of sulfuric acid before the temperature-controlled condenser. In this work, a sampling probe operating at 200°C was used. The probe consisted of three coaxial tubes, similar to the one shown in Figure 10 with two exceptions: 1) the temperature was controlled using a thermal oil system; and 2) the center tube was composed of quartz glass.

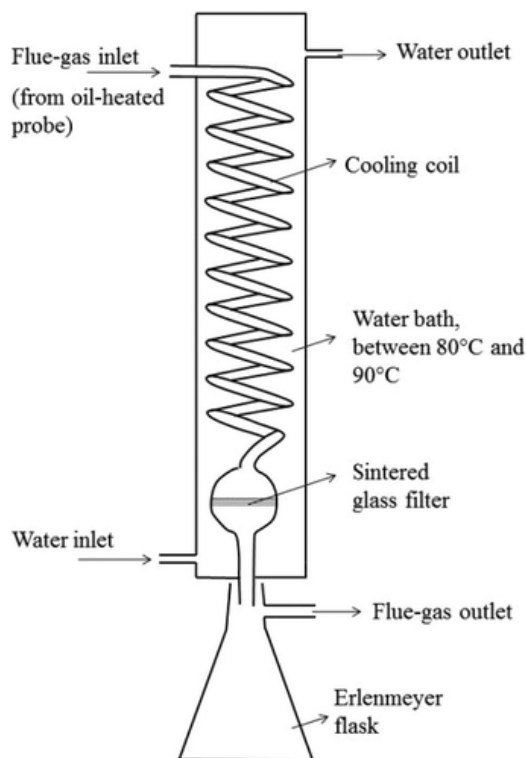


Figure 11. Schematic of the cooler system used for SO_3 measurements in this work.

4.2.1.2 IACMTM

The IACMTM (*in situ* alkali monitor) is an optical system for online measurements of alkali (potassium and sodium) chlorides developed by Vattenfall Research and Development AB. The IACMTM is patented in several European countries by Vattenfall AB (EP 1221036). According to the Lambert-Beers law, there is, for a fixed wavelength, a linear relationship between the absorption and concentration of an absorbing species. This relationship is used in the IACMTM system, in which the absorption spectra is analyzed using differential optical absorption spectroscopy (DOAS), which compares the minimum and maximum absorption values rather than the absolute absorption [113-115]. The IACMTM cannot distinguish between NaCl and KCl, however, since potassium is the only alkali metal used in the experiments presented here, the measured concentration will be referred to as the concentration of KCl. A UV-light source is used and the absorption at wavelengths between 225 nm and 310 nm is analyzed, giving a concentration of KCl. KCl must be in the gas phase to be able to absorb light at these wavelengths, which is why the condensation temperature of KCl restricts the temperature range within which IACMTM can be used. The system is calibrated for temperatures down to 650°C. Depending on the level of KCl in the flue gases, there is a risk that the detected concentration will be limited by the saturation of KCl in the gas phase [116].

In this work, the IACMTM system was used to measure the KCl concentration at M7 (Figure 8). A schematic of the setup is presented in Figure 12. High-intensity (150-W) UV-light is radiated from a L1314 Hamamatsu light source (1). The radiated light passes through two apertures (2) with a 90° off-axis parabolic mirror (3) in between. The light is collimated as it leaves the mirror, which has a UV-enhanced aluminum coating and a reflective focal length of 6 inches. Two ball valves (4) are mounted opposite each other at M7. Both ball valves have an internal quartz window that lets the light through without having flue gases leaking out from the furnace.

They also have one purge gas connector each. A small purge flow of N₂ or Ar was used to assure that the system only detected KCl over the 80-cm diameter of the furnace. N₂ and Ar were used during air-fuel and oxy-fuel firing, respectively. The light that exits the second ball valve is collected using a UV-enhanced parabolic collimator (5). The collimator is connected to the spectrometer (AVABENCH-75-2048) *via* an optical fiber. The signal from the spectrometer is then analyzed using a standard computer.

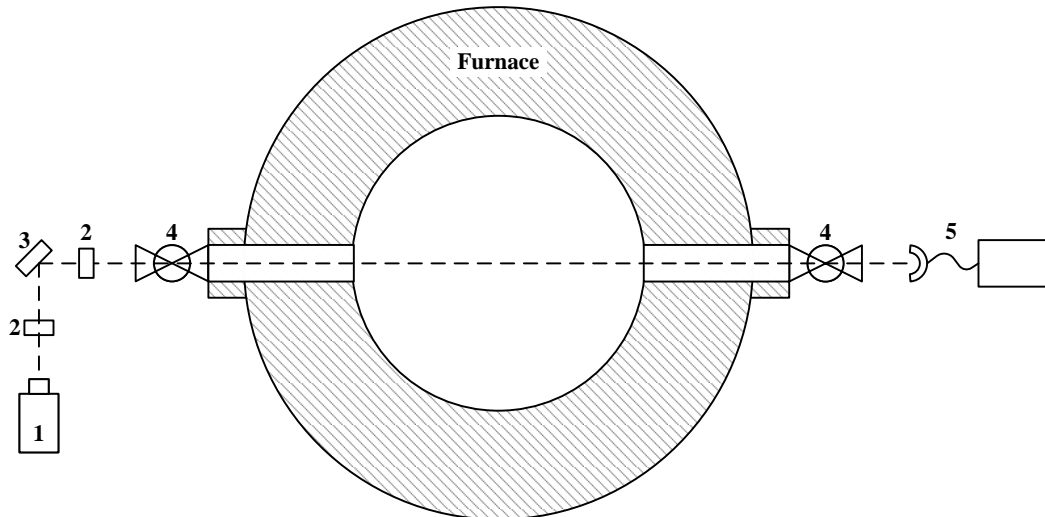


Figure 12. Schematic of the IACM™ setup used in this work to measure the concentration of KCl over the cross-section at M7. 1, UV-light source; 2, aperture; 3, parabolic mirror; 4, ball valve with window inside; 5, collimator connected to a spectrometer via an optical fiber.

4.2.2 Particle measurements

Most combustion processes form particulates, such as soot and inorganic aerosols. Measurements of such particulates at flue gas temperatures <500°C have been performed and presented in the literature for several different fuels and combustion technologies. In such measurements, different types of suction probes have been used [58-60, 62, 63, 117, 118]. These suction probes have in common a temperature-controlled tube with an inner tube through which the flue gases may be isokinetically sampled from the furnace. The probe is cooled using a cooling medium, and the sample gas is also cooled using a dilution gas injected into the probe tip. The extracted particles are then quantified and analyzed using suitable measurement techniques.

4.2.2.1 *Extraction of particles*

Extracting particles at high temperatures (>600°C) is difficult, especially during biomass combustion in which the concentrations of inorganic species (which typically condense at such temperatures) are relatively high. Condensation may affect the result by changing both the composition and the size of the particles during the extraction. Valmari et al. [119] avoided condensation by inserting the equipment into the flue gas path (convection path, about 650°C). Strand et al. [120] and Lind et al. [121] have performed high-temperature (750°C and 830°C, respectively) particle extractions using a suction probe that was designed to meet the criteria for cooling rate, dilution, and residence time, in order to avoid problems with agglomeration and/or the condensation of gaseous compounds. Wiinikka et al. [122] have presented results from particle extractions from a 8-kW wood pellet combustor for even higher temperatures, up to 1450°C, which corresponds to the in-flame temperature condition. Similar experimental setups have been used more recently, e.g., by Fernandes et al, [123], even though they measured at a lower temperature of around 900°C.

The extracted sample should be adjusted to a high dilution ratio (1:100), so that the vapor condensates on the probe walls instead of on the already existing particles, thereby minimizing the risk of an altered particle size distribution [120]. It is also important to have a cooling rate of >600°C/s so as favor homogenous nucleation over heterogeneous nucleation. This will produce many nano-sized particles, but keeps the sampled particles less affected [124, 125]. Coagulation of particles can take place spontaneously due to relative motion and is strongly dependent upon the particle concentration and residence time. A residence time of 0.2 s is sufficient for a particle concentration of 10^{18} to decrease by as much as a factor 1000. This will increase the mean particle diameter correspondingly [126]. A high dilution rate and a short residence time between the probe tip and the measurement equipment are therefore preferable.

4.2.2.2 *Our setup*

In this work, the particle measurements were performed by sampling at the center position of M3 using a suction probe. The probe, which was maintained at a temperature of 120°C using a thermal oil system, was connected to a vacuum pump that was used to extract the sample volume from the furnace. The sample was taken *via* the opening at the tip of the probe (indicated with a green arrow in Figure 13). Soon after the sample flow entered the probe, it was diluted with nitrogen (indicated with blue arrows in Figure 13), and the diluted sample exited the probe at the back end. The gas temperature at the probe inlet was <250°C, which enabled a sufficient cooling rate. The dilution rate of approximately five in the probe resulted in a residence time in the probe of about 0.5 s, which was too short for any significant wall condensation to occur.

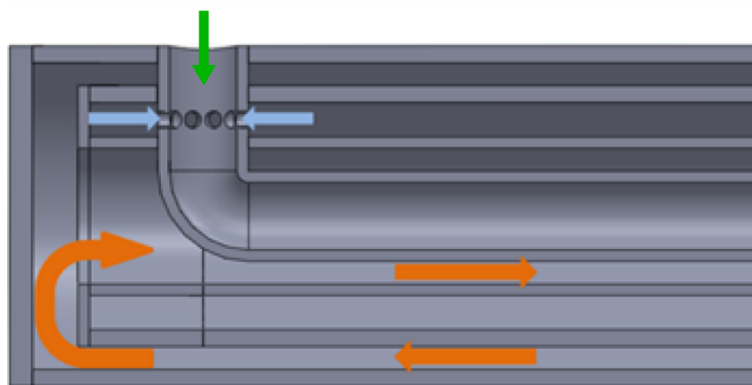


Figure 13. Cross-sectional drawing showing the tip of the particle-sampling probe used in this work. The green arrow indicates the hole through which the sample is taken. The blue arrows represent the dilution gas, and the orange arrows represent the flow of thermal oil.

The sample flow extracted using the suction probe was split after the probe, as indicated in Figure 14. The main part of the sample stream passed through the DLPI as well as the vacuum pump used to create the low pressure level needed for the DLPI. The system can be run also without the DLPI, in which case the pump is only used to create a suction flow through the probe. A slipstream can be used for analysis in a SMPS and VT-DMA. This slipstream was further diluted in two steps. After each dilution step, the main part of the flow was ejected so as to reduce the total flow downstream in the system. The flow going in to the SMPS and VT-DMA had a dilution rate of around 375 (including the dilution factor in the probe).

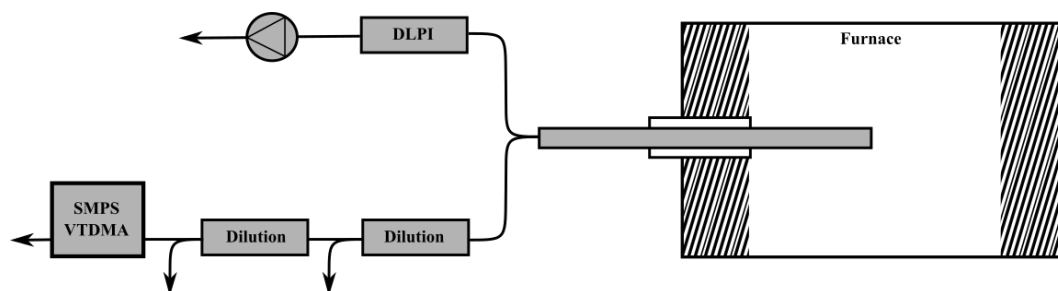


Figure 14. Schematic of the particle aerosol sampling and analysis system used in this work.

4.2.2.3 DLPI

The mass size classification of particles is usually accomplished using a low-pressure impactor (LPI), which separates particles in the range of 30 nm to 10 μm . A cascade impactor has a lower limit at 300 nm (see Figure 15 for a depiction of the impactor principle). Cyclones are used for collecting larger particles and for preventing large particles from filling the top stage of the LPI [58-60, 62, 63, 117, 118, 124, 125, 127]. Currently, the most commonly used LPI is the Dekati low-pressure impactor (DLPI). The DLPI has a slightly different design and has two additional stages (13 in total), giving better performance than the older-generation Berner low-pressure impactor (BLPI) [127].

The performance of a LPI is related to the temperature and pressure conditions. For a BLPI, an increase in temperature from 20°C to 160°C changes the cut diameter (also referred to as d_{50} , defined as the particle size collected with 50% efficiency) by 5%–50%; the largest deviation is found for the smallest particles [119]. It is therefore important to consider the LPI calibration conditions. Performance parameters for temperatures other than the calibration temperature may be estimated using correlations [119, 128]. In this work, the DLPI was heated to 100°C, which is higher than the calibrated temperature, in order to avoid condensation of the flue gas species within the DLPI.

In each of the LPI stages, there is a collector. The collectors usually consist of a piece of aluminum foil coated with vacuum grease (to prevent the particles from moving on the foil). If the LPI is operated at high temperatures, other materials are used for the collectors. The collectors should be heated both before and after operation, to dry the samples and minimize the possibility of a weighing error due to humidity [60, 63, 119, 121].

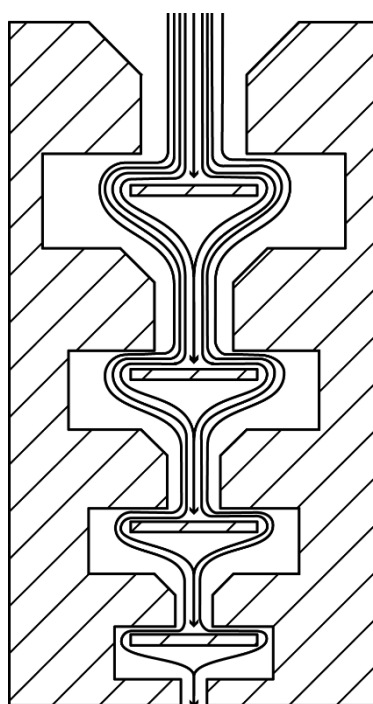


Figure 15. *Simplified drawing of an impactor used for measurements of gravimetric particle size distribution. The sample stream enters at the top into the first collection plate. The largest particles hit the plate, whereas the smaller particles tend to follow the gas stream to the next stage. Each stage is smaller than the previous one, which increases the flow speed and forces smaller particles to contact a collection plate.*

4.2.2.4 SMPS and VTDMA

The scanning mobility particle sizer (SMPS) is widely used for atmospheric particle measurements, as well as for measurements of particles in combustion processes [58, 63, 118, 120, 129]. The SMPS consists of two parts: a differential mobility analyzer (DMA), and a condensation particle counter (CPC) (Figure 16). The DMA technology, which has been used for a long time to characterize aerosols in gas flows [130], uses two coaxial cylinder electrodes to create an electrical field perpendicular to the sample stream. The electrodes are usually two coaxial cylinders, to avoid the end effects associated the use of plates [131]. The relationship between the electrical field and the particle velocity and diameter makes it possible to control

the size of the particles exiting the instrument. The particles are charged before entering the electrical field. In the SMPS system used in this work, the particles are charged *via* the bipolar diffusion created by a radioactive source (^{85}Kr). As shown in Figure 16 (left-hand side), the charged particles enter a laminar flow of inert gas, typically N_2 . Due to the laminar flow conditions applied, the horizontal motion of the particles is in principle only influenced by the electrical force between the particles and the charged cylinder in the middle of the chamber. The horizontal velocity will be higher for smaller particles (dark-blue dots in the figure) and therefore they will reach the center before they reach the openings in the center cylinder. The opposite will be the case for particles that are too large (red dots in the figure), as they will not reach the center or will do so first below the openings. By controlling the vertical velocity and the electrical field (the horizontal velocity), it is possible to choose the diameter of the particles leaving the DMA (green dots in the figure). Even though systems have been developed for the detection of particles with diameters down to 1 nm, the DMA system is the most commonly used for the detection of particles with diameters between 10 nm and 1000 nm. For particles with diameters of <10 nm, the risk for particle losses due to Brownian diffusion is increased, which would cause problems already upstream of the DMA [131-133].

The monodisperse particle flow exiting the DMA is introduced into the CPC, which counts the particles passing the detector (right-hand side of Figure 16). In this way, the SMPS determines the number of particles for a certain size of particulate. In the CPC, the particles are coated with a liquid (in this work, iso-butanol), which increases the particle diameter, before entering the detection chamber. The detection chamber consists of a light source and an optical detector for counting the particles.

A volatility tandem DMA (VTDAM) is created by adding a second DMA, together with an oven, prior to the SMPS. The VTDMA is used to quantify the volatility of the particles [132]. A monodisperse particle flow created by the first DMA is heated in the oven before entering the SMPS. It is then possible to estimate the degree of devolatilization by measuring the change in particle size distribution.

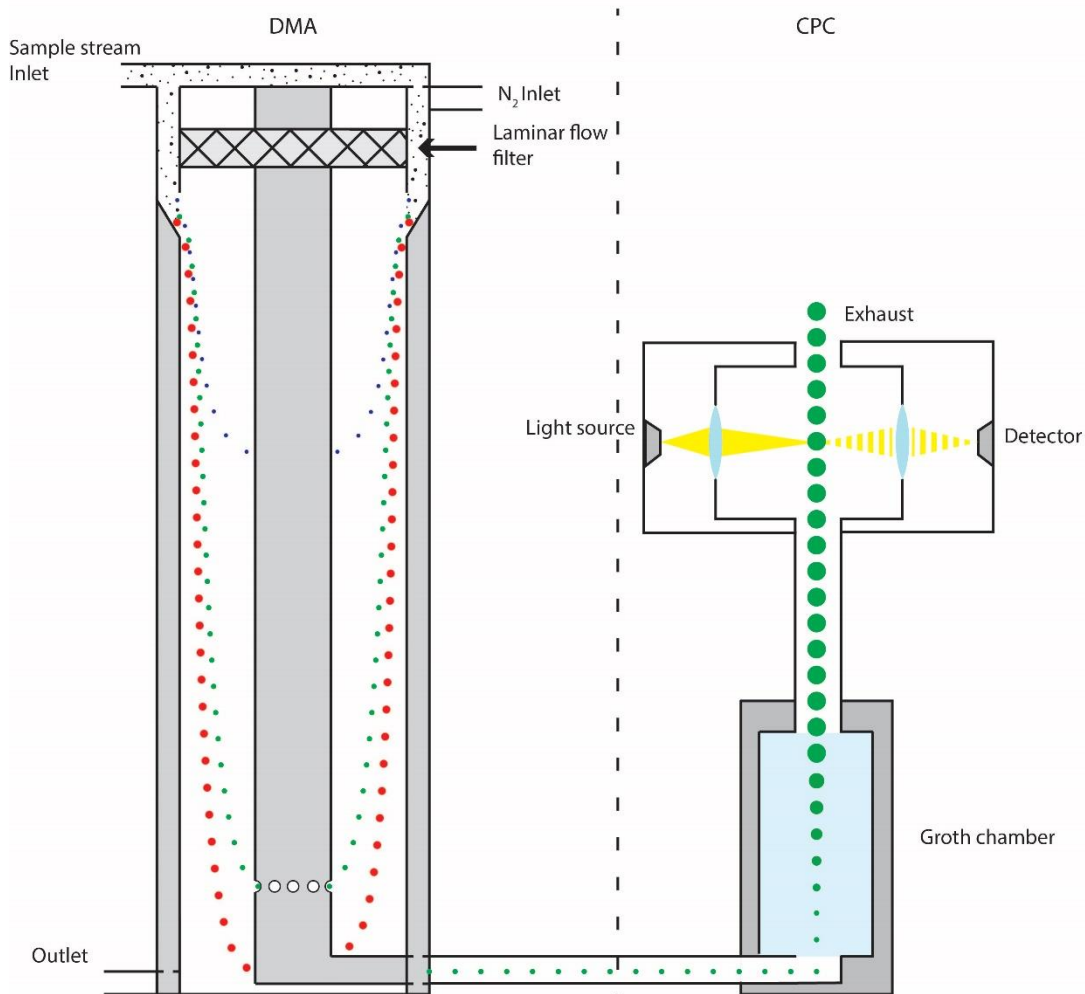


Figure 16. Schematic of a SMPS that consists of two parts: a DMA (left) and a CPC (right), connected in series.

4.2.3 Temperature measurements

The temperature of the gas inside the furnace was measured using a suction pyrometer. The suction pyrometer is a water-cooled suction probe equipped with a thermocouple (type B). The measuring point of the thermocouple is about 13 cm in front of the water-cooled probe. The thermocouple is shielded by two ceramic coaxial tubes, such that the outer tube has an inlet hole through which the sample gas enters (see Figure 17). The reason for having the ceramics protecting the thermocouple is to prevent it being influenced by radiation, which could otherwise influence the measurement. The flow of sample gas is created by connecting the probe to a pump and maintaining an appropriate gas velocity over the thermocouple. There is a trade-off between having an increased measuring error due to a low velocity and losing the accuracy of spatial precision, since the gas from a larger volume will enter the probe.

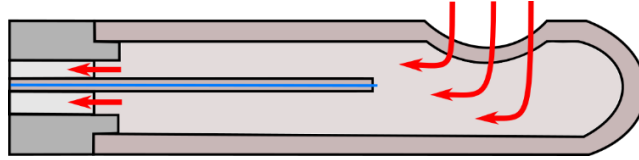


Figure 17. The thermocouple (blue line) is shielded by a ceramic tube with only the thermocouple junction being exposed to the flue gas flow. This point is about 13 cm in front of the water-cooled probe and is protected by a second ceramic tube with a hole through which the hot gases (red arrows) enter.

4.3 Evaluation of sulfation measurement methods

The development of an experimental setup suitable for investigating the alkali- and sulfur-related chemistries was also part of this work. This includes the injection system for aqueous solutions with KCl (see Section 4.1) and the evaluation of different methods for measuring the degree of sulfation under conditions relevant to this work. The degree of sulfation is defined as the ratio between the amount of potassium bound as sulfates and the total amount of potassium (Equation 1). Two methods based on gas composition measurements using FTIR (HCl) and the IACM™ (KCl) were tested, together with aerosol measurements using DLPI and SMPS in combination with a VT-DMA, giving a total of four different techniques. A short evaluation of each method is presented in this section.

$$\frac{2n_{K_2SO_4}}{n_{K_{tot}}} = \text{degree of sulfation} \quad \text{Equation 1}$$

4.3.1 HCl measurements (FTIR)

Using an FTIR system to determine the degree of sulfation by measuring the HCl concentration is an indirect method, since it does not involve any potassium-containing species. However, in the system used in the present work, the injected KCl was the only source of Cl, which meant that any chlorine found in the form of HCl had to have originated from the injected KCl. The potassium releases the chlorine not only when the final K_2SO_4 is formed, but also when K, KO or KOH is formed. The HCl measurements were performed at M8, where the temperature was $<600^\circ\text{C}$, which is why it is assumed that KCl and K_2SO_4 are the only potassium-containing species detected. This assumption is also supported by simulations. When using this method, the degree of sulfation is estimated using Equation 2:

$$\frac{n_{HCl}}{n_{K_{tot}}} \approx \text{degree of sulfation} \quad \text{Equation 2}$$

Figure 18 presents a continuous measurement of HCl for the OF25 case, in which the SO_2 concentration exceeded 2000 ppm. After 200 s, the injection of KCl was started and a clear increase in HCl concentration was observed. The opposite was observed at 600 s when the injection of KCl was terminated. The HCl concentration obtained when the KCl injection had stopped was slightly higher than that before the injection was started. When HCl was measured in a system that was completely free of HCl the instrument indicated a level of 0–3 ppm. Achieving this level again, after KCl had been injected, required several hours of operation and a slight increase in the “background” signal was therefore accepted. However, it should be noted that after a full day of experiments, the background level was never above 15 ppm. It is also noteworthy that the time required to reach a concentration of HCl lower than 3 ppm was drastically shortened when the SO_2 injection was stopped. When the injection was restarted, the

HCl level increased, which suggests that over time some KCl forms deposits that are slowly sulfated, resulting in a detectable amount of HCl. In the experimental work, only those measurements that showed a significant increase in HCl concentration, as a result of KCl injection, were considered to be accurate.

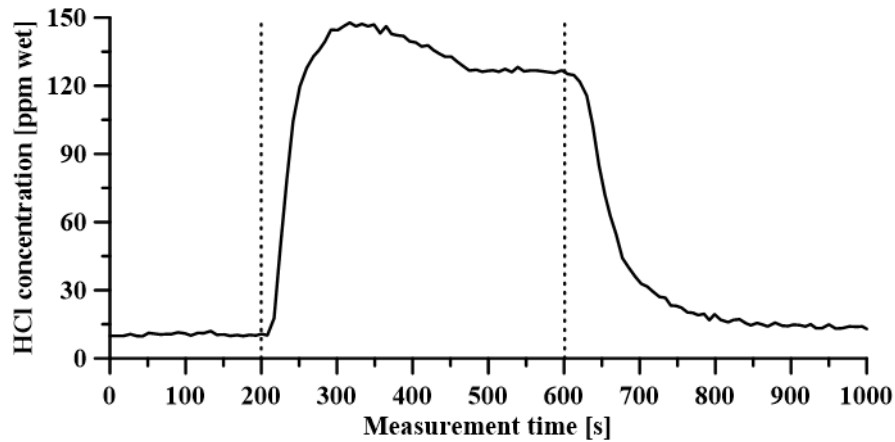


Figure 18. Continuous measurement of the HCl concentration using an FTIR during oxy-fuel operation with >2000 ppm of SO₂ in the flue gas. The injection KCl was started at 200 s and turned off again at 600 s.

The clear response profile of the HCl concentration obtained as a result of KCl injection indicates that the system works. As mentioned above, the method has value only under certain conditions, such as KCl being the only source of Cl and KCl and K₂SO₄ being the only potassium-containing species present. Based on this, the method is considered suitable for determination of the degree of sulfation at the flue gas exit (M8) for a combustion system such as that used in this work. It is, however, not suitable for flame measurements or for measurements that include solid fuels.

4.3.2 KCl measurements (IACM™)

The IACM™ system was used to determine the degree of sulfation by measuring the KCl concentration. Assuming that the only forms that potassium can take in the measuring location are KCl and K₂SO₄, it is possible to calculate the degree of sulfation based on the reduction in KCl concentration (Equation 3).

$$\frac{n_{KCl}^{inlet} - n_{KCl}}{n_{K_{tot}}} \approx \text{degree of sulfation} \quad \text{Equation 3}$$

Since the IACM™ measures the absorption of light, it is important to have a well-defined volume across which one can measure, in this case the diameter of the combustion unit (80 cm). A purge gas was used to prevent the flue gas from diffusing into the measuring ports. The temperature at the measuring position is also important, since it affects the density of the gas. The temperature was therefore measured along the diameter of M7, for both the air-fuel and oxy-fuel (OF25) combustion. This information was then implemented in the analysis software used to calculate the KCl concentration. One of the obtained KCl profiles is shown in Figure 19. The measurement was performed during air-fuel combustion and at time zero, neither KCl nor SO₂ was injected. The KCl injection was initiated after 3 minutes, and continued for 30 minutes before being turned off. There was a rapid increase in the KCl concentration as soon as the injection started. The measured KCl concentration varied between around 85 ppm and 105 ppm, with an average level of 96 ppm, which is close to the theoretical target of 100 ppm.

Similar trends were found in all the air-fired experiments, albeit with slightly different mean concentrations. The system used for KCl injection operated at 7 bar due to the pressure drop over the spray nozzle. When the pump was stopped, the injection continued but with a decreasing flow until the system was depressurized. This explains the slightly slower response of the KCl concentration when the injection was turned off, as compared to when it was started (Figure 19). Nevertheless, the overall response was rapid and the system, as expected, was capable of measuring the KCl concentration during air-fuel combustion. Therefore, this system was also used for the sulfation measurements at M7, where the aforementioned requirements were fulfilled.

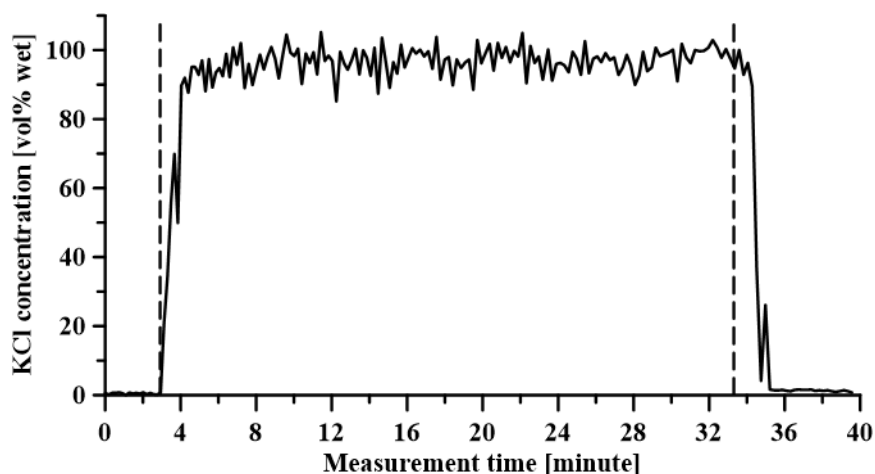


Figure 19. Continuous measurement of KCl at M7 using the IACMTM. At time 0, there is no injection of KCl. - KCl injection starts after 3 minutes and continues for 30 minutes.

The IACMTM system has been used in numerous experiments in both research and industrial facilities, all of which have been air-fired units. The present experimental series was the very first time that it was used to assay flue gases originating from oxy-fuel combustion. During this measurement campaign, the IACMTM did not perform as well during oxy-fuel combustion as during air-fuel combustion. When only KCl was injected during oxy-fuel combustion the measured concentration of KCl was lower than that detected for air-fuel combustion (around 85 ppm), even though it should theoretically have been higher due to the lower volumetric flue gas flow. In addition, the degree of sulfation assessed with the IACMTM was always much lower than that obtained with the FTIR or obtained from the simulations. Certain differences between air-fuel and oxy-fuel combustion could be important for the measurements, for example, the temperature, which was considered during the evaluation. Another difference is the replacement of nitrogen with carbon dioxide as the main flue gas component; at the time of the experiments, the IACMTM had never been calibrated for high CO₂ concentrations. CO₂ has been reported to absorb light at wavelengths in the range of 200–300 nm at temperatures >600°C [134]. This is in the same range as that used in the IACMTM, which could have influenced the result. On the one hand, SO₂ absorbs light at wavelengths between 290 nm and 310 nm, which is used by the instrument to measure also the SO₂ concentration. The IACMTM, on the other hand, had never been used to measure or had never been calibrated for such SO₂ concentrations as high as those found in the oxy-fuel cases in the present work. Due to these uncertainties, the IACMTM was used only for KCl measurements during air-fuel combustion. It is, however, possible to use the IACMTM also for oxy-fuel combustion, although some additional development work would be required.

4.3.3 Aerosol measurements

Aerosol measurements were conducted using the SMPS, VT-DMA, and DLPI. A representative result from the VT-DMA measurement campaign is shown in Figure 20. The measurement was performed for the Air case at the center of port M3 and compares the relative volume fractions for 80-nm particles during KCl injection, together with data for combined injection of KCl and SO₂. The monodisperse particle stream of 80 nm was heated before re-measurement of the size distribution, making it possible to detect changes caused by the increase in temperature. This relative loss in volume is presented for temperatures in the range of 400°–800°C in Figure 20. The main volume loss both with and without SO₂ injection occurred between 475°C and 550°C, although in the case of combined KCl and SO₂ injection about 6.7% of the mass was still measured for temperatures >600°C. The remaining volume found at these temperatures indicates that something other than KCl is detected – presumably K₂SO₄ – which has a much higher evaporation temperature than KCl. If the measurement had included higher temperatures, it would have been easier to classify the remaining mass.

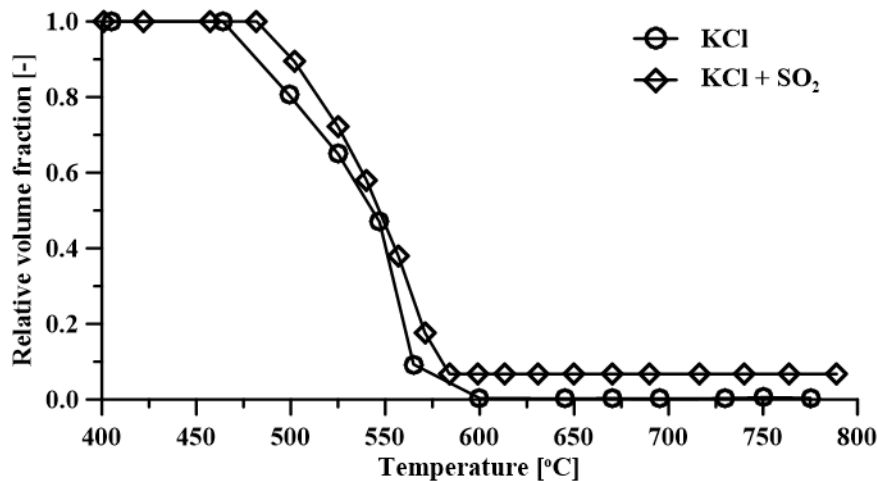


Figure 20. Relative volume fractions measured with VT-DMA at port M3(center position) during air-fuel combustion with KCl injection and with or without SO₂ injection. The measurements were performed for particles that had a diameter of 80 nm.

Using the DLPI, it was possible to collect the sampled particles (in this case, soot and potassium-containing aerosols) in 13 different size ranges. By weighing the foils before and after the particle sampling, the particle concentrations and size distribution (by mass) could be calculated. Unfortunately, accurate weighing could not be performed due to errors that occurred during the reference weighing. However, photographs of the first nine stages (d₅₀ 30 nm to 1060 nm) from measurements taken during the injection of KCl are shown in Figure 21. In these photographs, clear differences between the individual stages can be observed. There are visible aggregates of particles in stages 01–05. The aggregates are not as pronounced in stages 06 and 07, and in stages 08 and 09, there is only a thin white layer that is difficult to discern. The white layer can be found to varying extents in all the advanced stages. The aggregates are darker and larger on the plates used during the measurements without KCl injection. In addition, the white thin layer was not found in the foils from the experiments that did not involve KCl

injection. Therefore, this layer is believed to be the result of salt condensation or the condensation of water when the DLPI is cooled. Judging from the photographs in Figure 21, most of the particles appear to be smaller than 400 nm. DLPI measurements give, however, no information as to the composition of the particles, so additional analyses using, for example, SEM-EDX. In this way, the aerosols could be distinguished from the soot particles together with the composition.

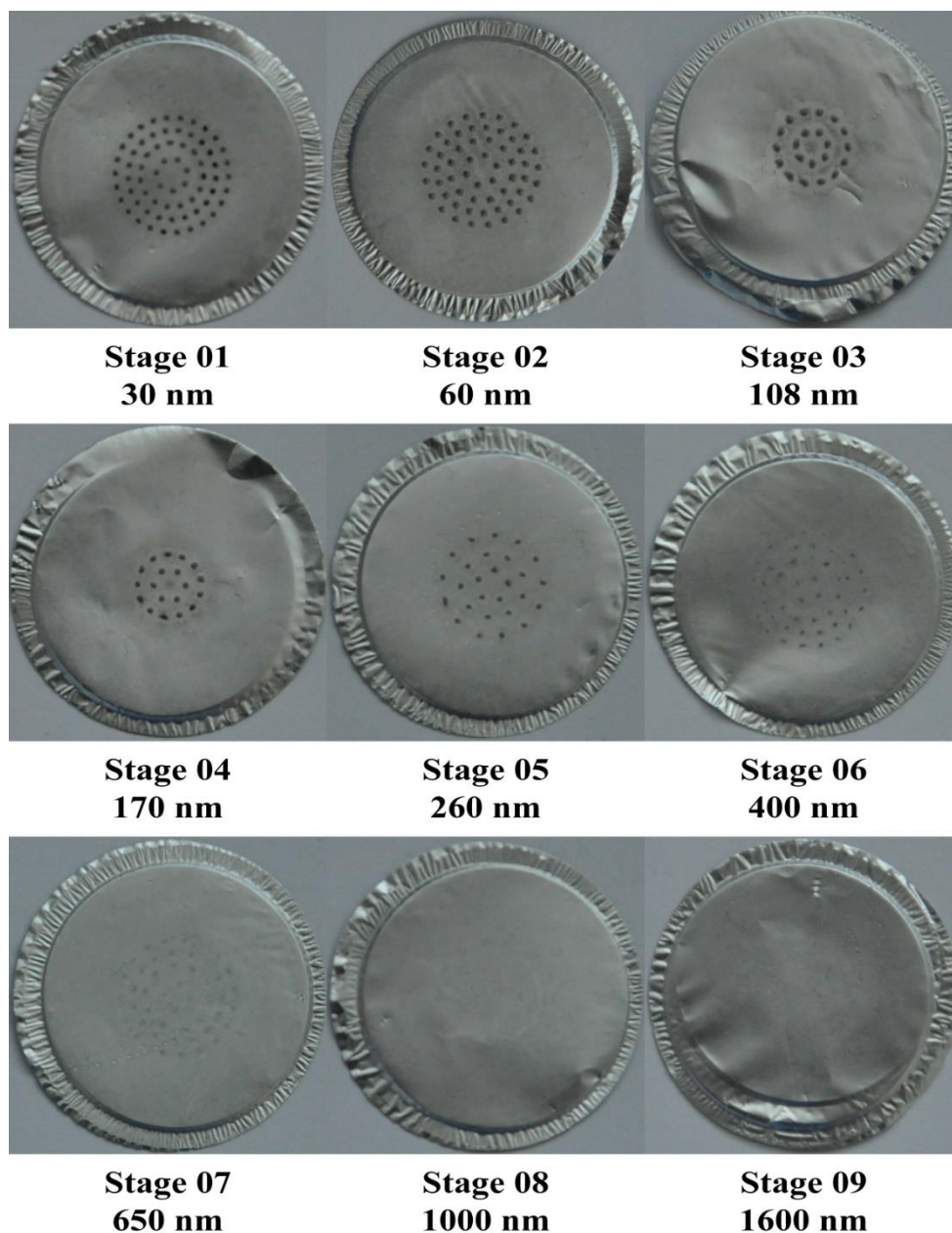


Figure 21. Photographs of the collecting foils used for the nine first stages (d_{50} 30 nm to 1060 nm) in the DLPI during the injection of KCl into the flame.

As measurement port M3 is relatively close to the burner, sampling at M3 should reflect an early stage of the sulfation process, and this turned out to be the case. The degree of sulfation detected using the VT-DMA (6.7%) was therefore considered plausible. To increase the level of accuracy, it would be important to cover the entire size distribution, since the individual shares of KCl and K_2SO_4 might vary for different particle sizes. Given the high melting

temperature of sulfated potassium, it would be expected to condensate almost immediately after formation. In contrast, one would expect the KCl to be found in the gas phase within the combustion unit. Aerosols are formed first during the sampling, where homogenous nucleation is favored, resulting in smaller particles. While tests were performed to include the whole size distribution, no useful data were obtained from these measurements. Two parts of the setup were considered to be problematic. First, the heating and cooling times of the oven used to heat-treat the particles were long, making this a very time-consuming measurement, especially when several size ranges were to be investigated separately. Second, instabilities in the sampling system, including the dilution steps, resulted in too-large fluctuations over time, making it impossible to draw any valid conclusions.

Due to the problems identified with our aerosol setup and the need for additional analysis using the DLPI, this setup was abandoned in the present work. Furthermore, the FTIR and IACM™ system was found to be suitable for this work. We believe that it is not only possible to improve the setup using these techniques (SMPS, VT-DMA and DLPI) to measure the degree of sulfation, but it is also a requirement if measurements are to be performed for which the use of FTIR and IACM™ is no longer considered valid, e.g., experiments involving the combustion of solid fuels or when performing flame measurements for gaseous fuels, as in this work.

5 Modelling

Simulations have been performed in all the papers included in this thesis. Each paper has an individual simulation set-up adapted for that specific investigation. The simulations can be divided into two types: 1) combustion simulations, in which fuel oxidation is included; and 2) flue gas simulations in which the oxidation of CO is included but there are no hydrocarbons present. All the simulations were performed using a PFR model in the Chemkin software, into which one of the three different mechanisms (Mechanisms A, B and C) used was implemented. More information about the mechanism can be found in Section 5.1.

5.1 Reaction mechanisms

As mentioned above, three different mechanisms are used in this work. The mechanisms contain all the reactions and reaction properties that are used in the simulations. A mechanism is divided into different subsets (groups of reactions). The development of these subsets is not part of this work, as all of them have been taken from the literature. It is important to point out that these subsets from the literature are used in combinations and with conditions for which they may not have been validated. The mechanisms are used to capture trends and general differences compared to the experimental data, and for this purpose, the mechanisms are assumed to be sufficient. A short description of the different mechanisms used is presented here and includes the different subsets used. The complete mechanisms with all their respective reactions can be found in the Appendix.

5.1.1 Mechanism A

Mechanism A, which is used in Papers I, III and IV, is taken from the work of Hindiyarti et al. [36], and it includes K, Cl, and S subsets, as well as a subset for CO/O/H reactions. Mechanism A also includes the estimation of K_2SO_4 condensation listed by Li et al. [74]. The mechanism presented by Hindiyarti et al. [36] uses a mechanism, earlier presented by Glarborg and Marshall [94], as its basis. The earlier mechanism included both potassium and sodium, while the latter was removed in this new mechanism for simplicity, based on the argument that potassium and sodium are very similar in their reactions (as has been discussed also earlier in this work). This is why it is possible to allow potassium to represent both alkali species. However, Hindiyarti and coworkers added a number of elementary reactions, together with two new potassium species, $KHSO_3$ and KSO_4 . Previously presented thermodynamic data were used when possible, otherwise they were estimated using the Gaussian 3 *ab initio* methods described elsewhere [94, 135, 136]. The sulfur subset used in this mechanism was taken from

the literature [33, 137, 138], and it covers the relationship between SO_2 and SO_3 , which is important for the sulfation of alkali-metals. For validation of their complete mechanism, Hindiyarti et al. used the results from the experimental studies of Iisa et al. [67], Jensen et al. [65], and Jimenez and Balester [139, 140]. The mechanism was developed to describe the sulfation of potassium in flue gases derived from combustion in air in the temperature range of 900°C – 1300°C .

5.1.2 Mechanism B

This mechanism, which was employed in Paper II, was used to study the sulfation process, including also the combustion of propane. All the subsets used in Mechanism A were also used in Mechanism B, with the addition of three subsets that describe the oxidation of C1-, C2-, and C3-hydrocarbons, respectively. The hydrocarbon oxidation subsets are based on the studies of Glarborg et al. [141, 142], Alzueta et al. [143] and Abián et al. [144]. This combination of subsets used in Mechanism B has not been validated, although the included subsets have been validated individually in a previous work. Therefore, the present work evaluates the influences of the C1–C3 subsets on the sulfation chemistry. An example from the evaluation is presented in Figure 22. Figure 22a shows the mole fraction of K_2SO_4 at the outlet of an isothermal PFR, calculated with and without the C1–C3 subsets. There is a noticeable difference at temperatures $<700^\circ\text{C}$, where sulfation is initiated at slightly lower temperatures. These temperatures are lower than those that Iisa et al. [67] applied in their work, a study which was used by Hindiyarti et al. [36] for validation purposes. Figure 22, b and c show the formation of K_2SO_4 at 660°C and 1000°C , respectively. For the lower temperature, the sulfation process is faster when the hydrocarbon chemistry is included (although no hydrocarbons are present). At higher temperatures, no difference is observed. The degree of sulfation and the equilibrium are not affected by including the C1–C3 subsets. In summary, a small but noticeable effect can be caused at temperatures $<700^\circ\text{C}$ by merging the two mechanisms, which is a phenomenon that deserves closer attention. In this work, the merged mechanism is used to evaluate the experimental study based on an 80-kW propane flame, which is obviously not an ideal setup for validating the mechanism. However, the combination of modeling and experimental results strongly indicates that the employed mechanism is appropriate for the purpose of this work.

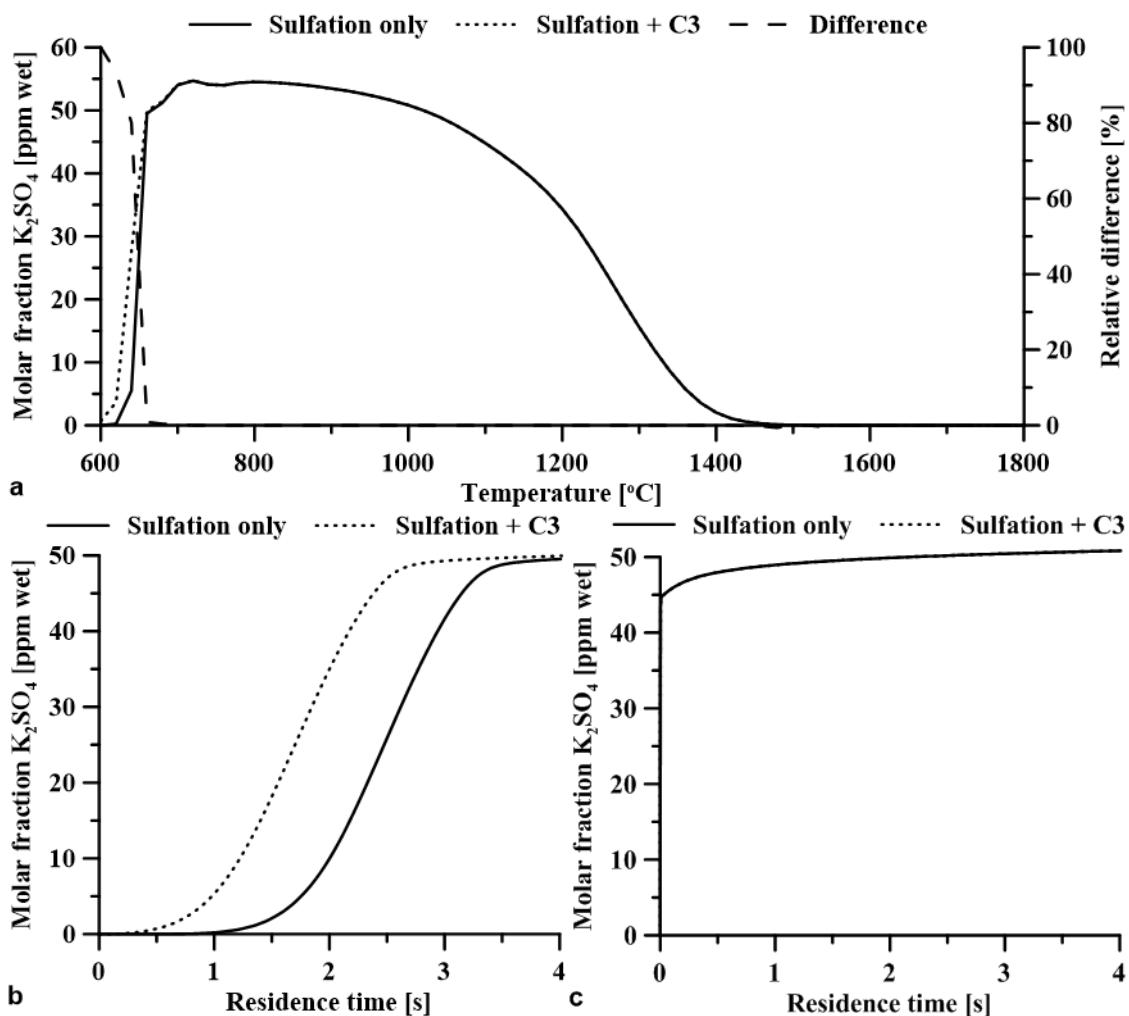


Figure 22. Results from an isothermal PFR model that includes only the sulfation mechanism and the sulfation mechanism together with the C1–C3 subsets. The PFR is fed with a gas flow with the following composition: 20% CO_2 , 20% CO , 12.5% O_2 , 400 ppm SO_2 , 100 ppm KCl , and N_2 set by difference. a) Molar fractions of K_2SO_4 at the outlet for temperatures in the range of 600°C – 1800°C , together with the relative differences between the two mechanisms. b) and c) Molar fractions of K_2SO_4 throughout the reactor at temperatures of 660°C and 1000°C , respectively.

5.1.3 Mechanism C

Similar to Mechanism B, Mechanism C covers the oxidation of hydrocarbons (C1–C3), for which the same subsets were used. In Mechanism B, these subsets were added to Mechanism A, which was not the case here. Instead, a mechanism that included the oxidation of hydrocarbons, as well as nitrogen and sulfur chemistry, was used. This mechanism has been used previously to compare the results of bench-scale experiments and experiments performed in the same combustion unit as that used in the present work [31, 109]. As mentioned, this mechanism has the same subsets that describe the oxidation of C1–C3, although in this mechanism, the CO/H/OH reactions are also taken from the studies of Glarborg et al. [141, 142] and Alzueta et al. [143]. The subsets that describe the nitrogen chemistry and its interactions with hydrocarbons are based on the works of Glarborg et al. [142, 145] and Dagaut et al. [146], and the sulfur chemistry is based on the studies of Giménez-López et al. [32] and Alzueta et al. [147]. The K and Cl subsets from Mechanism A were then added to the other subsets to create Mechanism C.

Mechanism C was used in Paper V, in which the influences of KCl and SO₂ on the NO chemistry were investigated. Therefore, it was important to maintain the nitrogen chemistry as accurately as possible when creating Mechanism C, which was the reason for adding the K and Cl subsets to the mechanism previously used by Fleig et al. [31, 109], instead of adding the nitrogen chemistry to Mechanism B. When comparing the different combinations of subsets it emerged that the nitrogen was affected by the differences in the CO/OH/H reactions. This is apparent in Figure 23, which shows the NO concentration profiles resulting from simulations similar to FR-Ref (see Table 5), where KCl is not present but still the different mechanisms behave differently. The concentration of NO is less than half that using Mechanism B+N compared to the other two mechanisms. Mechanism C was therefore assumed to be the most suitable mechanism for the purposes of Paper V.

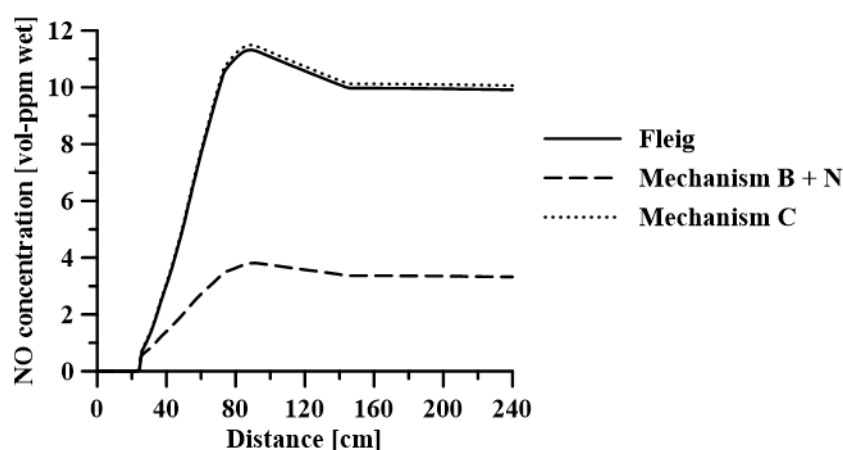


Figure 23. NO concentration profiles of the simulated PFR. The simulation settings are the same in all three cases and are also similar to the FR-Ref case (see Table 5), although the following three different mechanisms have been used: 1) the mechanism previously used by Fleig et al. [31, 109] (Fleig); 2) the mechanism where the nitrogen chemistry has been added to Mechanism B used in this work (Mechanism B+N); and 3) Mechanism C, as it is used in this work.

5.2 Sulfation simulations

The sulfation of potassium chloride is simulated in Paper I, II and III using two different mechanisms (Mechanism A and B) with three different approaches. The flue gas simulations are performed using Mechanism A. The work presented in Paper I includes an air-fired case and two oxy-fuel cases both with 25 % oxygen, but applying wet and dry flue gas recirculation denoted Air_{FG}, OF25_{FG} wet and OF25_{FG} dry, respectively. For these cases the temperature profile is linearly decreasing from 1600°C down to 500°C. In all three cases the same reactor geometry is used causing differences in residence time, see Table 3. The inlet composition, presented in Table 3, is based on complete combustion (stoichiometric-ratio equal to 1.2) of a fuel mix with 90% coal and 10% biomass. It is assumed that all S, K and Cl are released to the gas phase. For more details on how the inputs are derived, see Paper I.

Table 3 Inlet mole fractions used for flue gas simulations. The concentrations are presented on a wet basis. Source: Paper I

	Air _{FG}	OF25 _{FG} dry	OF25 _{FG} wet
N ₂	73.9%	6800 ppm	4820 ppm
CO ₂	14.5%	85.5%	60.7%
H ₂ O	8.30%	9.75%	34.8%
O ₂	3.27%	3.85%	3.85%
SO ₂	417 ppm	2245 ppm	1620 ppm
KCl	96 ppm	112 ppm	112 ppm
HCl	6 ppm	7 ppm	287 ppm
Residence time [s]	4.0	4.6	4.6
SO ₂ /KCl ratio	4.4	20	14

Mechanism A was used also in Paper III to investigate the influence of CO oxidation on the sulfation of KCl using a PFR model. The PFR was modeled isothermally at temperatures in the range of 800°C to 1800°C, and was set to have a constant velocity and to maintain a constant residence time of 10 s in all cases. The inlet concentrations represent flue gas compositions (N₂, O₂, H₂O and CO₂) and are based on complete combustion of propane in air with an air-to-fuel ratio of 1.15. For this case, 100 ppm of KCl and 600 ppm of SO₂ were added to the inlet composition. This case is the reference case used to represent a nitrogen based environment, N₂-Ref. A second reference case, CO₂-Ref, was created by replacing all nitrogen in N₂-Ref with CO₂. The influence of CO oxidation was studied by adding 3% CO to both reference cases and adjusting the O₂ and CO₂ concentrations while keeping the total mass flow constant. In all four cases, the oxygen was added through a separate inlet, to gradually oxidize the CO in the two CO cases. This was done using a linear injection profile between 0 s to 4 s residence time. The influences of the CO were investigated further by varying them from 0% up to 3%. The different cases are summarized in Table 4 and further details are found in Paper III.

Table 4. Summary of the inlet concentrations for the six cases investigated in this work. Source: Paper III.

		N ₂			CO ₂			Investigated interval
		Ref	CO	No O ₂	Ref	CO	No O ₂	
N ₂	mol%	bd	bd	Bd	0	0	0	0–3
CO ₂	mol%	10.2	7.2	7.2	bd	bd	bd	
H ₂ O	mol%	13.6	13.6	13.6	13.6	13.6	13.6	
O ₂	mol%	2.5	4.1	0	2.5	4.1	0	
CO	mol%	0	3	3	0	3	3	
KCl	ppm	100	100	100	100	100	100	
SO ₂	ppm	600	600	600	600	600	600	800–1800
Temp	°C							

bd = by difference

The combustion simulations basically include two cases that represent the Air and OF25 conditions that are investigated experimentally. Fuel oxidation is important in this study and therefore Mechanism B was applied. In order to keep the modelling and experimental results separated, the modelled cases will be denoted as Air_M and OF25_M. The same reactor geometries and temperature profile (see Figure 24 for the temperature profile) is used in both cases. However, due to different total flows, the reactor residence time is different between the two cases (4.4 s for the Air_M case and 5.6 s for the OF25_M case). To describe the influence of the radial mixing in the flame zone (which is assumed perfect in a PFR) the oxidizer is staged as is shown in Figure 24. The same cumulative oxidizer injection profile is used in both cases. The fuel (propane) feed and oxidizer inlet composition is the same as in the test unit during the experiments (see Table 2).

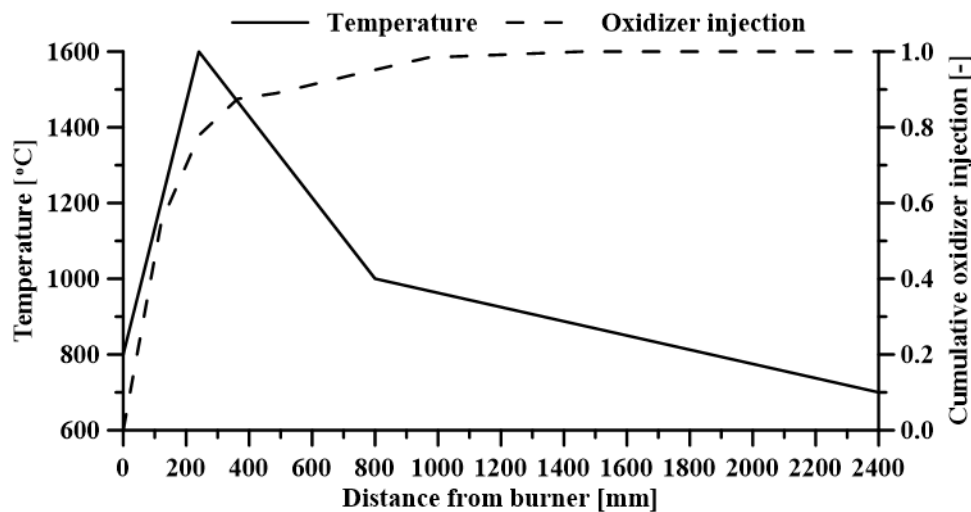


Figure 24. The temperature profile (solid line) and cumulative oxidizer injection profile (dashed line) used for the simulations including combustion of propane. Source: Paper II.

5.3 NO simulations

The combustion in a flame is limited by the mixing of fuel and oxygen in a diffusion process. A fuel-rich zone is formed that is surrounded by an oxygen-rich zone (see Figure 25a). When mixing takes place there will be two cases, either oxygen will be transported into the fuel-rich zone or combustibles will be transported out through the oxygen-rich zone. Since a PFR model is applied in this work no radial mixing occurs and therefore two scenarios are considered that will capture the different characteristics of both zones. Each case has an individual injection profile that represents the mixing of either oxygen into a fuel rich zone or fuel into a fuel lean zone (Figure 25b). The two cases also have individual temperature profiles, as presented in Figure 25c; both injection and temperature profiles are based on experimental results from measurements that are described in further detail in Paper V.

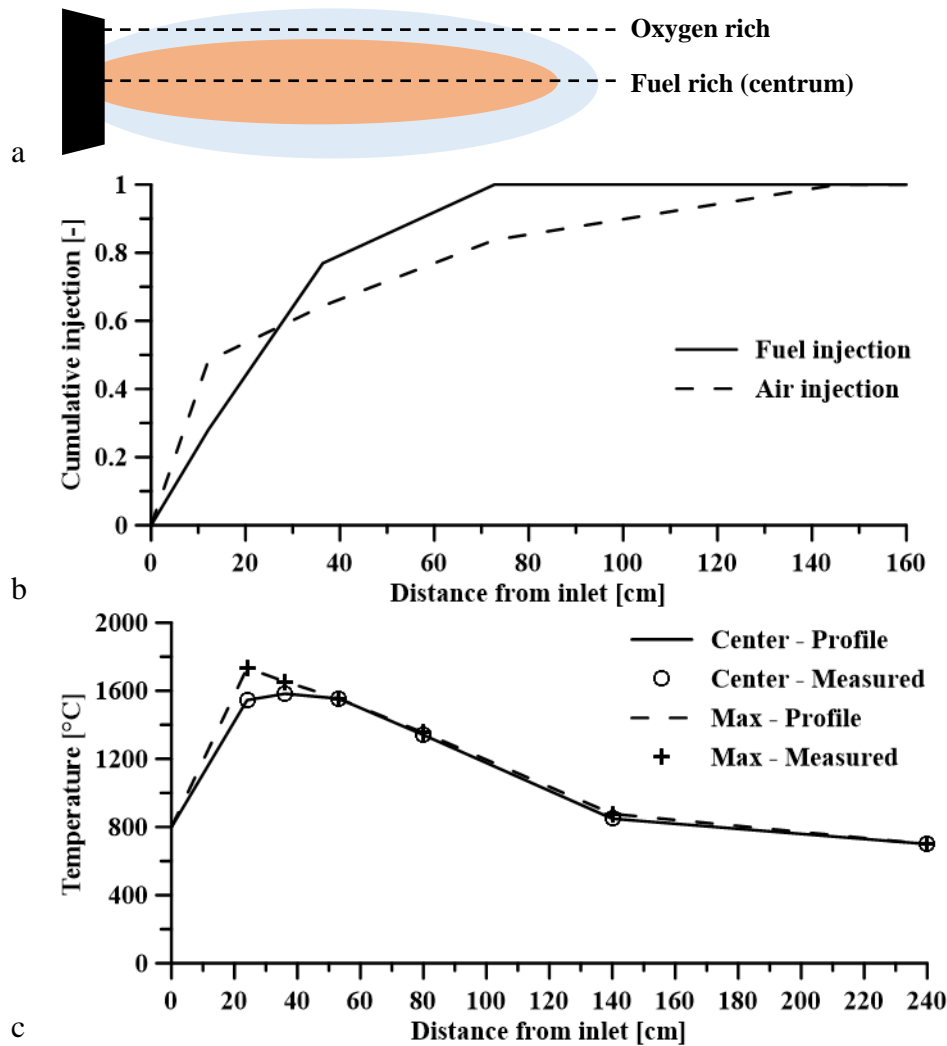


Figure 25. a) Schematic of a flame with the two different cases investigated in this work: fuel-rich and oxygen-rich. b) Cumulative injection profiles used in the simulations in order to mimic the effect of mixing. One used for injection of fuel (oxygen rich case) and one for injection of air (fuel rich case). c) Temperature profiles used in the simulations performed in this work. Both are based on experimental results that are presented in this work as well. One profile represents the center-line (dashed) and the other represents the highest temperature in axial direction (dotted). Source: Paper V.

The simulations that include nitrogen chemistry require Mechanism C, which also is implemented in the PFR model. The gas inlet compositions and flows are set to make the model comparable with experimental data. If the influence of KCl is investigated, the 8.5 mg/s of KCl are introduced together with the fuel stream. In those cases SO₂ is introduced at a feed rate of about 43.8 mg/s together with the oxidizer, i.e. about six times the KCl flow on a molar basis. These inputs are summarized in Table 5.

Table 5. Summary of input parameters used in the NO_x simulations based on the 100 kW combustion unit. Source: Paper V.

Case	Propane g/s	λ -	Profiles Temperature	Injection	KCl* mg/s	SO ₂ * mg/s
Fuel rich (FR)	1.73	1.15	Centrum	Air injection	8.4	43.6
Oxygen rich (OR)	1.73	1.15	Max	Fuel injection	8.4	43.6

*Note that KCl and SO₂ is not always included.

A sensitivity analysis on the impact on NO formation when switching the atmosphere from fuel-lean to fuel-rich was performed in an isothermal PFR set to 1400°C. Both the fuel (propane) and air was staged in this case according to Figure 26a. By doing this the conditions will switch back and forth between reducing and oxidizing conditions, as can be seen in the variations in air to fuel ratio presented in Figure 26b. Mechanism C was used also in this study.

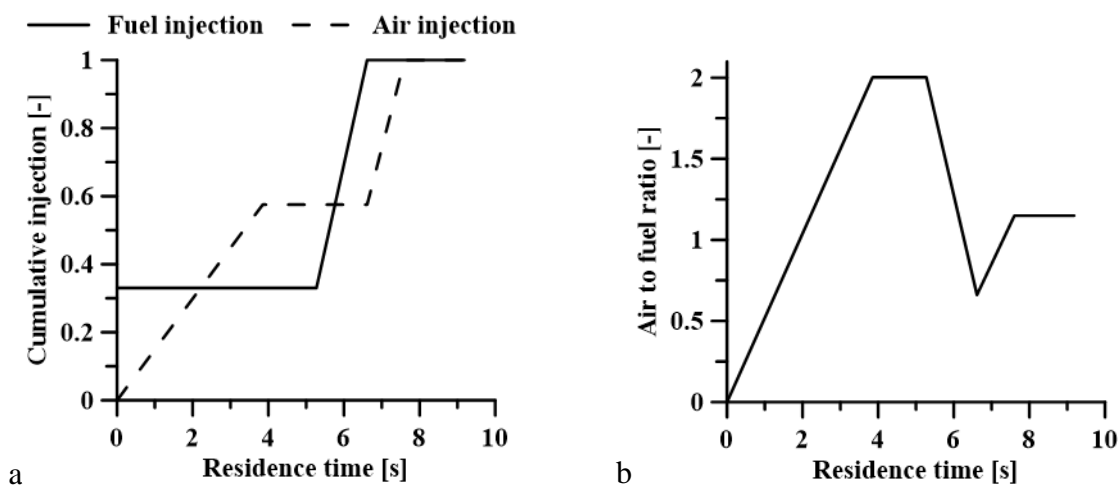


Figure 26. a) The cumulative injection profiles for both the air and the fuel stream used in the isothermal reactor and b) The variations in air to fuel ratio in the isothermal reactor. Source: Paper V.

6 Results

In this section, examples of the main results presented in Papers I–V are described, together with some additional results that are not included in those papers. These additional results are part of the same work and are presented here as a complement to the other data. The specific work from which the data are taken is indicated in the legend of the corresponding figure.

Figure 27 shows photos of the flame with and without KCl injection for the Air flame (Figure 27a and b respectively) and the OF25 flame (Figure 27c and d respectively). The photos of the Air flame are taken in port M2 while the OF25 photos are taken further downstream in M3. The change in color is due to the KCl injection and from a visual observation the KCl seems rather evenly distributed within the flame already in port M2 (air flame).

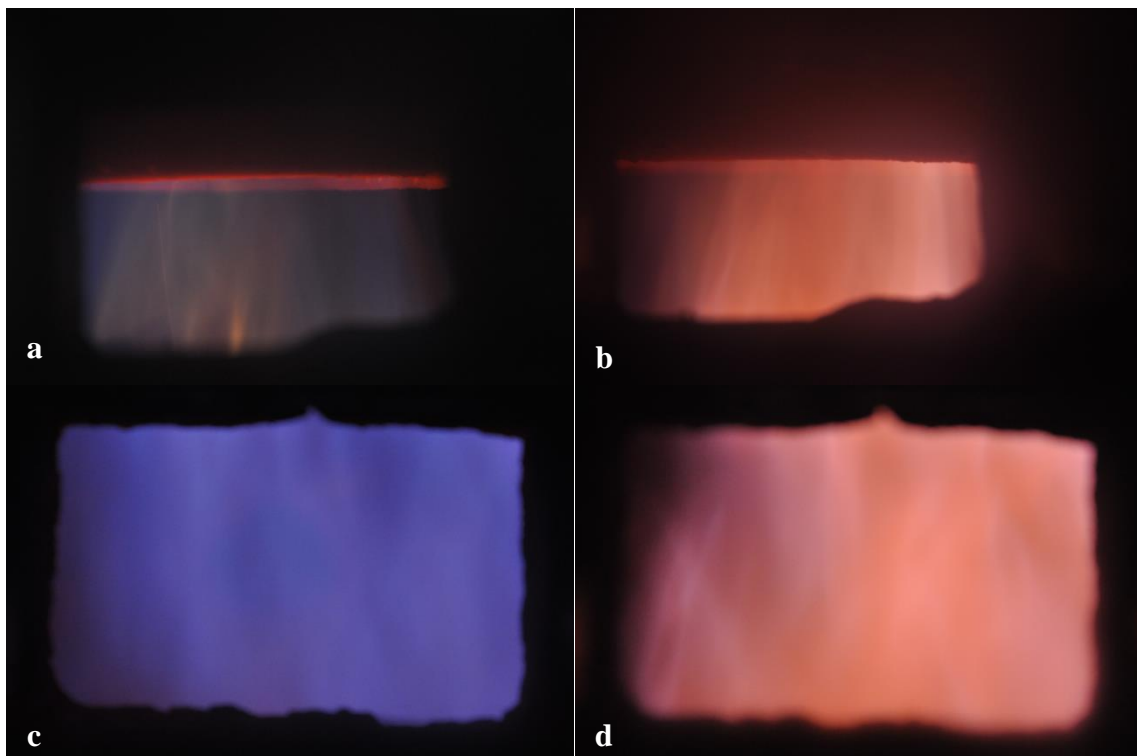


Figure 27. Photos of the flame taken during operation. The Air case both with and without KCl injection is shown in a) and b) respectively, both photos are taken in measurement port M2. The OF25 case is shown in c) and d) with and without KCl injection. The OF25 photos are from port M3.

Figure 28a shows the experimental and modeling results for the sulfation of KCl during the combustion of propane in the 100 kW test unit. Different S/K-ratios were tested by means of injection into the furnace, and the corresponding calculations were made using Mechanism B. As presented, the degree of sulfation was experimentally determined using two different measurement techniques, as indicated by the open (FTIR) and closed (IACMTM) symbols in Figure 28. The latter was, however, only used for air combustion experiments. As seen, the results show a good agreement between modeling and experiments for both combustion atmospheres. For the Air case, in which both measurement techniques were used, there is also good agreement between the experimental methods. The IACMTM sampling position is located upstream of that of the FTIR, which is a plausible explanation for those minor differences; the modeling results indicate that the sulfation process is still active at the measurement position of the IACMTM system. However, the difference is small and both methods agree well with the modeling results.

Due to the recirculation of the flue gas in oxy-fuel combustion, the concentration of sulfuric species is higher in the OF25 case than in the Air case when the same amount of SO₂ is fed to the system. In Figure 28b, the same data as in Figure 28a are plotted but now the actual S/K-ratios in the flue gases are presented for both cases. Even though the SO₂ concentrations are the same for both cases, the degree of sulfation obtained for the OF25 case is higher than that for the Air case for flue gas S/K-ratios lower than 14. It is evident that the amount of sulfur available in relation to the amount of potassium (S/K-ratio) is an important parameter for the sulfation process and this is shown to be valid for both air-fuel and oxy-fuel combustion atmospheres.

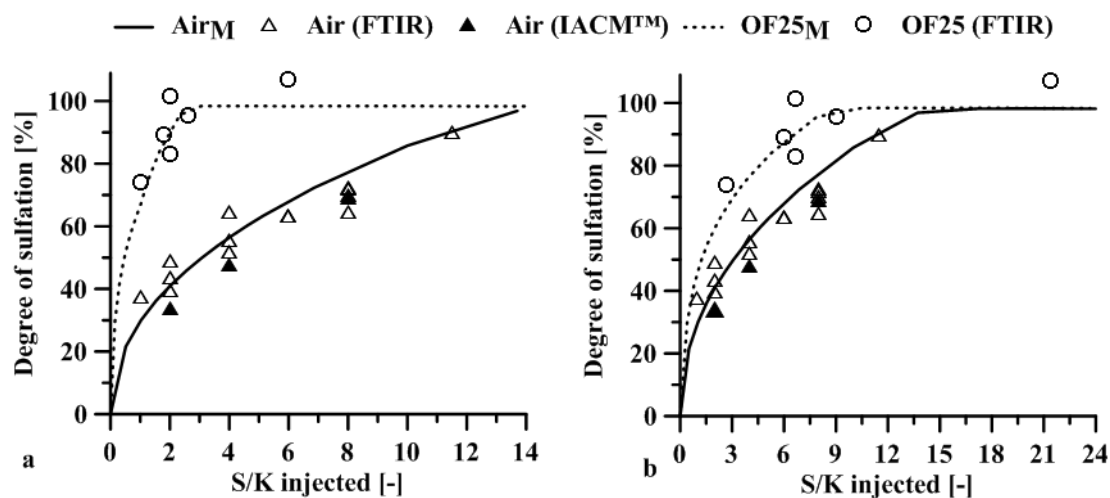


Figure 28. Comparison of the modeling and experimental results with respect to: a) the injected sulfur to potassium (S/K)-ratio; and b) the S/K-ratio in the flue gas. The solid and dotted lines represent the modeled values for the Air_M and OF25_M cases, respectively. Experimental values are indicated as follows: open symbols, FTIR measurements; and closed symbols, IACMTM measurements. Source: Paper II.

The degree of sulfation at the outlet of an isothermal PFR was modeled as part of the work presented in Paper II. The results are shown in Figure 29 for isothermal temperatures of between 800°C and 1800°C for N₂ and CO₂ atmospheres, both when CO is oxidized and with no oxidation of CO. Both the N₂-Ref and CO₂-Ref cases showed peak rates of sulfation at around 1050°C, and for all the tested temperatures they reached the same degree of sulfation. The two cases with CO oxidation (N₂-CO and CO₂-CO) displayed a trend similar to that of the reference cases in both the N₂ and CO₂ atmospheres at temperatures >1050°C. In contrast, at lower temperatures, both the N₂-CO case and the CO₂-CO case approached 100% sulfation.

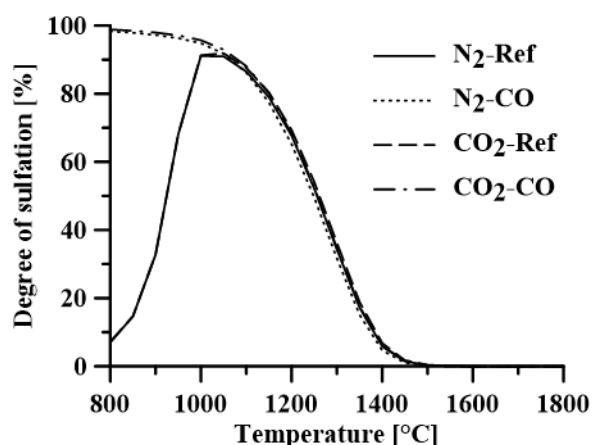


Figure 29. The degree of sulfation at the outlet of the isothermal PFR as a function of temperature for N₂ and CO₂ atmospheres, with and without CO oxidation. Source: Paper III.

At temperatures <1050°C, the most significant differences in the degree of sulfation achieved up to the PFR exit were found between the Ref-cases and CO-cases (Figure 29). The difference in CO concentration was generally large in those cases (either zero or 3.5 vol.%). Figure 30 shows the degrees of sulfation at the PFR exit for inlet CO fractions between 0.03 and 1E-7 when the temperature was set at 800°C, 900°C, and 1000°C, respectively. Here, a clear temperature-dependence is evident where the degree of sulfation is >90% for all the investigated inlet CO fractions. At 800°C and 900°C, a CO concentration in the range of 1–10 vol-ppm is sufficient to manifest a clear increase in the degree of sulfation. In addition, 0.1 vol.% CO at the inlet is sufficient to attain the highest degree of sulfation. The presented results are for the N₂-based environment. However, the same trend was noted for the CO₂ atmosphere, which is therefore not included in the figure.

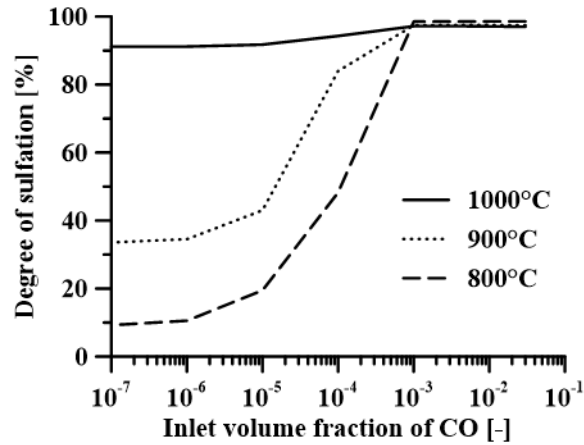


Figure 30. Degree of sulfation as a function of the inlet volume fraction of CO, presented for the three different temperatures of 800°C, 900°C, and 1000°C. The presented results are for an N_2 -based atmosphere. Source: Paper III.

A reaction path analysis of potassium compounds during sulfation of KCl is described in Paper I and presented in Figure 31. The figure demonstrates the differences in reaction activities between the three cases: Air_{FG}, OF25_{FG} dry, and OF25_{FG} wet, based on the flue gas compositions derived from the co-combustion of coal and biomass. The overall reaction activity is highest in the OF25_{FG} dry case, even though the formation of K_2SO_4 is not that much higher than in the OF25_{FG} wet case. The Air_{FG} case shows the lowest reaction activity of the three cases.

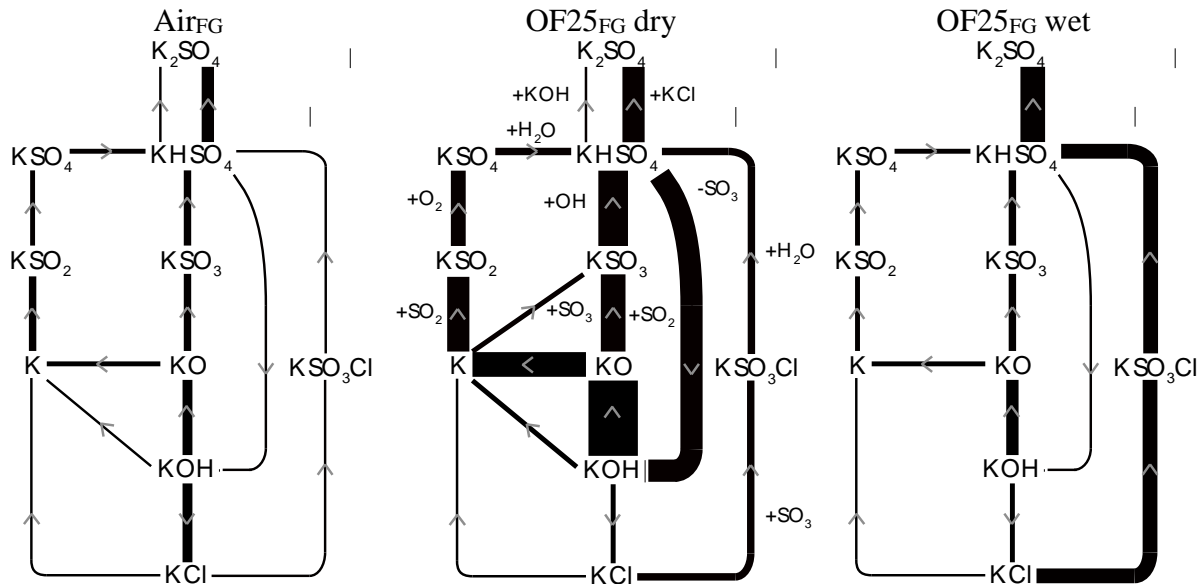


Figure 31. Modeling results for the activities of the important reaction paths involved in the sulfation of KCl in flue gases derived from the co-combustion of coal and biomass during air-fuel combustion (Air_{FG},) and oxy-fuel combustion with both dry (OF25_{FG} dry) and wet (OF25_{FG} wet) flue gas recirculation being applied. The relative thickness of each line indicates the relative activity of each individual pathway, normalized with respect to the overall highest activity for all three cases. Source: Paper I.

As indicated in the reaction path analysis (Figure 31), some of the reactions in the sulfation process involve SO_2 , while others are based on SO_3 . The relative importance of these two components varies depending on the flue gas composition, as shown in Figure 32. More than 50% of the K_2SO_4 formed in the OF25_{FG} wet case can be attributed to reactions that involve SO_3 . This is almost three-times the amount formed *via* SO_3 in the Air_{FG} and OF25_{FG} dry cases. However, the fraction of SO_3 is largest throughout the entire reactor in the OF25_{FG} dry case, as compared to both the Air_{FG} and OF25_{FG} wet cases (Figure 33). The peak fractions for both oxy-fuel cases are larger than the fraction found in the air-derived flue gases, almost 10-fold and 6-fold larger, respectively. In contrast, all the SO_3 is consumed in both the Air_{FG} and OF25_{FG} wet cases, whereas the exit fraction is almost 20 ppm in the OF25_{FG} dry case.

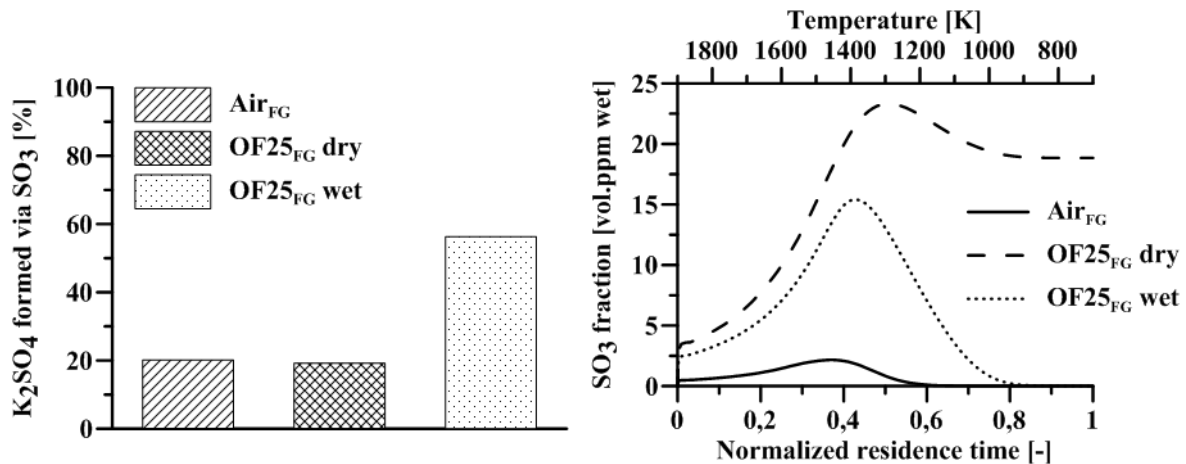


Figure 32. Percentages of the total amount of K_2SO_4 formed via reactions that included SO_3 for all cases. Source: Paper I.

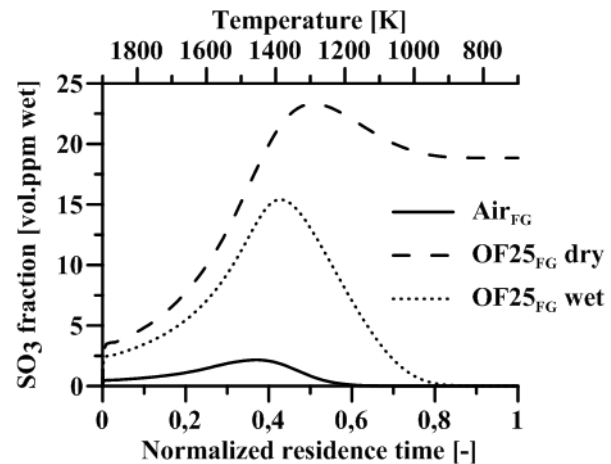


Figure 33. Variations in the SO_3 concentration throughout the reactor for all three flue gas cases investigated. Source: Paper I.

The SO_3 concentration was measured at M8 as part of the same measurement campaign as that in Paper II. The concentration was measured for different S/K-ratios when both KCl and SO_2 were injected (Figure 34). For an S/K ratio < 7 , the SO_3 concentration is around 10 ppm, and for higher S/K ratios, the SO_3 is clearly increasing; the same pattern is seen for both the Air and OF25 cases. According to the model, a noticeable SO_3 concentration is first detected after the S/K ratio exceeds 8 and 14 for the OF25_M and Air_M cases, respectively.

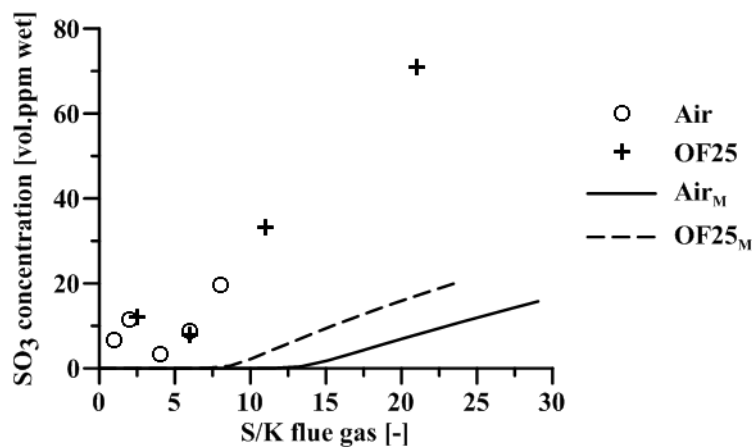


Figure 34. Measured SO_3 concentrations at M8 for the Air and OF25 cases (symbols). All the concentrations were measured when both SO_2 and KCl were injected. The exit concentrations of SO_3 from the modeled Air (M) and OF25 (M) cases are also included (lines).

We compared the degrees of sulfation when equilibrium was reached at various temperatures in a CO₂-rich atmosphere (Figure 35a) and in a modified CO₂-rich case with higher sulfur and HCl contents (Figure 35b). The N₂ and CO₂/H₂O cases were also investigated but are not shown, since the results were similar to those of the CO₂-rich case. The equilibrium favors complete sulfation at temperatures lower than 900°C, where the reaction instead is kinetically limited. The reaction rate is sufficiently high for sulfation to take place with a residence time of 4 s; the sulfation activity is initiated within a temperature window of 800°–1300°C (the case in Figure 35a). When the sulfur and chlorine concentrations increase, the sulfation rate decreases and the maximum reaction rate is shifted towards lower temperatures, with a temperature reduction of about 200°C. The equilibrium-driven sulfation is also shifted towards lower temperatures, as is clear from a comparison of the data in Figure 35a and Figure 35b.

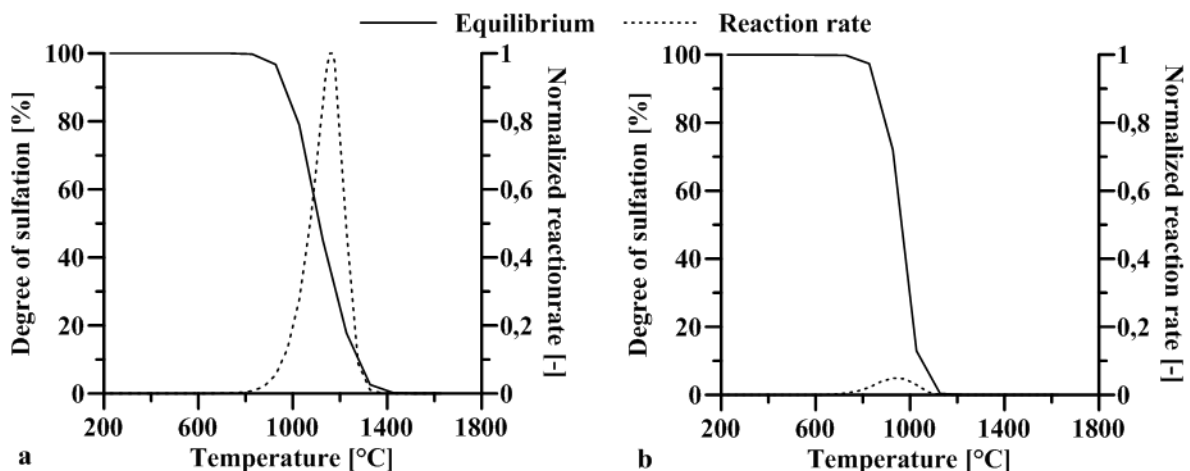


Figure 35. a) Degree of sulfation when equilibrium is reached for temperatures between 200°C and 1800°C in a CO₂ atmosphere. The reaction rate is shown for the same temperature interval. b) The same as in a) but for a CO₂ case with an S/K-ratio and Cl/K-ratio of 10. The reaction rates shown are normalized with respect to the maximum reaction rate in the case without HCl (Figure 35a).

Figure 36 gives the measured CO concentrations along the furnace centerline at different levels in the furnace, as measured in the work of Paper IV. Figure 36a shows the results from air-fuel combustion with different additives injected *via* the burner or *via* the oxidant, as described previously. No significant changes in the CO concentration are seen for any of the injected additives. The CO concentration declines with increasing distance from the burner until the oxidation is almost complete at a burner distance of 800 mm. The concentrations measured close to the burner (215 mm) suggest the presence of a slightly lower concentration of CO when the KCl is injected.

Figure 36b shows that the measured CO concentration in general is higher in oxy-fuel combustion than in air-fuel combustion. The figure also indicates that CO oxidation is completed more rapidly. In addition, during oxy-fuel operation, the effect on CO oxidation when KCl is injected is more significant. As shown, all the cases without KCl injection exhibit a higher concentration than those cases that include KCl, at every position from the burner inlet up to a distance of 800 mm when oxidation is complete. The effect on the measured CO concentration is substantial in the case in which the amount of injected KCl is doubled. However, despite this demonstrated effect of KCl injection on the in-flame CO concentration, the total time for CO oxidation remains in principle the same with and without KCl injection.

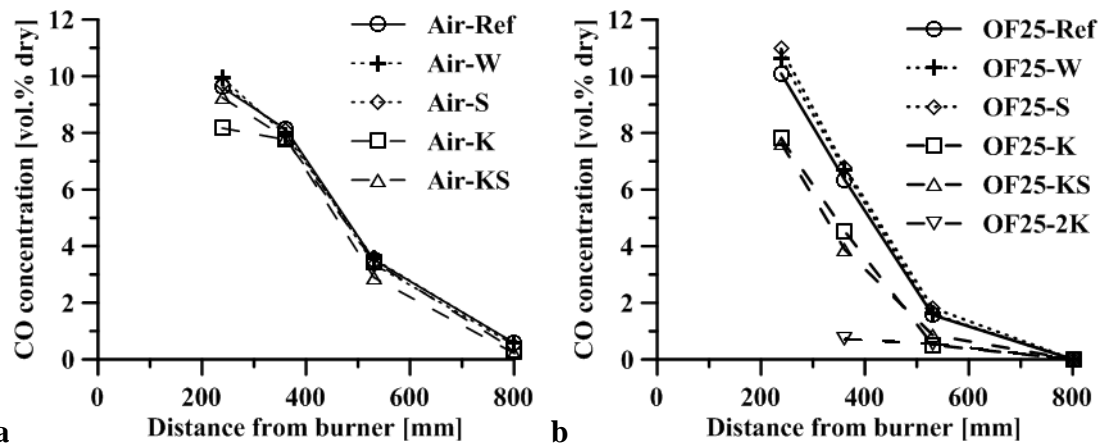


Figure 36. CO concentrations for five Air cases (a) and six OF25 cases (b) with and without injection of KCl, SO₂ and water. The cases are defined as follows; Ref, reference case (no injection), W – injection of pure water, K – injection of KCl, S – injection of SO₂, KS- injection of both KCl and SO₂ and 2K – double amount of KCl injected. Source: Paper IV.

The influences of KCl and SO₂ on the formation of NO during the combustion of propane in air was investigated in Paper V using two different mixing approaches. One approach represented the fuel-rich part of a flame (FR-cases) and the other represented the oxygen-rich (fuel-lean) region (OR-cases). The results of both approaches are presented in Figure 37, where the OR-cases show much higher NO formation than the FR-cases, as anticipated. Four variants of the FR-cases and OR-cases were modeled, in which KCl and SO₂ were included in the simulations, either separately or together. The results (Figure 37) show that while there are individual variations among the FR-cases and OR-cases, the OR-cases always have a concentration of NO >200 ppm at the outlet, as compared to the highest outlet concentration of 10 ppm among the FR-cases. Figure 37 includes the NO concentrations (70–110 ppm) measured at the exit of the 100-kW unit for the same four cases with and without KCl and SO₂. These are the average values taken from the continuous measurement made at the flue gas exit.

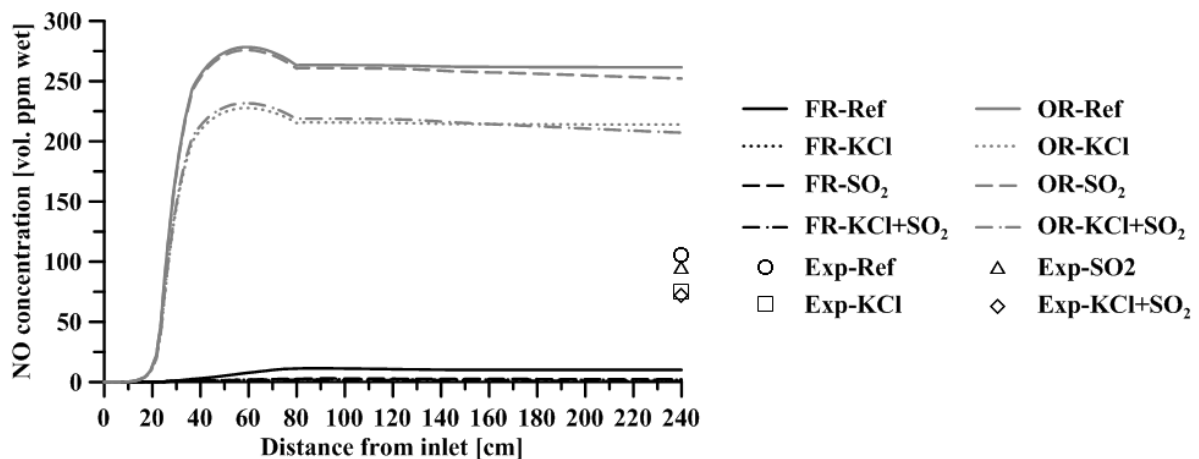


Figure 37. Simulated NO concentration profiles using the two different mixing approaches (FR and OR). Shown are the results from all eight cases, as well as the experimentally measured concentrations at the outlet of the 100-kW unit. Source: Paper V.

Figure 38 presents contour maps that are based on experimental data with measurements performed from port M2 down to M5. The figure compares the NO, CO and O₂ concentrations as well as gas temperature in the reference case (no injection) and the KCl case. There are no significant differences found for neither CO concentration, O₂ concentration nor temperature. For NO, on the other hand, there is a clear difference in concentration between the two cases with the reference case having the higher NO concentration. The general distribution is, however, similar also in the KCl case with two areas in the upper part around the center line and at 150 mm where the concentrations are very low.

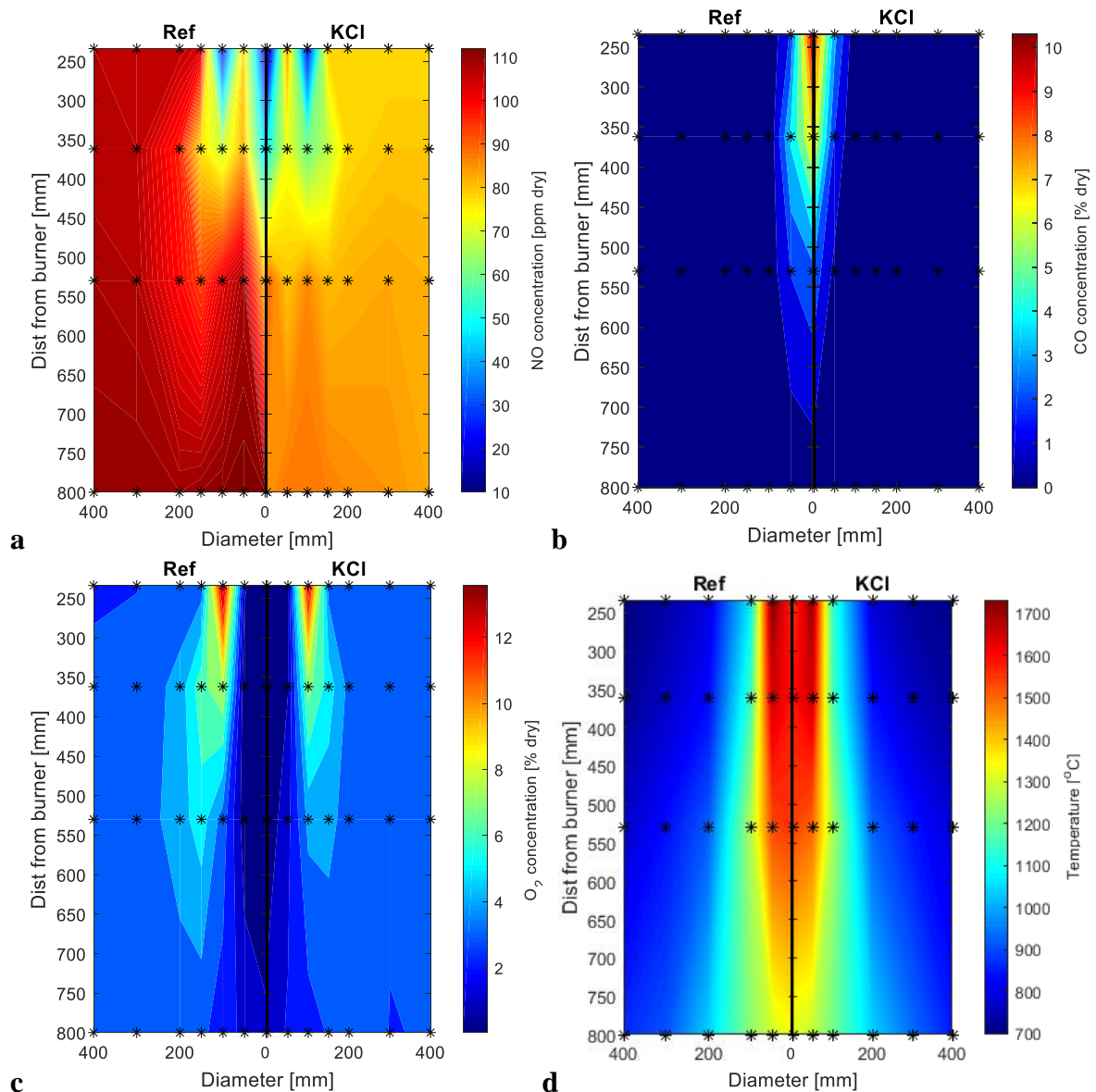


Figure 38. Color maps for NO concentration (a), CO concentration (b), O₂ concentration (c) and temperature (d) based on experimental data obtained in M2-M5 comparing the reference case and the case were KCl is injected. The x-axis indicates distance from the vertical center line. Note that the measurements are performed in the same location in both the Ref and KCl case, the x-axis in the KCl cases are however mirrored making the comparison easier. Source: Paper V.

The CO, O₂ and NO concentration profiles from an isothermal reactor operated at 1400°C are shown in Figure 39a and b respectively. The CO and O₂ concentrations vary as the fuel and air injection changes but there are no variations between the three cases why only one case is shown that represents all three. In the beginning the mixture is fuel rich and the CO concentration is increasing until the fuel injection stops. When all CO is oxidized the oxygen concentration increases until also the air injection is turned off after which the concentration remains constant until the fuel injection is started once again. Due to the fuel injection the CO concentration is increasing until additional air is introduced, air that oxidizes the CO and that brings up the O₂ level to its final concentration. The NO concentration varies substantially throughout the reactor as can be seen in Figure 39a. The formation of NO starts at 2.2 seconds in all three cases and continues until 6 seconds when the NO concentration immediately drops down to zero. After another 0.7 seconds the NO formation is rapidly initiated again and the concentration increases almost instantaneously; the formation rate becomes more moderate at 7 seconds but does not drop to zero.

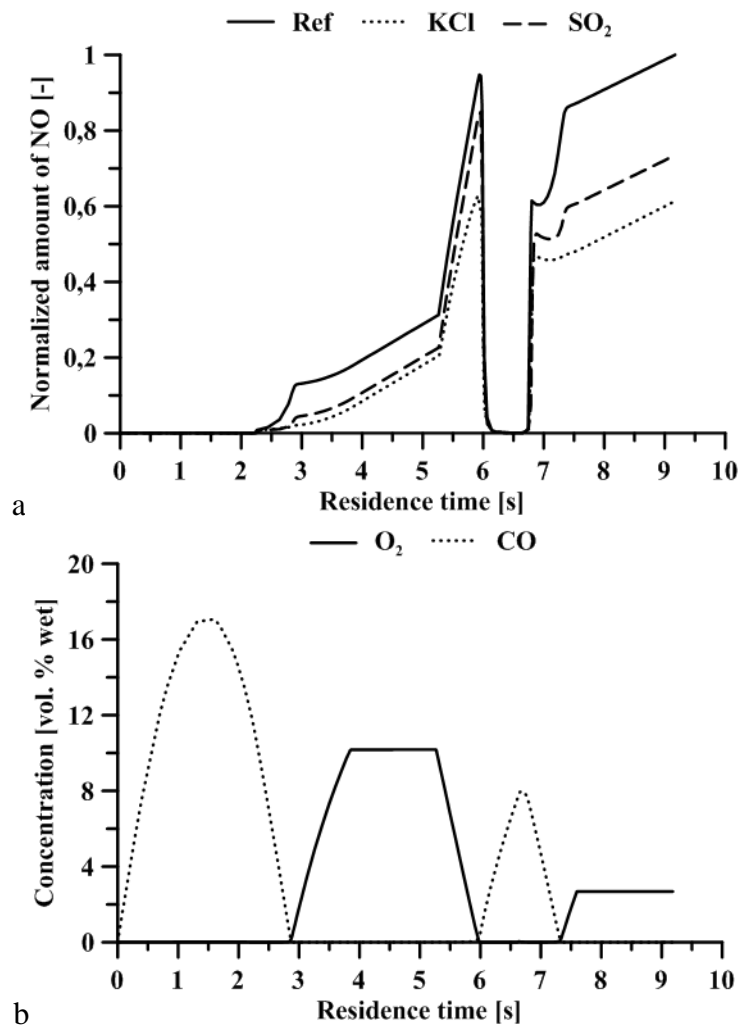


Figure 39. Concentration profiles showing the CO, O₂ and NO concentrations throughout an isothermal reactor changing from reducing to oxidizing conditions, back and forth. The NO concentrations are shown in figure a for the reference case and with KCl and SO₂ included individually. Source: Paper V.

7 Discussion

The sulfur content is important for the efficiency of the sulfation process which is clearly shown in this work; it was found that the S/K ratio in the flue gases needs to be significantly higher than one to reach complete sulfation (i.e. when all K has reacted with S). In an actual process this could be a limiting factor independent of practical conditions. That is, whether or not the KCl problems are to be mitigated by means of introducing a second fuel or a sulfur-based additive. In the example presented in Paper I, a 55 % degree of sulfation is reached during co-combustion of coal and biomass (90/10) and this results in a S/K ratio of 4.4. Now, 55 % is of course a noticeable level of sulfation but a higher degree of sulfation and/or a higher share of biomass can certainly be beneficial from both an economical and environmental perspective. The results from Paper I and Paper II, the latter also presented in Figure 28, show that this can be achieved if oxy-fuel combustion is applied. According to Figure 28a only one fifth of the sulfur is required in the OF 25 case compared to Air-fired conditions to reach complete sulfation. It is important to note that only homogenous gas phase reactions are considered in this work. In a commercial process, where solid fuels are combusted, the sulfation will be affected also by the overall fuel composition which will affect the availability of K and S in the gas phase. Solid fuel experiments need to be performed in order to examine if these effects will increase or reduce the benefit of applying flue gas recirculation, as found in this work.

As already mentioned, sulfur has a major influence on the sulfation of KCl. There are, however, other parameters that cause the higher degree of sulfation found in the OF25 case compared to the Air case as can be seen in Figure 28b. In the sensitivity analysis performed in Paper II both residence time and oxygen concentration was found to influence the sulfation even though neither of them could explain the difference found between OF25 and Air, *i.e.* effects not already caused by an increased sulfur concentration. The increased CO₂ concentration was, on the other hand, found to be capable to cause the difference. The increase in CO₂ concentration in oxy-combustion will influence the CO chemistry which could have an important influence on the sulfation of KCl. If the CO is oxidized at temperatures lower than 1100°C, the degree of sulfation could approach 100 % instead of zero as the temperature is descending (Figure 29). Oxidation of a few ppm of CO is sufficient for temperatures below 900°C to see an increase in the degree of sulfation and the most pronounced effect observed is reached just before 0.1 vol.% of CO (Figure 30). In the work presented in Paper III it was also shown that for temperatures higher than 1050°C, for which no effect of CO oxidation was found after 10 seconds in residence time, the oxidation of CO still made the sulfation faster. This could be important in a real process where the residence time at certain temperatures can be a limiting factor. It would be desirable to perform lab scale experiments to verify this effect that, so far, only is based on the simulation work presented in Paper III.

The described sulfation process becomes kinetically limited for temperatures below 1000°C as shown in Figure 36. At higher temperatures the process is limited by equilibrium. Both equilibrium and kinetics are influenced by the overall gas composition which is seen when comparing Figure 35a and b. The equilibrium favors a complete sulfation for all gas compositions investigated in this work when sulfur and free oxygen is available. Obviously, if it would be possible to boost the kinetics where those are limiting and where equilibrium concentrations are high, then there would be a lot to gain from a sulfation efficiency perspective. This is important to consider when discussing about general measures to reduce alkali-related HTC problems for commercial combustion systems where the overall composition may vary.

The reaction path analysis presented in Figure 31 shows that an increase in overall reaction activity in the OF25_{FG} dry case compared to the other two that is larger than the increase in degree of sulfation. Comparing the Air_{FG} and OF25_{FG} dry case the degree of sulfation in the Air_{FG} case is almost half of what is found in the OF25_{FG} dry case. The overall reaction activity is on the other hand only one fifth making the difference in reaction activity larger than in the actual degree of sulfation. A noticeable difference is the increased formation of SO₃, which is a result from desulfation of KHSO₄ through which KOH and SO₃ are formed. A similar net production of SO₃ from the sulfation of KCl was also seen in Paper III when the reaction activity is increased due to CO oxidation. The influence of the SO₃/SO₂ ratio is discussed in the literature to be important for the sulfation; SO₃ is typically assumed to be the most reactive form of the SO_x species in the sulfation of alkali species. The results from Paper I, as presented in Figure 32, show that around 20 % of the sulfation proceeds via SO₃ in both the Air_{FG} and OF25_{FG} dry cases despite the difference in reaction activity with respect to the formation of SO₃ itself, as observed in Figure 31. It is also shown in Figure 33 that the calculated SO₃ concentration along the PFR is much higher in the OF25_{FG} dry case compared to the Air_{FG} case. This is probably due to the much higher total amount of sulfur that is present in the oxy-fuel cases. On the other hand, the outlet concentration of SO₃ is zero also in the case with wet flue gas recirculation, which also has a relatively high sulfur concentration. Over half of the K₂SO₄ is formed via SO₃ in the OF25_{FG} wet case which of course affects the concentration of SO₃. This might be caused by the much higher water as well as HCl concentrations. HCl seems to inhibit the sulfation, whereas water is shown to promote the sulfation (Paper I). The promoting effect by the water could be due to its influence on the oxidation of SO₂ to SO₃. When observing the comparison between measured and modeled SO₃ concentrations in Figure 34 the measurement data never reached a zero signal (or concentration), which it should reach according to the calculations. It was also found from the experiments that the SO₃ concentration increases for S/K ratios above five. The modeling, on the other hand, suggests no significant SO₃ concentration at the outlet until a S/K ratio of 8 and 14 for the OF25_M and Air_M cases respectively. This is due to complete sulfation in both atmospheres. Thus, there is a clear difference between experimental and modelling observations: all SO₃ is consumed by the sulfation in the calculations but not according the experimental data.

It has been shown in this work that oxidation of CO promotes alkali sulfation. It was, however, also shown that KCl could have a promoting effect on CO oxidation. The results (Figure 36) show a clear reduction in CO concentration during injection of KCl for oxy-fuel combustion experiments independent of the presence of SO₂. It is also shown that the effect on CO oxidation is increased when the amount of KCl is doubled. No clear influence of KCl on CO oxidation could, however, be seen for the Air case. It is therefore suggested that a switch from N₂ to CO₂-rich environments will increase the sensitivity of CO-oxidation to KCl injection. This theory is supported by the sensitivity analysis performed in Paper IV. Although it was not possible to reproduce the exact same scenario as was observed in the experiments it was still possible to see that the effect of KCl on CO oxidation changed from inhibiting to promoting conditions for temperatures in the range of 1100°C to 1400°C and for CO₂ concentrations above around 20 vol% (wet basis).

According to both experimental and modelling results, both KCl and SO₂ seems to influence the NO concentration (see Figure 37 and Figure 38a). The way by which the NO concentration is affected depends on the choice between the two additives. KCl inhibits the actual formation of NO, but SO₂ on the other hand, promotes oxidation of NO to NO₂. The later has a lower impact on the overall NO concentration and takes place in the post flame region whereas the effect of KCl takes place in the flame zone. The flame zone might be divided into two theoretic sub-zones: one fuel-rich and one fuel-lean zone, respectively. Both zones are included in the modelling work and there is a large difference in the NO formation between these zones (as expected), which is shown in Figure 37.

Figure 39 presents the concentration profiles of NO (Fig. 36a), CO and O₂ (Fig. 36b) in an isothermal PFR which was run at 1400°C where propane and air both are injected according to the profiles presented in Figure 26. With this approach, the conditions switch between reducing and oxidizing conditions. When observing the NO concentrations in Figure 39a the formation starts after about 2 seconds when the CO concentration decreases, *i.e.* in line with theory. The conditions found between 2.5 s and 3 s are similar to those around 80 cm in the FR case and so are also the results with most NO formed when nothing is added. Between 3 s and 5 s, and, between 7.5 s and 9 s, the conditions are oxidizing and the slope of the NO profiles are the same for all three cases which indicates that KCl and SO₂ does not influence the formation under oxidizing conditions. After 5.3 s the NO formation increases, in all three cases, until 6 s into the simulation. The rates are however not the same in this time window with the least NO being formed in the KCl case. At this point, fuel is introduced to an oxygen rich environment similar to the OR cases in which the NO formation was stronger compared to the FR cases (Figure 37). What happens is that the KCl reduces the amount of both OH and H radicals in relation to the reference case. The same can be seen between 2.5 s and 3 s where there also was a clear difference between these cases with respect to radical pool composition. During the period between 6 s and 6.8 s when the CO is present and fuel is injected the NO concentration is rapidly reduced and is converted mainly into NH₃ and HCN. These compounds form NO once the air injection starts again, but the NO concentration does not reach the same level as before (similar to typical fuel staging behavior). After the first rapid NO formation before 7 s there is a subsequent NO increase before 7.5 s in the reference case but not in the case with KCl. At this point, between 7 to 7.5 s, when all NH₃ and HCN is consumed there is a peak in availability of OH and H radicals which also at this point is lower in the KCl case, compared to both the

reference and SO₂ cases that results in a much slower NO formation. No further analysis of what happens after 6s in Figure 39 is included in this work but an investigation for similar conditions is recommended for future work since it involves reactions and species associated with reburning and NO formation from fuel-related volatiles.

In Figure 38 it is shown that there are no or low levels of NO where both the oxygen and CO concentrations are high. However, at about 50 mm from the reactor center line, there is a relatively high NO concentration. This is the reaction front where the highest temperatures occur and the main part of the combustibles are mixed with oxygen.

It is worth mentioning that the injection of KCl was done in the form of an aqueous solution that was sprayed into the flame. This set-up could potentially influence the mixing as well as the temperature in the flame. The mixing is a limiting step in the oxidation of a fuel during flame combustion. Increasing the mixing would increase the probability for oxygen and fuel/CO to react and this would hence tend to improve CO oxidation. As mentioned, a spray could potentially also lower the flame temperature a fact that could have a reducing effect on thermal NO formation. Injection of pure water was therefore conducted as a reference since any of these effects would occur also for such a set-up. Any difference in both CO and NO concentration between injection of water and KCl is assumed to be an effect of KCl. It was shown in Figure 38 that the injection had no significant impact on the flame temperature. The NO concentration was lower also during injection of pure water compared to the reference case but it was reduced even further during KCl injection. For our experimental conditions, water had a small but inhibiting effect on CO oxidation, i.e. opposite to what was found for KCl. The effect found during injection of KCl on both NO formation and CO oxidation is therefore assumed to be of chemical nature rather than a thermal or mixing effect created by the spray.

8 Summary & outlook

The use of biomass and waste as fuels for combustion processes is expected to increase during the coming years since this represents a possibility to reduce fossil CO₂ emissions. The relatively high content of alkali metals and chlorine found in biomass compared to coal increases the risk for problems related to deposition and high-temperature corrosion. The related chemistry is therefore important in order to utilize the biomass in the best way possible, i.e. in order to maximize the thermal efficiency in power plants. This work focuses on the K-Cl-S chemistry relevant for combustion in flames, sulfation of KCl and the influence of these species on the CO oxidation and nitrogen chemistry. The work includes experiments performed in a 100 kW combustion test unit together with kinetic modelling performed using Chemkin.

Sulfur is mainly found as SO₂ in the flue gas and SO₂ promotes alkali sulfation. Coal has, in general, a higher sulfur content compared to biomass and therefore more alkali sulfates will form when biomass is co-combusted with coal. Alkali sulfates are less problematic with respect to HTC compared to alkali chlorides and it is therefore beneficial to co-combust coal and biomass from an HTC perspective. The concentration of SO₂ will be even higher during oxy-fuel combustion compared to air combustion, and, as a result, the degree of sulfation will typically be higher for oxy-fuel compared to air-combustion, as also observed in the presented experiments. Thus, the main reason for enhanced sulfation is the higher concentration of SO₂ in oxy-combustion but oxidation of CO also has an influence. The latter is found to increase the kinetics, especially at temperatures for which the sulfation is kinetically limited. In addition, KCl seems to have a promoting effect on CO oxidation for high temperatures and CO₂ concentrations.

The relation between SO₂ and SO₃ influences the formation of alkali sulfates according to the simulations. SO₃ may enhance the sulfation but the SO₃ concentration is less important when the overall SO_x concentration is high. A high water concentration has also been shown to favor sulfation via SO₃ which increases the importance of SO₂ oxidation also for high S/K ratios. The experiments does, however, indicate that not all SO₃ has to be consumed by the sulfation.

The formation of NO differs strongly between fuel rich and fuel lean conditions and this has to be considered when performing calculations, especially when using a PFR model. In such a case no radial mixing is considered and it is there for common to follow one specific path for example the center line of a flame which could influence the results. It is also found that the nitrogen chemistry can be influenced by both KCl and SO₂. KCl is found to inhibit the formation of NO via its interactions with the radical pool. SO₂, on the other hand, does not seem to influence the formation of NO but instead promotes its oxidation to NO₂ during post flame conditions.

The present work has shown that there is a potential to mitigate HTC related problems that are connected to alkali species and chlorine during biomass combustion in oxy-fuel atmospheres. HTC issues in oxy-fuel combustion are therefore expected to be easier to handle compared to conventional air-fuel combustion systems. These findings are based on isolated gas phase reactions. In a real solid fuel combustion system the sulfation will also be influenced by the release of gaseous species together with ash-related reactions. How this chemistry is influenced when switching from air-fuel to an oxy-fuel system will be important for the sulfation of alkali metals in a real combustion system. Future work is therefore suggested to include experiments that examine the behavior of biomass fuel particles during oxy-fuel combustion.

It is also suggested that future work should include bench scale reactor experiments. In such a reactor, the fundamental chemistry can be controlled and investigated in more detail in order to obtain an improved understanding of the CO-KCl and K-S-N interactions found in this work. The interaction between alkali species, soot and aerosols is another important area that needs further advancement.

Nomenclature

BECCS	Bio energy with carbon capture and storage
BLPI	Berner low-pressure impactor
CCS	Carbon capture and storage
CFB	Circulating fluidized bed
CPC	Condensation particle counter
d ₅₀	Size of particles collected with 50% efficiency
DMA	Differential mobility analyzer
DOAS	Differential optical absorption spectroscopy
DLPI	Dekati low-pressure impactor
FB	Fluidized bed
FTIR	Fourier transform infrared spectroscopy
HTC	High temperature corrosion
IACM	In situ alkali monitor
IEA	International Energy Agency
IR	Infrared
LPI	Low-pressure impactor
NO _x	Generic term for nitrogen oxides; NO and NO ₂
PFR	Plug flow reactor
SMPS	Scanning mobility particle sizer
SO _x	Generic term for sulfuric oxides; SO, SO ₂ and SO ₃
UV	Ultra violet
VT-DMA	Volatility tandem differential mobility analyzer

References

1. IPCC, 2013: *Climate Change 2013: The Physical Science Basis.*, in *Contribution of Working Group I to the Fifth Assessment Report of the Intergovernmental Panel on Climate Change*, T.F. Stocker, D. Qin, G.-K. Plattner, M. Tignor, S.K. Allen, J. Boschung, A. Nauels, Y. Xia, V. Bex and P.M. Midgley, Editor. 2013: Cambridge University Press, Cambridge, United Kingdom and New York, NY, USA, 2013. p. 1535.
2. IEA, *Renewables Information 2016*. 2016, International Energy Agency, ISBN 978-92-64-25867-9.
3. IEA, *CO2 Emissions from Fuel Combustion*. 2016, International Energy Agency, ISBN 978-92-64-25856-3.
4. IEA, *Electricity Information 2016*. 2016, International Energy Agency, ISBN 978-92-64-25865-5.
5. Wang, M., A. Lawal, P. Stephenson, J. Sidders, and C. Ramshaw, *Post-combustion CO2 capture with chemical absorption: A state-of-the-art review*. Chemical Engineering Research and Design, 2011. **89**(9): p. 1609-1624.
6. Toftegaard, M.B., J. Brix, P.A. Jensen, P. Glarborg, and A.D. Jensen, *Oxy-fuel combustion of solid fuels*. Progress in Energy and Combustion Science, 2010. **36**(5): p. 581-625.
7. Markström, P., C. Linderholm, and A. Lyngfelt, *Chemical-looping combustion of solid fuels - Design and operation of a 100kW unit with bituminous coal*. International Journal of Greenhouse Gas Control, 2013. **15**: p. 150-162.
8. Bachu, S., *CO 2 storage in geological media: Role, means, status and barriers to deployment*. Progress in Energy and Combustion Science, 2008. **34**(2): p. 254-273.
9. Azar, C., D.J.A. Johansson, and N. Mattsson, *Meeting global temperature targets - The role of bioenergy with carbon capture and storage*. Environmental Research Letters, 2013. **8**(3).
10. Aho, M., T. Envall, and J. Kauppinen, *Corrosivity of flue gases during co-firing Chinese biomass with coal at fluidised bed conditions*. Fuel Processing Technology, 2013. **105**: p. 82-88.
11. Kassman, H., J. Pettersson, B.M. Steenari, and L.E. Åmand, *Two strategies to reduce gaseous KCl and chlorine in deposits during biomass combustion - Injection of ammonium sulphate and co-combustion with peat*. Fuel Processing Technology, 2013. **105**: p. 170-180.
12. Khan, A.A., W. de Jong, P.J. Jansens, and H. Spliethoff, *Biomass combustion in fluidized bed boilers: Potential problems and remedies*. Fuel Processing Technology, 2009. **90**(1): p. 21-50.
13. Olanders, B. and B.M. Steenari, *Characterization of ashes from wood and straw*. Biomass and Bioenergy, 1995. **8**(2): p. 105-115.
14. Saleh, S.B., J.P. Flensburg, T.K. Shoulaifar, Z. Sárossy, B.B. Hansen, H. Egsgaard, N. Demartini, P.A. Jensen, P. Glarborg, and K. Dam-Johansen, *Release of chlorine and sulfur during biomass torrefaction and pyrolysis*. Energy and Fuels, 2014. **28**(6): p. 3738-3746.
15. Andersson, K., R. Johansson, S. Hjærtstam, F. Johnsson, and B. Leckner, *Radiation intensity of lignite-fired oxy-fuel flames*. Experimental Thermal and Fluid Science, 2008. **33**(1): p. 67-76.

16. Andersson, K., R. Johansson, F. Johnsson, and B. Leckner, *Radiation intensity of propane-fired oxy-fuel flames: Implications for soot formation*. Energy and Fuels, 2008. **22**(3): p. 1535-1541.
17. Andersson, K. and F. Johnsson, *Flame and radiation characteristics of gas-fired O₂/CO₂ combustion*. Fuel, 2007. **86**(5-6): p. 656-668.
18. Fleig, D., K. Andersson, F. Normann, and F. Johnsson, *SO₃ Formation under oxyfuel combustion conditions*. Industrial and Engineering Chemistry Research, 2011. **50**(14): p. 8505-8514.
19. Fleig, D., F. Normann, K. Andersson, F. Johnsson, and B. Leckner. *The fate of sulphur during oxy-fuel combustion of lignite*. in *International Conference on Greenhouse Gas Control Technologies*. 2008. Washington DC, USA: Elsevier.
20. Normann, F., K. Andersson, F. Johnsson, and B. Leckner, *NO_x reburning in oxy-fuel combustion: A comparison between solid and gaseous fuels*. International Journal of Greenhouse Gas Control, 2011. **5**(SUPPL. 1): p. S120-S126.
21. Normann, F., K. Andersson, B. Leckner, and F. Johnsson, *Emission control of nitrogen oxides in the oxy-fuel process*. Progress in Energy and Combustion Science, 2009. **35**(5): p. 385-397.
22. Leckner, B., *Co-combustion - A summary of technology*. Thermal Science, 2007. **11**(4): p. 5-40.
23. Savolainen, K., *Co-firing of biomass in coal-fired utility boilers*. Applied Energy, 2003. **74**(3-4): p. 369-381.
24. Spliethoff, H. and K.R.G. Hein, *Effect of co-combustion of biomass on emissions in pulverized fuel furnaces*. Fuel Processing Technology, 1998. **54**(1-3): p. 189-205.
25. Harb, J.N. and E.E. Smith, *Fireside corrosion in pc-fired boilers*. Progress in Energy and Combustion Science, 1990. **16**(3): p. 169-190.
26. Åmand, L.E., B. Leckner, D. Eskilsson, and C. Tullin, *Ash deposition on heat transfer tubes during combustion of demolition wood*. Energy and Fuels, 2006. **20**(3): p. 1001-1007.
27. Pisa, I. and G. Lazaroiu, *Influence of co-combustion of coal/biomass on the corrosion*. Fuel Processing Technology, 2012. **104**: p. 356-364.
28. Pettersson, J., J.E. Svensson, and L.G. Johansson, *Alkali induced corrosion of 304-type austenitic stainless steel at 600°C; comparison between KCl, K₂CO₃ and K₂SO₄*. Materials Science Forum, 2008. **595-598**: p. 367-375.
29. Pettersson, A., A.L. Elled, A. Möller, B.M. Steenari, and L.E. Amand. *The impact of zeolites during co-combustion of municipal sewage sludge with alkali and chlorine rich fuels*. 2009.
30. Syed, A.U., N.J. Simms, and J.E. Oakey, *Fireside corrosion of superheaters: Effects of air and oxy-firing of coal and biomass*. Fuel, 2012. **101**: p. 62-73.
31. Fleig, D., K. Andersson, and F. Johnsson, *Influence of operating conditions on SO₃ formation during air and oxy-fuel combustion*. Industrial and Engineering Chemistry Research, 2012. **51**(28): p. 9483-9491.
32. Giménez-López, J., M. Martínez, A. Millera, R. Bilbao, and M.U. Alzueta, *SO₂ effects on CO oxidation in a CO₂ atmosphere, characteristic of oxy-fuel conditions*. Combustion and Flame, 2011. **158**(1): p. 48-56.
33. Rasmussen, C.L., P. Glarborg, and P. Marshall, *Mechanisms of radical removal by SO₂*. Proceedings of the Combustion Institute, 2007. **31 I**: p. 339-347.
34. Kassman, H., M. Broström, M. Berg, and L.E. Åmand, *Measures to reduce chlorine in deposits: Application in a large-scale circulating fluidised bed boiler firing biomass*. Fuel, 2011. **90**(4): p. 1325-1334.

35. Kassman, H., F. Normann, and L.-E. Åmand, *The effect of oxygen and volatile combustibles on the sulphation of gaseous KCl*. *Combustion and Flame*, 2013. **160**(10): p. 2231-2241.
36. Hindiyarti, L., F. Frandsen, H. Livbjerg, P. Glarborg, and P. Marshall, *An exploratory study of alkali sulfate aerosol formation during biomass combustion*. *Fuel*, 2008. **87**(8-9): p. 1591-1600.
37. Slack, M., J.W. Cox, A. Grillo, and R. Ryan, *Potassium kinetics in heavily seeded atmospheric pressure laminar methane flames*. *Combustion and Flame*, 1989. **77**(3-4): p. 311-320.
38. Johansen, J.M., J.G. Jakobsen, F.J. Frandsen, and P. Glarborg, *Release of K, Cl, and S during pyrolysis and combustion of high-chlorine biomass*. *Energy and Fuels*, 2011. **25**(11): p. 4961-4971.
39. Glarborg, P., *Hidden interactions-Trace species governing combustion and emissions*. *Proceedings of the Combustion Institute*, 2007. **31 I**: p. 77-98.
40. Johansen, J.M., M. Aho, K. Paakkinen, R. Taipale, H. Egsgaard, J.G. Jakobsen, F.J. Frandsen, and P. Glarborg, *Release of K, Cl, and S during combustion and co-combustion with wood of high-chlorine biomass in bench and pilot scale fuel beds*. *Proceedings of the Combustion Institute*, 2013. **34**(2): p. 2363-2372.
41. Knudsen, J.N., P.A. Jensen, and K. Dam-Johansen, *Transformation and release to the gas phase of Cl, K, and S during combustion of annual biomass*. *Energy and Fuels*, 2004. **18**(5): p. 1385-1399.
42. Pommer, L., M. Öhman, D. Boström, J. Burvall, R. Backman, I. Olofsson, and A. Nordin, *Mechanisms behind the positive effects on bed agglomeration and deposit formation combusting forest residue with peat additives in fluidized beds*. *Energy and Fuels*, 2009. **23**(9): p. 4245-4253.
43. Ferrer, E., M. Aho, J. Silvennoinen, and R.V. Nurminen, *Fluidized bed combustion of refuse-derived fuel in presence of protective coal ash*. *Fuel Processing Technology*, 2005. **87**(1): p. 33-44.
44. Knudsen, J.N., P.A. Jensen, W. Lin, and K. Dam-Johansen, *Secondary capture of chlorine and sulfur during thermal conversion of biomass*. *Energy and Fuels*, 2005. **19**(2): p. 606-617.
45. Wei, X., C. Lopez, T. Von Puttkamer, U. Schnell, S. Unterberger, and K.R.G. Hein, *Assessment of chlorine-alkali-mineral interactions during co-combustion of coal and straw*. *Energy and Fuels*, 2002. **16**(5): p. 1095-1108.
46. Müller, M., K.J. Wolf, A. Smeda, and K. Hilpert, *Release of K, Cl, and S species during co-combustion of coal and straw*. *Energy and Fuels*, 2006. **20**(4): p. 1444-1449.
47. Wu, H., M. Castro, P.A. Jensen, F.J. Frandsen, P. Glarborg, K. Dam-Johansen, M. Røkke, and K. Lundtorp, *Release and transformation of inorganic elements in combustion of a high-phosphorus fuel*. *Energy and Fuels*, 2011. **25**(7): p. 2874-2886.
48. Yue, M., Y. Wang, and X. Li, *Experimental study on the release characteristics of chlorine and alkali metal during co-firing of wheat straw and lean coal*. 2012. p. 3799-3802.
49. Cullis, C.F. and M.F.R. Mulcahy, *The kinetics of combustion of gaseous sulphur compounds*. *Combustion and Flame*, 1972. **18**(2): p. 225-292.
50. Glarborg, P. and P. Marshall, *Oxidation of reduced sulfur species: Carbonyl sulfide*. *International Journal of Chemical Kinetics*, 2013. **45**(7): p. 429-439.
51. Bassilakis, R., Y. Zhao, P.R. Solomon, and M.A. Serio, *Sulfur and nitrogen evolution in the Argonne coals: Experiment and modeling*. *Energy & Fuels*, 1993. **7**(6): p. 710-720.

52. Glarborg, P., A.D. Jensen, and J.E. Johnsson, *Fuel nitrogen conversion in solid fuel fired systems*. Progress in Energy and Combustion Science, 2003. **29**(2): p. 89-113.
53. Pohl, J.H. and A.F. Sarofim, *Devolatilization and oxidation of coal nitrogen*. Symposium (International) on Combustion, 1977. **16**(1): p. 491-501.
54. Baxter, L.L., R.E. Mitchell, T.H. Fletcher, and R.H. Hurt, *Nitrogen Release during Coal Combustion*. Energy & Fuels, 1996. **10**(1): p. 188-196.
55. Blair, D.W., J.O.L. Wendt, and W. Bartok, *Evolution of nitrogen and other species during controlled pyrolysis of coal*. Symposium (International) on Combustion, 1977. **16**(1): p. 475-489.
56. Rigby, J., J. Ma, B.W. Webb, and T.H. Fletcher, *Transformations of coal-derived soot at elevated temperature*. Energy and Fuels, 2001. **15**(1): p. 52-59.
57. Chen, J.C., C. Castagnoli, and S. Niksa, *Coal devolatilization during rapid transient heating. 2. Secondary pyrolysis*. Energy & Fuels, 1992. **6**(3): p. 264-271.
58. Wierzbicka, A., L. Lillieblad, J. Pagels, M. Strand, A. Gudmundsson, A. Gharibi, E. Swietlicki, M. Sanati, and M. Bohgard, *Particle emissions from district heating units operating on three commonly used biofuels*. Atmospheric Environment, 2005. **39**(1): p. 139-150.
59. Valmari, T., T.M. Lind, E.I. Kauppinen, G. Sfiris, K. Nilsson, and W. Maenhaut, *Field study on ash behavior during circulating fluidized-bed combustion of biomass. 1. Ash formation*. Energy and Fuels, 1999. **13**(2): p. 379-389.
60. Boman, C., A. Nordin, D. Boström, and M. Öhman, *Characterization of inorganic particulate matter from residential combustion of pelletized biomass fuels*. Energy and Fuels, 2004. **18**(2): p. 338-348.
61. Christensen, K.A. and H. Livbjerg, *A field study of submicron particles from the combustion of straw*. Aerosol Science and Technology, 1996. **25**(2): p. 185-199.
62. Johansson, L.S., C. Tullin, B. Leckner, and P. Sjövall, *Particle emissions from biomass combustion in small combustors*. Biomass and Bioenergy, 2003. **25**(4): p. 435-446.
63. Pagels, J., M. Strand, J. Rissler, A. Szpila, A. Gudmundsson, M. Bohgard, L. Lillieblad, M. Sanati, and E. Swietlicki, *Characteristics of aerosol particles formed during grate combustion of moist forest residue*. Journal of Aerosol Science, 2003. **34**(8): p. 1043-1059.
64. Alkemade, U. and K.H. Homann, *Gas-Phase Dimerization of Sodium Halides and Formation of Mixed Sodium/Phenyl Iodides*. Berichte der Bunsengesellschaft für physikalische Chemie, 1989. **93**(4): p. 434-439.
65. Jensen, J.R., L.B. Nielsen, C. Schultz-Møller, S. Wedel, and H. Livbjerg, *The Nucleation of Aerosols in Flue Gases with a High Content of Alkali - A Laboratory Study*. Aerosol Science and Technology, 2000. **33**(6): p. 490-509.
66. Blomberg, T., *A thermodynamic study of the gaseous potassium chemistry in the convection sections of biomass fired boilers*. Materials and Corrosion, 2011. **62**(7): p. 635-641.
67. Iisa, K., Y. Lu, and K. Salmenoja, *Sulfation of potassium chloride at combustion conditions*. Energy and Fuels, 1999. **13**(6): p. 1184-1190.
68. Sengeløv, L.W., T.B. Hansen, C. Bartolomé, H. Wu, K.H. Pedersen, F.J. Frandsen, A.D. Jensen, and P. Glarborg, *Sulfation of condensed potassium chloride by SO₂*. Energy and Fuels, 2013. **27**(6): p. 3283-3289.
69. Lindberg, D., R. Backman, and P. Chartrand, *Thermodynamic evaluation and optimization of the (Na₂SO₄ + K₂SO₄ + Na₂S₂O₇ + K₂S₂O₇) system*. Journal of Chemical Thermodynamics, 2006. **38**(12): p. 1568-1583.

70. Steinberg, M. and K. Schofield, *The controlling chemistry of surface deposition from sodium and potassium seeded flames free of sulfur or chlorine impurities*. Combustion and Flame, 2002. **129**(4): p. 453-470.
71. Schofield, K. and M. Steinberg, *Sodium/sulfur chemical behavior in fuel-rich and -lean flames*. The Journal of Physical Chemistry, 1992. **96**(2): p. 715-726.
72. Steinberg, M. and K. Schofield, *The chemistry of sodium with sulfur in flames*. Progress in Energy and Combustion Science, 1990. **16**(4): p. 311-317.
73. Boonsongsup, L., K. Iisa, and W.J. Frederick Jr, *Kinetics of the Sulfation of NaCl at Combustion Conditions*. Industrial and Engineering Chemistry Research, 1997. **36**(10): p. 4212-4216.
74. Li, B., Z. Sun, Z. Li, M. Aldén, J.G. Jakobsen, S. Hansen, and P. Glarborg, *Post-flame gas-phase sulfation of potassium chloride*. Combustion and Flame, 2013. **160**(5): p. 959-969.
75. Christensen, K.A. and H. Livbjerg, *A plug flow model for chemical reactions and aerosol nucleation and growth in an alkali-containing flue gas*. Aerosol Science and Technology, 2000. **33**(6): p. 470-489.
76. Hynes, A.J., M. Steinberg, and K. Schofield, *The chemical kinetics and thermodynamics of sodium species in oxygen-rich hydrogen flames*. The Journal of Chemical Physics, 1983. **80**(6): p. 2585-2597.
77. Jensen, D.E., *Alkali-metal compounds in oxygen-rich flames. A reinterpretation of experimental results*. Journal of the Chemical Society, Faraday Transactions 1: Physical Chemistry in Condensed Phases, 1982. **78**(9): p. 2835-2842.
78. Jensen, D.E. and G.A. Jones, *Kinetics of flame inhibition by sodium*. Journal of the Chemical Society, Faraday Transactions 1: Physical Chemistry in Condensed Phases, 1982. **78**(9): p. 2843-2850.
79. Jensen, D.E., G.A. Jones, and A.C.H. Mace, *Flame inhibition by potassium*. Journal of the Chemical Society, Faraday Transactions 1: Physical Chemistry in Condensed Phases, 1979. **75**: p. 2377-2385.
80. Birchall, J.D., *On the mechanism of flame inhibition by alkali metal salts*. Combustion and Flame, 1970. **14**(1): p. 85-95.
81. Bulewicz, E.M. and B.J. Kucnerowicz-Polak, *The action of sodium bicarbonate and of silica powder on upward propagating flame in a vertical duct*. Combustion and Flame, 1987. **70**(2): p. 127-135.
82. Dewitte, M., J. Vrebosch, and A. van Tiggelen, *Inhibition and extinction of premixed flames by dust particles*. Combustion and Flame, 1964. **8**(4): p. 257-266.
83. Dodding, R.A., R.F. Simmons, and A. Stephens, *The extinction of methane-air diffusion flames by sodium bicarbonate powders*. Combustion and Flame, 1970. **15**(3): p. 313-315.
84. Friedman, R. and J.B. Levy, *Inhibition of opposed-jet methane-air diffusion flames. The effects of alkali metal vapours and organic halides*. Combustion and Flame, 1963. **7**(1): p. 195-201.
85. Kim, H.T. and J.J. Reuther, *Temperature dependence of dry chemical premixed flame inhibition effectiveness*. Combustion and Flame, 1984. **57**(3): p. 313-317.
86. Rosser Jr, W.A., S.H. Inami, and H. Wise, *The effect of metal salts on premixed hydrocarbon-air flames*. Combustion and Flame, 1963. **7**(1): p. 107-119.
87. Sridhar Iya, K., S. Wollowitz, and W.E. Kaskan, *The mechanism of flame inhibition by sodium salts*. Symposium (International) on Combustion, 1975. **15**(1): p. 329-336.
88. Wei, X., U. Schnell, X. Han, and K.R.G. Hein, *Interactions of CO, HCl, and SOx in pulverised coal flames*. Fuel, 2004. **83**(9): p. 1227-1233.

89. Hindiyarti, L., F. Frandsen, H. Livbjerg, and P. Glarborg, *Influence of potassium chloride on moist CO oxidation under reducing conditions: Experimental and kinetic modeling study*. Fuel, 2006. **85**(7-8): p. 978-988.
90. Roesler, J.F., R.A. Yetter, and F.L. Dryer, *Detailed kinetic modeling of moist CO oxidation inhibited by trace quantities of HCl*. Combustion science and technology, 1992. **85**(1-6): p. 1-22.
91. Roesler, J.F., R.A. Yetter, and F.L. Dryer, *Kinetic interactions of CO, NO_x, and HCl emissions in postcombustion gases*. Combustion and Flame, 1995. **100**(3): p. 495-504.
92. Roesler, J.F., R.A. Yetter, and F.L. Dryer, *Inhibition and oxidation characteristics of chloromethanes in reacting CO/H₂O/O₂ mixtures*. Combustion science and technology, 1996. **120**(1-6): p. 11-37.
93. Mueller, C., P. Kilpinen, and M. Hupa, *Influence of HCl on the homogeneous reactions of CO and NO in postcombustion conditions - A kinetic modeling study*. Combustion and Flame, 1998. **113**(4): p. 579-588.
94. Glarborg, P. and P. Marshall, *Mechanism and modeling of the formation of gaseous alkali sulfates*. Combustion and Flame, 2005. **141**(1-2): p. 22-39.
95. Zamansky, V.M., V.V. Lissianski, P.M. Maly, L. Ho, D. Rusli, and W.C. Gardiner Jr, *Reactions of sodium species in the promoted SNCR process*. Combustion and Flame, 1999. **117**(4): p. 821-831.
96. Zamansky, V.M., P.M. Maly, L. Ho, V.V. Lissianski, D. Rusli, and W.C. Gardiner Jr, *Promotion of selective non-catalytic reduction of NO by sodium carbonate*. Symposium (International) on Combustion, 1998. **1**: p. 1443-1449.
97. Wei, X., X. Han, U. Schnell, J. Maier, H. Wörner, and K.R.G. Hein, *The effect of HCl and SO₂ on NO_x formation in coal flames*. Energy and Fuels, 2003. **17**(5): p. 1392-1398.
98. Campbell, I.M. and B.A. Thrush, *Reactivity of hydrogen to atomic nitrogen and atomic oxygen*. Transactions of the Faraday Society, 1968. **64**: p. 1265-1274.
99. Lavole, G.A., J.B. Heywood, and J.C. Keck, *Experimental and theoretical study of nitric oxide formation in internal combustion engines*. Combustion Science and Technology, 1970. **1**(4): p. 313-326.
100. Zeldovich, J., *The oxidation of nitrogen in combustion and explosions*. European Physical Journal A - Hadrons and Nuclei, 1946. **21**: p. 577-628.
101. Fenimore, C.P., *Formation of nitric oxide in premixed hydrocarbon flames*. Symposium (International) on Combustion, 1971. **13**(1): p. 373-380.
102. Wendt, J.O.L., C.V. Sternling, and M.A. Matovich, *Reduction of sulfur trioxide and nitrogen oxides by secondary fuel injection*. Symposium (International) on Combustion, 1973. **14**(1): p. 897-904.
103. Wendt, J.O.L., J.T. Morcomb, and T.L. Corley, *Influence of fuel sulfur on fuel nitrogen oxidation mechanisms*. Symposium (International) on Combustion, 1979. **17**(1): p. 671-678.
104. Wendt, J.O.L. and J.M. Ekmann, *Effect of fuel sulfur species on nitrogen oxide emissions from premixed flames*. Combustion and Flame, 1975. **25**: p. 355-360.
105. Pfefferle, L.D. and S.W. Churchill, *Effect of fuel sulfur on nitrogen oxide formation in a thermally stabilized plug-flow burner*. Industrials and Engineering Chemistry Research®, 1989. **28**(7): p. 1004-1010.
106. Zhao, Z., W. Li, J. Qiu, and B. Li, *Effect of Na, Ca and Fe on the evolution of nitrogen species during pyrolysis and combustion of model chars*. Fuel, 2003. **82**(15-17): p. 1839-1844.

107. Zhao, Z., W. Li, J. Qiu, and B. Li, *Catalytic effect of Na-Fe on NO-char reaction and NO emission during coal char combustion*. Fuel, 2002. **81**(18): p. 2343-2348.
108. Zhao, Z., J. Qiu, W. Li, H. Chen, and B. Li, *Influence of mineral matter in coal on decomposition of NO over coal chars and emission of NO during char combustion*. Fuel, 2003. **82**(8): p. 949-957.
109. Fleig, D., M.U. Alzueta, F. Normann, M. Abián, K. Andersson, and F. Johnsson, *Measurement and modeling of sulfur trioxide formation in a flow reactor under post-flame conditions*. Combustion and Flame, 2013. **160**(6): p. 1142-1151.
110. Kühnemuth, D., F. Normann, K. Andersson, F. Johnsson, and B. Leckner, *NOX REBURNING IN OXY-FUEL COMBUSTION AN EXPERIMENTAL INVESTIGATION*, in *International Pittsburgh Coal Conference*. 2010: Istanbul, Turkey.
111. Fleig, D., E. Vainio, K. Andersson, A. Brink, F. Johnsson, and M. Hupa, *Evaluation of SO₃ measurement techniques in air and oxy-fuel combustion*. Energy and Fuels, 2012. **26**(9): p. 5537-5549.
112. Maddalone, R.F., S.F. Newton, R.G. Rhudy, and R.M. Statnick, *Laboratory and field evaluation of the Controlled Condensation System for SO₃ measurements in flue gas streams*. Journal of the Air Pollution Control Association, 1979. **29**(6): p. 626-631.
113. Forsberg, C., M. Broström, R. Backman, E. Edvardsson, S. Badiei, M. Berg, and H. Kassman, *Principle, calibration, and application of the in situ alkali chloride monitor*. Review of Scientific Instruments, 2009. **80**(2).
114. Platt, U. and D. Perner, *MEASUREMENTS OF ATMOSPHERIC TRACE GASES BY LONG PATH DIFFERENTIAL UV/VISIBLE ABSORPTION SPECTROSCOPY*. Springer Series in Optical Sciences, 1983. **39**: p. 97-105.
115. Mellqvist, J. and A. Rosén, *DOAS for flue gas monitoring—II. Deviations from the Beer-Lambert law for the U.V./visible absorption spectra of NO, NO₂, SO₂ and NH₃*. Journal of Quantitative Spectroscopy and Radiative Transfer, 1996. **56**(2): p. 209-224.
116. Leffler, T., C. Brackmann, M. Berg, M. Aldén, and Z.S. Li, *Development of an alkali chloride vapour-generating apparatus for calibration of ultraviolet absorption measurements*. Review of Scientific Instruments, 2017. **88**(2).
117. Strand, M., J. Pagels, A. Szpila, A. Gudmundsson, E. Swietlicki, M. Bohgard, and M. Sanati, *Fly ash penetration through electrostatic precipitator and flue gas condenser in a 6 MW biomass fired boiler*. Energy and Fuels, 2002. **16**(6): p. 1499-1506.
118. Wiinikka, H. and R. Gebart, *Critical parameters for particle emissions in small-scale fixed-bed combustion of wood pellets*. Energy and Fuels, 2004. **18**(4): p. 897-907.
119. Valmari, T., E.I. Kauppinen, J. Kurkela, J.K. Jokiniemi, G. Sfiris, and H. Revitzer, *Fly ash formation and deposition during fluidized bed combustion of willow*. Journal of Aerosol Science, 1998. **29**(4): p. 445-459.
120. Strand, M., M. Bohgard, E. Swietlicki, A. Gharibi, and M. Sanati, *Laboratory and field test of a sampling method for characterization of combustion aerosols at high temperatures*. Aerosol Science and Technology, 2004. **38**(8): p. 757-765.
121. Lind, T., T. Valmari, E. Kauppinen, K. Nilsson, G. Sfiris, and W. Maenhaut, *Ash formation mechanisms during combustion of wood in circulating fluidized beds*. Symposium (International) on Combustion, 2000. **28**(2): p. 2287-2294.
122. Wiinikka, H., R. Gebart, C. Boman, D. Boström, A. Nordin, and M. Öhman, *High-temperature aerosol formation in wood pellets flames: Spatially resolved measurements*. Combustion and Flame, 2006. **147**(4): p. 278-293.
123. Fernandes, U., M. Guerrero, Á. Millera, R. Bilbao, M.U. Alzueta, and M. Costa, *Oxidation behavior of particulate matter sampled from the combustion zone of a domestic pellet-fired boiler*. Fuel Processing Technology, 2013. **116**: p. 201-208.

124. Davis, S.B., T.K. Gale, J.O.L. Wendt, and W.P. Linak, *Multicomponent coagulation and condensation of toxic metals in combustors*. Symposium (International) on Combustion, 1998. **2**: p. 1785-1791.
125. McNallan, M.J., G.J. Yurek, and J.F. Elliott, *The formation of inorganic particulates by homogeneous nucleation in gases produced by the combustion of coal*. Combustion and Flame, 1981. **42**(C): p. 45-60.
126. Wiinikka, H., *High Temperature Aerosol Formation and Emission Minimisation during Combustion of Wood Pellets*, in *Applied Physics and Mechanical Engineering*. 2005, Luleå University of Technology: Applied Physics and Mechanical Engineering. p. 57.
127. Wang, C., W.S. Seames, M. Gadgil, J. Hrdlicka, and G. Fix, *Comparison of coal ash particle size distributions from Berner and Dekati low pressure impactors*. Aerosol Science and Technology, 2007. **41**(12): p. 1062-1075.
128. Biswas, P. and R.C. Flagan, *High-velocity inertial impactors*. Environmental Science and Technology, 1984. **18**(8): p. 611-616.
129. Jiménez, S. and J. Ballester, *Formation and emission of submicron particles in pulverized olive residue (orujillo) combustion*. Aerosol Science and Technology, 2004. **38**(7): p. 707-723.
130. Zeleny, J., *The distribution of mobilities of ions in moist air*. Physical Review, 1929. **34**(2): p. 310-334.
131. De La Mora, J.F., L. De Juan, T. Eichler, and J. Rosell, *Differential mobility analysis of molecular ions and nanometer particles*. TrAC - Trends in Analytical Chemistry, 1998. **17**(6): p. 328-339.
132. Park, K., D. Dutcher, M. Emery, J. Pagels, H. Sakurai, J. Scheckman, S. Qian, M.R. Stolzenburg, X. Wang, J. Yang, and P.H. McMurry, *Tandem measurements of aerosol properties - A review of mobility techniques with extensions*. Aerosol Science and Technology, 2008. **42**(10): p. 801-816.
133. Knutson, E.O. and K.T. Whitby, *Aerosol classification by electric mobility: apparatus, theory, and applications*. Journal of Aerosol Science, 1975. **6**(6): p. 443-451.
134. Schulz, C., J.D. Koch, D.F. Davidson, J.B. Jeffries, and R.K. Hanson, *Ultraviolet absorption spectra of shock-heated carbon dioxide and water between 900 and 3050 K*. Chemical Physics Letters, 2002. **355**(1-2): p. 82-88.
135. Curtiss, L.A., K. Raghavachari, P.C. Redfern, V. Rassolov, and J.A. Pople, *Gaussian-3 (G3) theory for molecules containing first and second-row atoms*. Journal of Chemical Physics, 1998. **109**(18): p. 7764-7776.
136. Curtiss, L.A., P.C. Redfern, V. Rassolov, G. Kedziora, and J.A. Pople, *Extension of Gaussian-3 theory to molecules containing third-row atoms K, Ca, Ga-Kr*. Journal of Chemical Physics, 2001. **114**(21): p. 9287-9295.
137. Yilmaz, A., L. Hindiyarti, A.D. Jensen, P. Glarborg, and P. Marshall, *Thermal dissociation of SO₃ at 1000-1400 K*. Journal of Physical Chemistry A, 2006. **110**(21): p. 6654-6659.
138. Hindiyarti, L., P. Glarborg, and P. Marshall, *Reactions of SO₃ with the O/H radical pool under combustion conditions*. Journal of Physical Chemistry A, 2007. **111**(19): p. 3984-3991.
139. Jiménez, S. and J. Ballester, *Influence of operating conditions and the role of sulfur in the formation of aerosols from biomass combustion*. Combustion and Flame, 2005. **140**(4): p. 346-358.
140. Jiménez, S. and J. Ballester, *Formation of alkali sulphate aerosols in biomass combustion*. Fuel, 2007. **86**(4): p. 486-493.

141. Glarborg, P., M.U. Alzueta, K. Kjærgaard, and K. Dam-Johansen, *Oxidation of formaldehyde and its interaction with nitric oxide in a flow reactor*. Combustion and Flame, 2003. **132**(4): p. 629-638.
142. Glarborg, P., M.U. Alzueta, K. Dam-Johansen, and J.A. Miller, *Kinetic modeling of hydrocarbon/nitric oxide interactions in a flow reactor*. Combustion and Flame, 1998. **115**(1-2): p. 1-27.
143. Alzueta, M.U., M. Borruely, A. Callejas, A. Millera, and R. Bilbao, *An experimental and modeling study of the oxidation of acetylene in a flow reactor*. Combustion and Flame, 2008. **152**(3): p. 377-386.
144. Abián, M., J. Giménez-López, R. Bilbao, and M.U. Alzueta, *Effect of different concentration levels of CO₂ and H₂O on the oxidation of CO: Experiments and modeling*. Proceedings of the Combustion Institute, 2011. **33**(1): p. 317-323.
145. Glarborg, P., M. Østberg, M.U. Alzueta, K. Dam-Johansen, and J.A. Miller, *Twenty-Seventh Symposium (International) on Combustion Volume One The recombination of hydrogen atoms with nitric oxide at high temperatures*. Symposium (International) on Combustion, 1998. **27**(1): p. 219-226.
146. Dagaut, P., P. Glarborg, and M.U. Alzueta, *The oxidation of hydrogen cyanide and related chemistry*. Progress in Energy and Combustion Science, 2008. **34**(1): p. 1-46.
147. Alzueta, M.U., R. Bilbao, and P. Glarborg, *Inhibition and sensitization of fuel oxidation by SO₂*. Combustion and Flame, 2001. **127**(4): p. 2234-2251.